IJEST

ISSN: 0973-6255
Vol. 11 No.2
July - December 2017

Indian Journal of Engineering, Science, and Technology

A Refereed Research Journal

Published by

BANNARI AMMAN INSTITUTE OF TECHNOLOGY

(Autonomous Institution Affiliated to Anna University of Technology, Coimbatore - Approved by AICTE - Accredited by NBA and NAAC with "A" Grade)
Sathyamangalam - 638 401 Erode District Tamil Nadu India
Ph: 04295-226340 - 44 Fax: 04295-226666
www.bitsathy.ac.in E-mail: ijest@bitsathy.ac.in

Indian Journal of Engineering, Science, and Technology

IJEST is a refereed research journal published half-yearly by Bannari Amman Institute of Technology. Responsibility for the contents rests upon the authors and not upon the IJEST. For copying or reprint permission, write to Copyright Department, IJEST, Bannari Amman Institute of Technology, Sathyamanagalam, Erode District - 638 401, Tamil Nadu, India.

Indian Journal of Engineering, Science, and Technology

ISSN: 0973-6255

Volume 11 Number 2 **July - December 2017**

CONTENTS

Excerpt from the National Conference on Communication, Computation and Networks (NCCCN) held at BIT - 23-24 Feb 2017

S.No.	Title	Page.No.
1	**Design of Compact Microstrip Dipole Antenna** S.Anusha and L.Gomathi	01
2	**An Efficient Compression Technique for Image Multiplication** N. Savithaa, C.S. Manikandababu and G.G. Renuga Devi	08
3	**Measurement and Detection of Cisterna Magna in Fetal Brain based on LMS Method** V. Praveen Kumar and S. Deepak	14
4	**Fault Diagnosis of Three Phase Induction Motors by Using Kernal Based SVM Classifiers** R. Senthil Kumar and K. Sarasvathi	19
5	**Deployment of IoT in Railway System** M. Gayathri Devi and E. Esakki Vigneswaran	25
6	**Performance Analysis of MPPT Algorithms for PV Array Fed SEPIC Converter** S.Kirthika	31
7	**Dynamic Power Tracking Using Intelligence Technique for WECS With Sepic Converter** P. Alageswari and S. Dinesh Kumar	37
8	**Design of High Throughput Redundant Binary Technique for Image Processing Application** P.Nathiya, S.Padmapriya and K.Dhatchayani	45
9	**Estimation of Micro Calcification in Mammogram Images** C.Santhi, S.M.Shayeela Banu, S.Suvetha, V.Thenmozhi and M.Manikandan	50

Design of Compact Microstrip Dipole Antenna

S.Anusha[1] and L.Gomathi[2]
Department of Electronics and Communication Engineering
M.Kumarasamy College of Engineering, Karur - 639 113, Karur, Tamil Nadu
E-mail: anushapoongodi@gmail.com, gomathilece@gmail.com

Abstract

We present a broadband microstrip different dipole endыre planar receiving wires that is sensible for applications in microwave, submillimeter (sub-mm), and millimeter (mm) wavelengths. We have related two dipoles of various lengths in course of action to grow the transmission limit of microstrip gathering contraptions. Two printed administrators and a ground plan which is truncated are comprehensively used to achieve high front-to-back get extent. The parallel stripline which is acclimated to feeding the gathering mechanical assembly's drivers is related particularly to microstrip without a direct stage. This direct radio wire setup can be viably consolidated into microstrip circuits. In this paper, we focus principally on the blueprint of a Ku- band gathering mechanical assembly with 7 GHz transmission limit. Plan and examination of the microstrip receiving wire were performed using intensive electromagnetic amusements and we likely researched the execution of the gathering contraption by measuring the bar radiation outlines and moreover the entry loss of a radio wire created on a Roger RO 4350 printed circuit board. The ordinary microstrip- reinforced twofold dipole gathering mechanical assembly with simplиыed balun is modиыed to extend the usable information exchange limit by growing the security of the radiation plans in the microstrip dipole receiving wires. The radio wire showed here moreover contains two parallel dipoles of various lengths to get two basic resonances. The partition between the two dipoles is changed to decrease the landing adversity between the rule resonances. A wide usable transmission limit practically more than 84% is procured with high radiation plan . The proposed microstrip dipole radio wire is fundamental in framework and little in size. Finally, we indicate two unmistakable representation uses of the receiving wire in the sub-mm and mm discoverers extend. The delayed consequences of a modиыed two-part show conыguration of the microstrip gathering device exhibit that it is helpful for wideband group applications.

Keywords: *Dipole radio wires, Microstrip reception apparatuses, Planar receiving wires, Staged exhibits, Ultra-wideband radio wires, Yagi–Uda clusters.*

1. INTRODUCTION

The idea of microstrip dipole reception apparatuses was ыrst proposed in the 1950s [1]. Be that as it may, this thought of microstrip reception apparatus needed to hold up almost up to 20 years to be acknowledged after the prevalent advancement of the printed circuit board (PCB) innovation in the 1970s [2,3]. From that point forward, microstrip design, predominant convenience, reasonable for a wide range of exhibits, simple for creation in the printed circuit board, and simple coordination with all kind of microwave solid incorporate circuits [4–7]. These reception apparatuses have been generally utilized for the non military personnel and military applications, for example, wide pillar examining, TV, communicate radio correspondence, portable frameworks, worldwide situating framework (GPS vehicle crash evasion and impact recognition framework, satellite interchanges, observation frameworks, course establishing), radio-recurrence identiыcation (RFID), various info numerous yield systems(MIMO) , radar frameworks, remote detecting, natural imaging in provincial territories, rocket direction, thus on [8]. Notwithstanding the many favourable circumstances of ordinary microstrip dipole receiving wires, they likewise have three essential inconveniences: They have low increase, limit transfer speed and are respectably broad size.

The thin exchange speed is one of the major drawbacks of these sorts of microstrip dipole receiving wires. Microstrip gathering contraptions are straight forward system for improving the information exchange limit is extending the substrate thickness. In any case, surface wave force of the microstrip receiving wire increments and radiation control diminishes with the

expanding substrate thickness, which prompts to poor radiation eьiciency. Therefore, different procedures are disclosed to give wide-impedance data transmissions of various wavelength in microstrip dipole radio wires, including impedance coordinating systems utilizing single or twofold stub and negative capacitor/inductor , microstrip opening receiving wires utilizing the L, U, T, and upset T spaces in the ground arrange, surface wave smothering utilizing magnet dielectric substrate and electromagnetic vitality bandgap(EBG) structures, and composite-resonator microstrip reception apparatuses utilizing meta material resonators .Another issue to be tackled is the low pick up for customary microstrip dipole reception apparatus component. Pit backing methods has been utilized to wipe out the bidirectional radiation design, along these lines furnishing higher pick up contrasted and traditional microstrip dipole radio wire. Focal point covering is an option approach to accomplish pick up and radiation design improvement. The focal point with accepted proьile, as curved, hemi circular, hyper- hemispherical and semi circular, broadened hemispherical, used to center the radiation design shaft from the radiator components. The coordinated focal point of microstrip dipole receiving wire can be dealt with as composite reception apparatus joined by microstrip radiator components and dielectrics, which is extremely valuable for high frequencies (optical waves, terahertz (THz), sub-mm and mm). The applications of the antenna in the sub-mm and mm detectors area. The results of a modiьed two-element array conьguration from this antenna show that it is very good for wideband phased array applications.

Whatever remains of the paper is sorted out as takes after: In Section 2, we portray related work on various sort microstrip reception apparatuses topology. In Section 3, we depict the models, investigation, and calculations our system. Area 4, we depict the use of our structure to outline proficient receiving wires. Area 5 gives an execution assessment. At last, we had finish up the paper in Section 6.

2. RELATEDWORKS

The microstrip reception apparatus has been broadly contemplated in the previous decades as one of the standard planar microstrip radio wires, despite everything it has an immense potential for further advancements and assumes critical part in military applications. The paper [1] proposes three ranges for further research in light of the past takes a shot at microstrip dipole receiving wire components and clusters. One is investigating the assortment of microstrip dipole radio wire topologies to meet the sought prerequisite, for example, all inclusive band (UWB), high pick up, scaling down, ease, round polarization, multi energized, et cetera. Another is to apply microstrip dipole reception apparatus to shape composite radio wire which is more potential than the individual receiving wire. The execution of receiving wire is developing towards exceptionally mix of reception apparatus exhibit and sustaining system at generally high frequencies and data transfer capacity, similar to sub-millimeter wave or millimeter or terahertz(THz) waveguide, by utilizing the progressed machining techniques.[2]A novel microstrip-to-waveguide move using coplanar segments of the Yagi-like radio wire is introduced. The X-band move of the microstrip dipole receiving wire shows around 40% data transmission with return misfortune is greatly improved than - 12dB. This move ought to discover wide bar examining applications because of its high similarity with MMIC innovation at low creation cost [6].

We portray a waveguide to thin-ьilm microstrip move for superior the submillimetre wave and terahertz applications. The proposed consistent sweep test couples thin-ьilm microstrip dipole line, to full stature rectangular waveguide with superior to 99% effciency (Voltage standing wave proportion <1.20) and 45% partial transmission capacity. It chips away at the Broad HFSS reproductions are supported by scale-show estimations. By selecting the substrate material of the radio wire and test range, any genuine impedance between the strip is ≅15-60 Ω can be accomplished effectively. The spiral test gives signiьicantly enhanced execution over different outlines talked about in the microstrip dipole reception apparatus. Despite the fact that our essential application is submillimetre wave in super directing blenders, we demonstrate that layer methods of the radio wire ought to permit expansive band waveguide segment to be developed for the THz recurrence run.

In this [12] we depict a novel broadband microstrip dipole radio wire in light of the exemplary Yagi–Uda dipole exhibit. This semi Yagi reception apparatus accomplishes a deliberate 48% of transmission capacity for Voltage Standard Wave Proportion 2 and which is superior to anything 12 dB front-to-back proportion, littler than 15 dB of cross polarization, 3–5 dB total pick up and an ostensible effectiveness is around 93% over the working data transmission of the microstrip. Limited contrast and the time-space

reproduction is utilized as a part of the radio wire for the improvement and the outcomes are exceptionally well with the estimation of recurrence. Moreover, an increase upgraded plan of microstrip dipole receiving wire is introduced, where higher pick up has been accomplished at the cost of diminished transmission capacity and recurrence. These semi Yagi receiving wires are utilized on a high dielectric t substrate and are totally good with microstrip dipole hardware and in the strong state gadgets. The reception apparatus ought to locate the wide bar checking applications in remote correspondence frameworks, staged exhibits, control consolidating and dynamic clusters, and in addition millimeter-wave imaging varieties of the receiving wire.

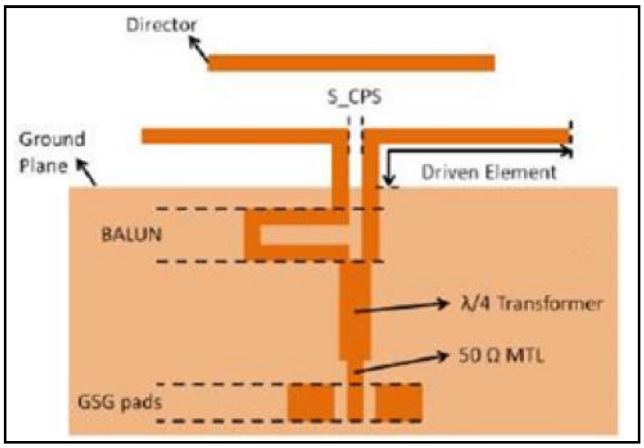

Fig.2.1 Schematic View of a Yagi-uda Antenna Including Measurement Pads

A basic sort of a free-space planar radio wire is a uniplanar dipole fed with a coplanar stripline (CPS). This essential gathering contraption structure, in any case it requires a snared CPS-to-microstrip balun to change the RF movement into the microstrip circuit[5], and a lone dipole receiving wire encounters contract transmission limit operation. To broaden the information exchange limit, we course two dipoles of different lengths in plan to make two resonances centered at two fairly remarkable frequencies [6], surrounding a truncated log-periodic like receiving wire as showed up in Figure 2.1. The biplanar drivers are supported with a parallel stripline, where the top stripline is related with one part of the dipoles and the base stripline is related with the other half, confining two back to back "F-shapes" structures disconnected by a thin dielectric layer. To upgrade the F/B get extents and to get the endűre far-field shaft outlines, we use two planar administrators arranged before the twofold dipole driver and a truncated ground plane as a reflecting part by expanding the base stripline the separation to the edges. This structures a move from the parallel stripline to a microstrip line. A preliminary arrangement is gotten by understanding that the working repeat and the information transmission of the receiving wire are mainly controlled by the two quarter-wavelength dipoles. The shorter and the more drawn out dipoles pick the higher and the lower rehash resonances, autonomously. The radio wire get and the passage episode are controlled by the parcel between the two dipoles and by the length of the parallel stripline that interfaces the back dipoles and the ground plane. The width of the parallel stripline controls the yield impedance and ought to along these lines be fit in with encourage the yield impedance of the twofold dipole. Every one of these estimations, including the length of the overseers, are then streamlined utilizing HFSS for the required transmission cutoff and radiation diagrams.

3.OUR PROPOSED FRAME WORK

In context of this framework, we have shaped and made a radio wire that can efűciently transmit and get RF developments in the Ku-band (11–18GHz).The social event contraption was engraved on both sides of Roger RO4350 substrate and the microstrip was connected with a standard SMA connector. The űnal geometry of the streamlined radio wire is checked. To compose the receiving wire to the impedance of the SMA connector, two extra microstrip segments were consolidated (0.4 and 0.5 mm wide freely) after the yield port of the social occasion mechanical get together to shape a quarter wavelength arranging transformer. Figure 3.1 demonstrates the HFSS replicated far-field radiation instance of the receiving wire at the consigned focal rehash 15 GHz. Both E-and H-plane radiation traces show endűre bar qualities, with a roughly 18-dB F/B get degree. The 3-dB (full-width half-most over the top, FWHM) segment width of the E-plane representation is by and large at 15 GHz, while the H-plane FWHM bar is to some degree more noteworthy at around in perspective of the nonappearance of planning fragments reverse to the radio wire's plane. The arrival loss of the receiving wire was measured utilizing a vector orchestrate analyser (VNA) in conjunction with an Anritsu thorough test fixture. The receiving wire (without the SMA connector) was adjusted and held to the test fixture's K-connector stick utilizing aching stacked jaw, and the setup was screened with high-hardship microwave securities to take out reűection impediment. The contemplate return loss of the radio wire concurs exceedingly well with the HFSS imitated result. All the

consider reverberation jumps take after certainly the course of action rehash positions, next to that the contemplate upper frequencies and resounding (around 17.5 GHz) are to some degree lower than anticipated. Never the less, there turn incident remains underneath 9dB in a repeat extent of 11–18GHz, contrasting with an information transmission of about 1.64:1 The metallization on the base plane is a truncated microstrip ground, which fills in as the reflector part for the gathering device. The parasitic boss segment on the top plane in the meantime arranges the gathering mechanical assembly expansion toward the endfire heading, and goes about as an impedance planning segment. Additionally as with the model Yagi–Udaantenna, real arrangement requires careful upgrade of the driver, official, and reflector parameters, which consolidate segment scattering, length, and width.

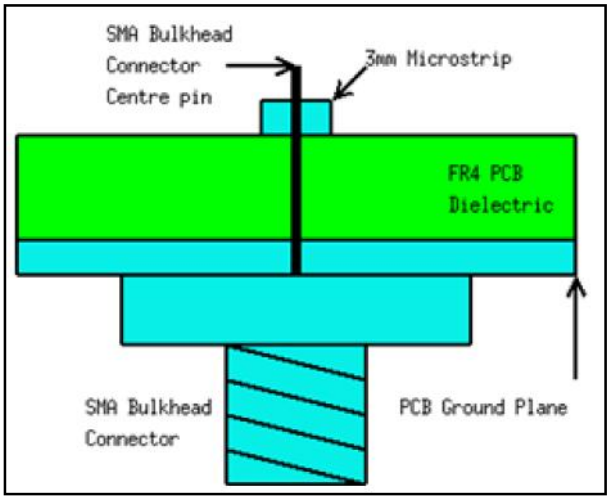

Fig. 3.1 Micro strip Connector

4. DISCUSSIONS

4.1. Highly Integration and Highly Operating Frequency Antennas and Data Transfer Capacity Based on Advanced Machining Techniques

It is understood that the microstrip radio wire was ыrst made using PCB development in 1970s, around 20 years after its machining procedures, we prescribe that a third research domain of microstrip dipole reception apparatuses is always presenting a novel progressed machining procedures in the field of receiving wires. In the accompanying, two cases will be disclosed to show how critical the progressed machining method is to create miniaturized scale strip dipole receiving wires. One of the reception apparatus is the exceptionally incorporate wide band microstrip dipole receiving wire exhibit created utilizing MPCB innovation. Another sort is THz wave planar coordinated dynamic microstrip receiving wire utilizing MEMS innovation. The VSWR of total and difference port of the mono heartbeat roundabout spellbound DCWS receiving wire cluster. This idea was ыrst introduced in 1950s. Obviously, the improvement of microstrip dipole receiving wires is firmly related with the machining strategies. As of late, different machining procedures including low temperature co-fired pottery (LTCC), multilayer printed circuit board (MPCB), smaller scale electro mechanical frameworks (MEMS), and corresponding metal oxide semiconductor (CMOS) are exceptionally built up, the opening open doors for imaginative microstrip dipole radio wires, for example, dynamic and inactive components of microstrip receiving wires, reconыgurable reception apparatuses, THz receiving wires, meta material- based reception apparatuses, et cetera. The radio wires with the accessibility of high exactness and furthermore the fast progressed machining methods, microstrip dipole receiving wires are developing towards exceptionally combination of reception apparatus, bolster arrange and working at moderately high frequencies and furthermore data transfer capacity. Since they reception apparatuses are l in light of the propelled innovation.

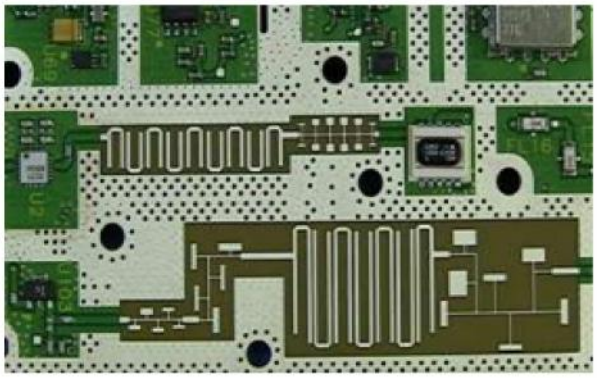

Fig 4.1 Micro strip Distributed Element Filter Technology

4.2. Exceedingly Integrated Broad-Band Microstrip Antenna Array Using Multilayer Printed Circuit Board (MPCB) Technology.

At this moment, with the progression of the multilayer printed circuit board (MPCB) advancement, the microstrip dipole radio wires can be made and arranged from one- dimensional (1D) to two dimensional(2D) and even three dimensional(3D) structures. In perspective of the multilayer printed circuit board (MPCB) advancement, a high consolidated broadband Ku-band microstrip dipole gathering contraption bunch is laid out, manufactured and

measured. This reception apparatus comprises of a parasitic fix, a determined fix two executives, a stripline encouraging system, some covered screw openings an expansive band coaxial line to stripline move and some through the gaps. The bolstering system is coordinated in base of the substrate layer of the microstrip dipole receiving wire. As the greater part of the structures of the radio wires are created immediately, the precision and the consistency can be guaranteed to be consistent. Two receiving wires of this sort are measured. The deliberate Voltage Standing Wave Ratio, pick up ,and radiation design at the inside recurrence. The deliberate outcomes demonstrate that this receiving wire keeps up great radiation design and coordinating exhibitions with relative data transmission of 13% and at fantastic recurrence. They have likewise demonstrated great consistency by utilizing multilayer printed circuit board (MPCB) innovation. A composite antenna, which is used in THz systems are made up of microstrip log-periodic antenna and dielectric lens.

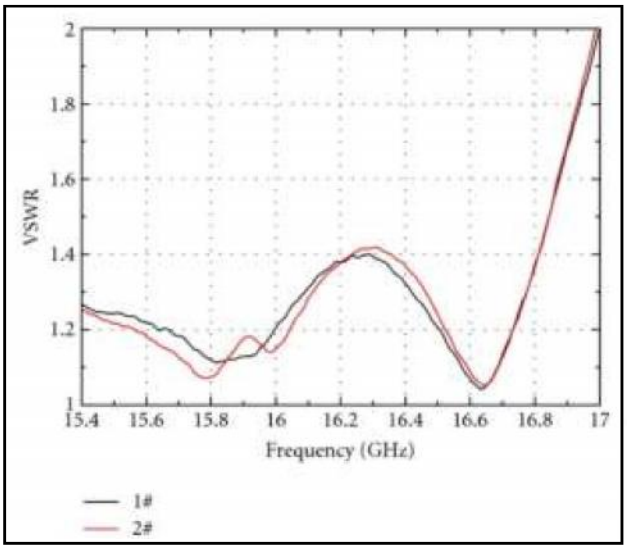

Fig. 4.2.2 The VSWR of the High Incorporate Wide Band Microstrip Receiving Wire Cluster Utilizing MPCB Innovation

4.3 Microstrip Dipole Antenna Using Micro-Electromechanical Systems Technology

THz waves are normally consolidate frequencies in the range in the region of 0.1THz and 10THz. THz development is directly transforming into a promising advancement which has potential applications in all ьields, for instance, short-run correspondence, imaging national security,space investigation and correspondence, biosensor, etcetera. To acknowledge THz handset framework, microstrip receiving wire is a fundamental segment. We frequently utilize focal point radio wire, horn receiving wire and dielectric explanatory reception apparatus for THz frameworks. In any case, they are difficult to coordinate with typical solid incorporate circuits. In spite of the fact that the microstrip receiving wire has the benefits of little volume light weight and simple combination with the solid circuit, it is diьicult to be utilized as a part of high-recurrence areas.

Miniaturized scale electro mechanical frameworks (MEMS) innovation opens the best approach to plan of THz reception apparatuses, circuits, and frameworks. THz solid receiving wire manufactured utilizing MEMS innovation and which is secured by a dielectric focal point, the reception apparatus can be viewed as a composite radio wire, are planned, created, and measured utilizing solid circuits. Diodes have the elements of blending or balancing the transporter wave motion with the primary flag. It is an efficient approach to decrease the engendering way for indicators application by incorporating the microstrip reception apparatus and diode. The developed hyper hemi circular dielectric focal point is utilized to build the pickup and recurrence of the microstrip dipole reception apparatus. A reception apparatus comprises of a coupled identifier coordinated with a dielectric focal point is composed and created by solid circuits is dependent upon THz. The planar microstrip log-period reception apparatus and log-winding receiving wire have been created utilizing smaller scale electromechanical framework innovation. The deliberate reactions of the radio wire coupled finder working at diferent recurrence groups, which can be considered to decide the effective working frequencies. This identifier gave a substantial reaction from 12GHz to 110GHz frequencies. The outcomes demonstrate the legitimacy and practicality of the THz receiving wire planned utilizing small scale electro mechanical frameworks (MEMSs) innovation.

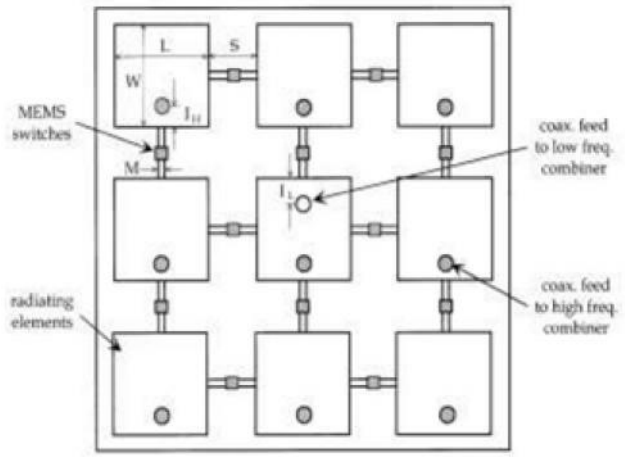

Fig. 4.3 MEMS Technology

5. PERFORMANCE EVALUATIONS

Our motivation in working up the above-depicted twofold dipole radio wire is to use it as a maintain for the super driving section crossing point discoverers for the most part created for sub-mm infinite recipients. These sub-mm discoverer chips are routinely mounted in the E-plane of a rectangular waveguide of little estimations, and the RF control from the wave guide is coupled to the device by method for a waveguide-to-microstrip move. It required to make the locator square and to mount each identifier chip absolutely in the waveguide. This is particularly repetitive in the midst of the hidden testing of another period of pointer devices since concentrated reiterated testing are required to depict and grasp their properties. It would in this way be generously more accommodating to make an assortment of discoverers each supported by a free-space twofold dipole receiving wire as showed up in Figure 6(a), and test these locator devices in the meantime by illuminating the display with a sub-mm source at a required repeat [9]. The locator show can be made using proclamation and photolithography taking care of on a lone wafer, allowing a straightforward and brisk depiction of then discoverer layout. Consequently, we have scaled and enhanced the double dipole gathering gadget to work at the 700-GHz frequencies augment.The radio wire was confined using a 400-nm-thick niobium nitride superconducting ылm as the top metallization layer and a niobium thin ылm of an undefined thickness from the base layer, with a 460-nm silicon dioxide as the ensuring layer. The entire receivingwire structure was created on a 1- m thick silicon nitride layer onto 200-m silicon substrate, which is cut away toward the complete of the get ready. The microchip is then mounted at the E-plane of a rectangular waveguide. The streamlined geometry for the sub-mm gathering contraption.

The cross-coupling between two receiving wires set at around one wavelength (400 m) a long way from each other along the gathering device plane is seemed, by all accounts, to be under 0.1% over the band. The cross-coupling augmentations to around 20dB of the segment between the two radio wires is part. The radiation case of the individual gathering device in his two-segment display also stays, as it were, unaltered from the single-segment radio wire. Another appealing usage of the radio wire in the sub-mm identifiers range is to use it as a move from waveguide to planar circuit. This is a basic part in mm and sub-mm astronomical recipients as the RF banner is assembled by an electromagnetic horn and coupled to a discoverer chip from the waveguide. The advantages of the twofold dipole radio wire in this application over the consistently used extended test [10], [11] are that it has a data impedance like the exhausted waveguide. It can without quite a bit of an extend be grounded to the waveguide, and it doesn't require the making of an unequivocally machined back short. The reenacted control coupling and return hardship execution of a twofold dipole receiving wire arranged at the E-plane of a rectangular waveguide, which shows that it can be used as a better waveguide-than planar-circuit move at mm and sub- mm wavelengths

6. CONCLUSIONS

We have displayed the blueprint and the likely measured the execution of a planar microstrip dipole endfire receiving wire that is moderate and impeccable with microwave circuit development. We fell two dipoles to finish wide band operation, and utilized a truncated ground plane and two printed officials to fulfill high F/B get extent and end fire far-field radiation trademark. The receiving wire has a particularly fundamental geometry and is supported particularly by microstrip line. We made a Ku-band radio wire in light of this layout and measured the far- field column illustrations and return setback execution. The consider results agreed particularly well with the reenacted execution. In spite of the way that the genuineness of the framework was appeared at microwave frequencies, our reenactments exhibit that it has engaging applications at sub-mm wave lengths, both as a free-space radio wire and as a waveguide-to-microstrip move.

REFERENCES

[1] A. Castillo, R. Deulofeut, A.Critz and A.Sola, "Prevention of Retinopathy Of Prematurity In Preterm Infants Through Changes In Clinical Practice and SpO(2) Technology", 2010.

[2] Davicurone, Emanuele Lindo Secco, Laura Caldani, "Assessment of Sensing Fire Fighters Uniforms For Physiological Parameters Measurement In Harsh Environment", IEEE Transaction on Information Technology in Biomedicine, Vol.16, No.3, 2012.

[3] G. DeJean and M. Tentzeris, "A New High-Gain Microstrip Yagi Array Antenna with A High

Front-To-Back (F/B) Ratio For Wlan And Millimeter-Wave Applications", IEEE Trans. Antennas Propag., Vol. 55, No. 2, Feb. 2007, pp. 298–304,

[4] A. A. Eldek, "Design of Double Dipole Antenna With Enhanced Usable Bandwidth For Sideband Phased Array Applications", Prog. Electro- magn. Res., Vol. 59, 2006, pp. 1-15.

[5] P. Forget, F. Lois, M. de Kock, "Goal-Directed Fluid Management Based on the Pulse Oximeter-Derived Pleth Variability Index Reduces Lactate Levels and Improves Fluid Management", 2010

[6] MW. Jopling, PD. Mannheimer, DE.Bebout, "Issues in the Laboratory Evaluation of Pulse Oximeter Performance", Jan2002.

[7] N. Kaneda, Y. Qian and T. Itoh, "A Broad-band Microstrip-to-wave- guide Transition using Quasi-Yagi Antenna", IEEE Trans. Microw. Theory Tech., Vol.47, No.12, Dec. 1999, pp.2562-2567.

[8] N. Kaneda, W. Deal, Y. Qian, R. Waterhouse and T. Itoh, "A Broad- band Planar Quasi-Yagi antenna", IEEE Trans. Antennas Propag., Vol. 50, No.8, Aug.2002, pp.1158-1160.

[9] J. Kooi *et al.,* "A Full-Height Waveguide to Thin-film Microstrip Tran- Sition with Exceptional RF Bandwidth And Coupling Efficiency", Int. J. Infrared Millim. Waves, Vol.24, No.3, 2003, pp. 261-284.

[10] V.Kavitha, V.Palanisamy, "New Burst Assembly and Scheduling T technique for Optical Burst Switching Networks", Journal of Computer Science, Vol. 9, Issue 8, 2013, pp.1030-1040.

[11] Y. Liu, *et al*., "Some Recent Developments of Microstrip Antenna", Int.J.Antennas Propag., Vol.2012, Article ID 428284, pp.1-10, 428-284.

[12] A. Lymberis and A. Dittmar, "Advanced Wearable Health Systems And Applications Research And Development Efforts", IEEE Eng. Med. Biol. Mag., Vol. 26, No.3, 2007, pp. 29-33.

[13] S.Palanivel Rajan, "Review and Investigations on Future Research Directions of Mobile Based Tele care System for Cardiac Surveillance", Journal of Applied Research and Technology, Vol.13, No.4, 2015, pp.454-460.

[14] S.Palanivel Rajan, K.Sheik Davood, "Performance Evaluation on Automatic Follicles Detection in the Ovary", International Journal of Applied Engineering Research, Vol.10, No.55, 2015, pp.1-5.

[15] S.Palanivel Rajan, M.Paranthaman, Dr.C.Vivek, "Design and Enhancement of Wideband Reconfigurability using Two E-Shaped Patch Antenna", Asian Journal of Research in Social Sciences and Humanities, ISSN : 2249-7315, Vol.6, No.9, 2016, pp. 317-327.

[16] R. Paradiso, G. Lorigavol, "A Wearable Healthcare System Based on Knitted Integrated Sensors", IEEE Trans. Inf. Tech. Biomed, 2005, pp.337-344.

[17] K. Sundaravadivu and S. Bharathi, "STBC Codes for Generalized Spatial Modulation in MIMO Systems", IEEE International Conference ON Emerging Trends in Computing, Communication and Nanotechnology (ICECCN), Tirunelveli, 2013, pp.486-490.

[18] B. K. Tan, G. Yassin, P. Grimes, and K. Jacobs, "650 GHz SIS Mixer Fabricated on Silicon-on-Insulator Substrate", Electron. Lett., Vol.49, No. 20, Sep. 2013, pp.1273-1275.

[19] B. K. Tan, G. Yassin, S. Withington and D. Goldie, "Broadband Planar Yagi Antenna for Millimetre & Sub- millimetre Detectors", in Proc. 6th UCMMT, Sep. 2013, pp. 1-2.

[20] C.Vivek, S.Palanivel Rajan, "Z-TCAM : An Efficient Memory Architecture Based TCAM", Asian Journal of Information Technology, Vol.15, No.3, 2016, pp.448-454.

[21] S. Withington *et al.*, "A 350 GHz Radial-probe SIS Mixer for Astronom-ical Imaging Arrays", Int. J. Infrared Millim. Waves, Vol.22, No.9, 2001, pp. 1305-1312.

[22] G. Zheng, A. Kishk, A. Glisson and A. Yakovlev, "Simplified Feed for Modified Printed Yagi Antenna", Electron. Lett., Vol. 40, No.8, 2004, pp. 464-466.

[23] J. Zmuidzinas and P. L. Richards, "Superconducting Detectors and Mixers for Millimeter and Submillimeter Astrophysics," Proc. IEEE, Vol. 92, No.10, Oct. 2004, pp. 1597-1616.

An efficient Compression Technique for Image Multiplication

N. Savithaa, C.S. Manikandababu and G.G. Renuga Devi
Sri Ramakrishna Engineering College, Coimbatore - 641 022, Tamil Nadu

Abstract

Data compression is a widely used technique in digital signal processing applications such as multimedia and image processing to deliver the information/data in a compact size. Approximate computing is an interesting concept in arithmetic designs. While dealing with these application, the most important aspect to be considered is power,area and delay reduction. This paper deals withthe design of four different compression schemes that are analyzed for a 8X8 Dadda multiplier and its application on image processing where pixel by pixel multiplication is been carried out. The result shows that there is a significant reduction in power,area and delay when compared to the existing design;also two of the proposed designs show excellent capabilities for image multiplication in terms of Peak Signal to Noise Ratio(PSNR).

Keywords: *Approximate design, Dadda Multiplier, Image Blending, Peak-to-Signal Noise Ratio(PSNR), 4:2 Compressor*

1. INTRODUCTION

The digital logic circuits which operate with high degree of reliability and precision are used to implement many arithmetic applications. Several image and video processing algorithms are implemented by these digital circuits and for human visibility it seems to be accurate though it remains numerically approximate. The numerical accuracy relaxation provides some freedom to carry out approximate computation. This idea provides low-power designs with less area and delay in different abstraction levels. Approximate and probabilistic adders determined by its figure of merit for inexact computing are been compared using several adders and new metrics by Liang *et al*.[10].

Error Distance (ED) is a parameter in image processing which is described as the difference between the actual output and an error output for a given input [10]. Peak Signal-To-Noise Ratio often abbreviated PSNR is used to determine the quality of reconstruction of lossy compression codecs (e.g., for image compression).PSNR is an approximation to human perception of reconstruction quality and easily defined via the Mean Squared Error (MSE).

This paper is organized as follows: Chapter 2 explains the survey of different multipliers in existence. Chapter 3 gives the detailed description of exact 4:2 compressors.Chapter 4 presents the proposed approximate 4:2 compressors. Chapter 5 deals with the implementation of approximate compressors in Dadda multiplier.

In Chapter 6, results and discussions are clearly manifested. Chapter 7 infers the application of multipliers on Image processing. Finally, Chapter 8 concludes the paper.

2.SURVEY OF DIFFERENT MULTIPLIERS

Multiplication plays a major role in digital signal processing. In fact it is the most commonly used operation in various processes.Parallel multipliers are a high speed multiplier which requires high area implementation. Therefore it is not an effective multiplication method.On the other hand,Truncated multiplier multiplies the data by adding the most significant columnsof the multiplication matrix,along with a correction constant term[11].It achieves low area consumption of rounded output multipliers. Various signal processing algorithms and architectures are in need of low power designs for multimedia devices.

Fast multiplier design widely uses compressors in order to speed up the partial product reduction tree and to reduce the power dissipation[5].Optimized 4-2 compressors have been proposed in [3],[5],[6].In neural network applications, an imprecise array multiplier[10] has been used by omitting few of the least significant bits in the partial products(hence by removing some adders in the array).An approximate multi-bit adder cell is designed using imprecise or approximate full adder

with reduced circuit complexity at transistor level. It produces17 incorrect results out of 32 states and thus it becomes inefficient.

3. EXACT 4:2 COMPRESSOR DESIGN

In the multiplication process, compressors are normally used to serve two major purposes, (i)to speed up the operation (ii)to reduce the number of stages in the partial product generation. The main goal of this exact compressor is to provide an accurate output but with high power consumption, area and delay. Basically 4:2 compressor came into existence to replace the usage of more number of full adders.The general block diagram of 4:2 compressor is shown in Fig.1. It consists of X1,X2,X3,X4 as 4 inputs with a carry in(Cin) and sum,carry as outputs with a carry out(Cout) for propagation.

$$Sum = x1 \oplus x2 \oplus x3 \oplus x4 \oplus Cin \quad (1)$$
$$Cout = (x1 \oplus x2)x3 + \overline{(x1 \oplus x2)}x1 \quad (2)$$
$$Carry = (x1 \oplus x2 \oplus x3 \oplus x4)Cin + \overline{(x1 \oplus x2 \oplus x3 \oplus x4)}x4 \quad (3)$$

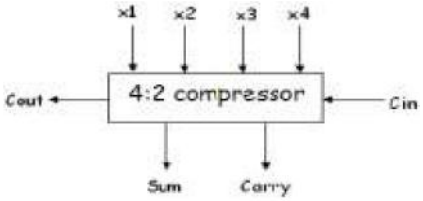

Fig.1 Block Diagram of 4:2 compressor

The carry out (Cout) is a one bit binary number with higher significance whereas the four inputs and sum output carry the same weight. Since the carry in (Cin) bit acts as one of the inputs to the compressor, it will have lower significance while the output Carry out (Cout) comes with higher significance. There are two types of implementation for the exact compressor as follows:

(i)Using two Full Adders (FA).

(ii)Using XOR-XNOR module with a multiplexer.

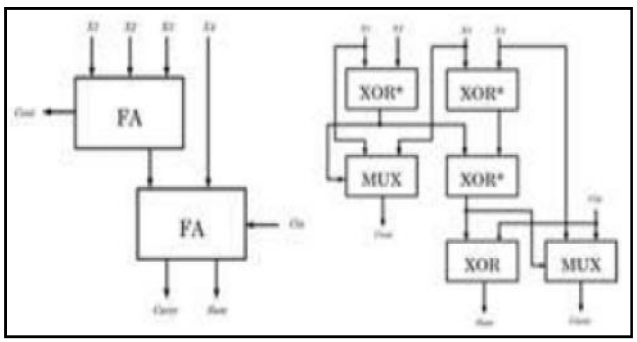

Fig. 2 Compressor using two full adders and XOR-XNOR module

The first method is implemented by a series of two full adders is shown in figure 2. Each will possess 3 inputs and 2 outputs. The Carry of first FA will be propagated to the next FA as Cin and thus producing Sum and carry as final outputs. The second method XOR-XNOR denoted by XOR* produces XOR and XNOR signals simultaneously which is shown in figure 2 as well. The multiplexer will have a select line with which the input signals are chosen for output.

4. APPROXIMATE 4:2 COMPRESSORS

In this section, two approximate compressor designs are proposed. There were ample methods that could be substituted for approximation but they are not efficient in terms of accuracy and optimization. In [9], an approximate full adder cell has been substituted in the place of an exact full adder cell but it produces at least 17 incorrect results out of 32 possible outputs, therefore the error rate is more than 53 percent (error rate is calculated by the ratio of erroneous outputs to the total number of outputs).Here, two designs are proposed to reduce these errors so as to improve the performance with respect to area, power and delay.

4.1 Design-1 Approximate Compressor

In an exact compressor, the output carry has the same value ofCin in 24 out of 32 states.While designing an approximate compressor, this feature must be considered.

$$Carry = Cin \quad (4)$$
$$Sum = \overline{Cin}(\overline{x1 \oplus x2} + \overline{x3 \oplus x4}) \quad (5)$$
$$Cout = \overline{\overline{x1x2} + \overline{x3x4}} \quad (6)$$

In Design 1, the carry is made equal to Cin by changing the value of other eight outputs.Since the output carry gains the higher weight of a binary bit, an error value of this signal will be producing a difference value of two in the output. The substantial difference may not be acceptable but it can be compensated /reduced by sum and Cout simplifications. This simplification of sum to a value of 0 in the second half of truth table reduces the difference between exact and approximate outputs as well as the design complexity.

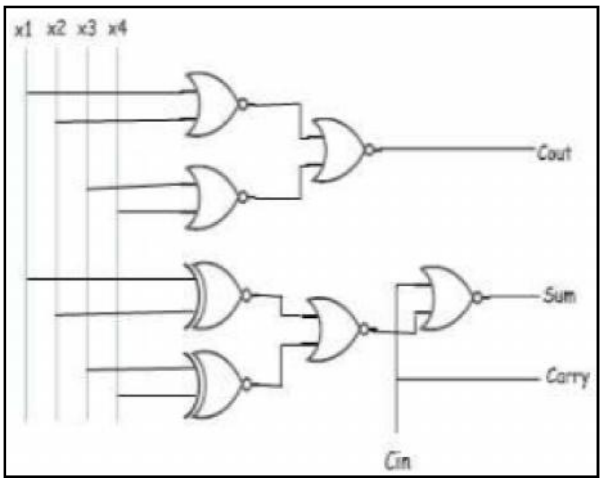

Fig.3 Logic Diagram of Design 1 Compressor

There occurs some errors on the sum signal which will result in the reduction in the overall delay of the design (critical path). This design contains 12 incorrect outputs out of 32 outputs (error rate =37.5%) which is less than the approximate full- adder cell.

4.2 Design-2 Approximate Compressor

Design 2 is proposed for two main reasons, to increase the performance and to reduce the error rate.The carry and Cout outputs have the same weight; therefore the equations for the carry and Cout in the previous design can be interchanged. Cin and Cout can be ignored in the hardware design since they will be zero in all stages (i.e.,Cin is zero in the first stage).

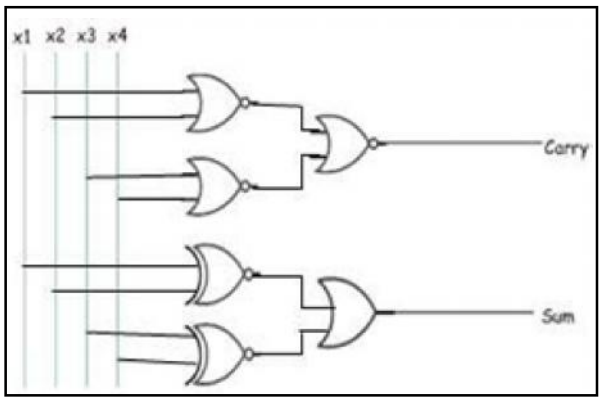

Fig.4 Logic Diagram of Design 2 compressor

This proposed design contains 4 incorrect outputs out of 16 outputs, so its error rate has been reduced to 25 percent. This seems to be a positive approach because the amount of imprecision found to be smaller than the existing schemes.

$$Sum = \overline{x1 \oplus x2} + \overline{x3 \oplus x4} \quad (7)$$

$$Carry = \overline{x1x2} + \overline{x3x4} \quad (8)$$

4.3 3:2 Compressor

The full adders are replaced by 3:2 compressor high speed and low power consumption. It consists of XOR gates and Multiplexer so as to minimize the number of logic gates, power and delay. The functionality remains the same as the full adder but structurally different. The first two stages of multiplier uses3:2 compressor for effective performance.

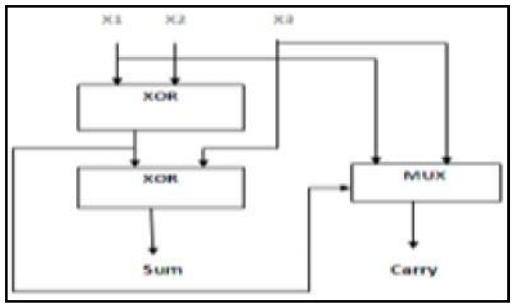

Fig 5 : Block Diagram of 3:2 Compressor

5.MULTIPLICATION

In this section, the implementation of proposed compressors on multiplier is analyzed. An exact multiplier with high speed is composed of three modules.

(i)Partial Product Generation.
(ii)A Carry Save Adder (CSA) tree for the reduction of partial products.
(iii)A Carry Propagation Adder (CPA) for final computation of result.

In a multiplier design, the second module plays a major role with respect to delay, power consumption and circuit complexity. Compressors are usually used to increase the speed of the CSA tree and decrease its power dissipation in order to achieve low-power operation.These approximate compressors lead to the design of approximate multipliers.

An unsigned 8*8 Dadda tree multiplier is chosen for the usage of proposed compressors in multipliers. Figure 6 illustrates the reduction circuit of an exact multiplier where two half-adders, two 3:2 compressors (instead of full adders) and eight 4:2 compressors are utilized in the first stage to reduce the partial products to at most four rows. In the very next stage, one half-adder, one 3:2 compressor and ten compressors are

used to calculate the 2 final rows of partial products. Hence, 2 stages of reduction and 3 half adders, three 3:2 compressors and 18 compressors are needed in this reduction of 8x8 Dadda tree multiplier.

In this work, we considered four cases to design an approximate multiplier.

Case 1 – Multiplier 1 :

Design-1 4:2 compressors are used all over the stages (figure 6).Totally 3 half adders, three 3:2 compressors and 18 4:2 compressors are utilized.

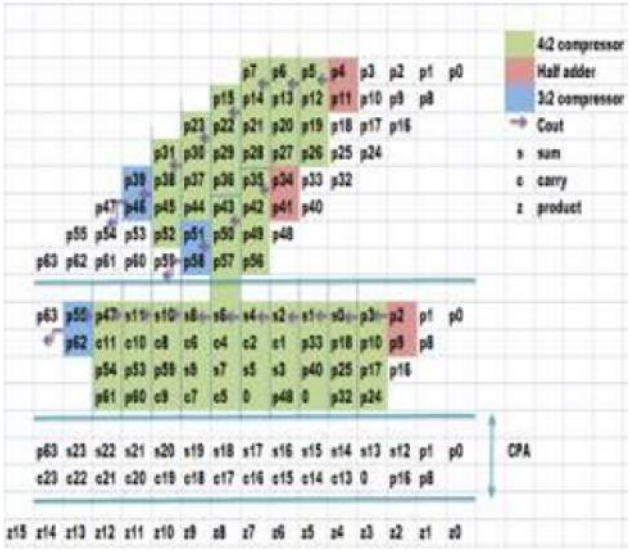

Fig.6 Dadda Multiplier usingDesign-1 compressor

Case 2 – Multiplier 2 :

Design-2 4:2 compressors are used. Less number of compressors are required for the reduction circuitry since Cin and Cout are absent (figure 7).This multiplier uses 6 half adders, one 3:2 compressor and 17 4:2 compressors.

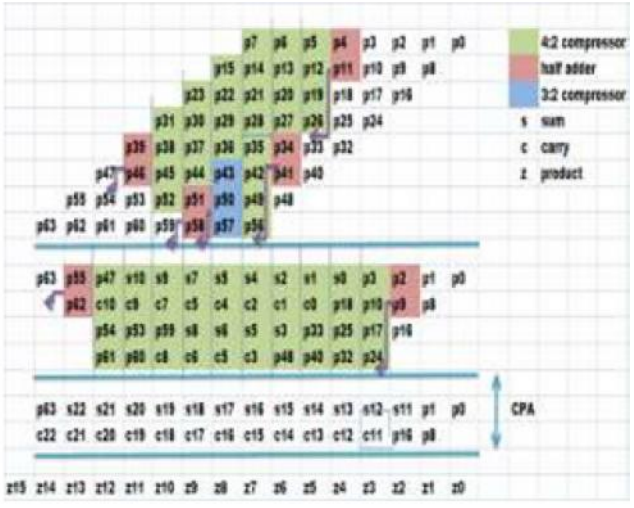

Fig 7 :Dadda Multiplier using Design-1 compressor

Case 3 – Multiplier 3 :

Two combinations are used in this case. The 'n' most significant columns in the reduction circuitry design uses exact 4:2 compressors and 'n-1' least significant columns uses Design-1 4:2 compressor. This in turn will improve the accuracy by reducing the error rate as shown in figure 8.

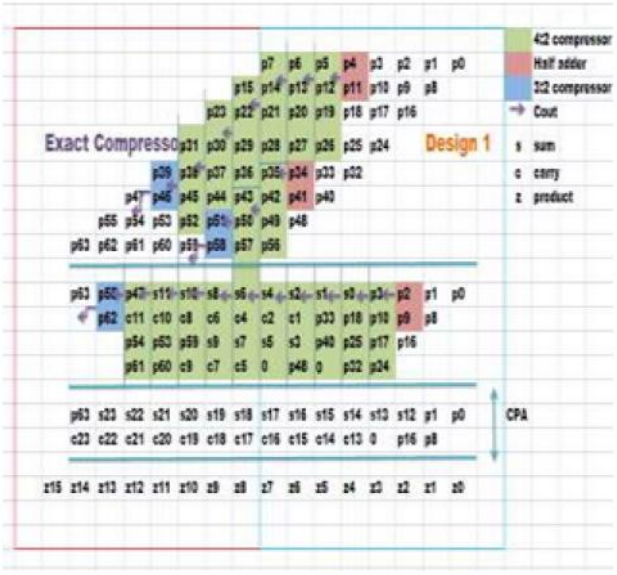

Fig.8 Dadda Multiplier using Exact and Design-1 Compressor

Case 4 – Multiplier 4 :

The 'n' most significant columns in the reduction circuitry design uses exact 4:2 compressors and 'n-1' least significant columns uses Design-2 4:2 compressor as shown in figure 9. This gives more appropriate solution when compared to the multiplier-3.

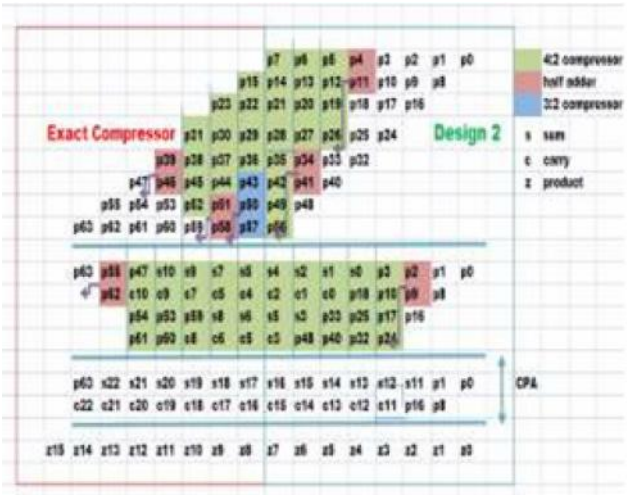

Fig.9 Dadda Multiplier using Exact and Design-2 Compressor

6. PERFORMANCE ANALYSIS

The performance analysis is done using CADENCE and XILINX ISE toolsto analyzethe efficiencyof the design on both ASIC and FPGA. It is found that Design-2 works more efficient in terms of power, delay and area than Design-1.For improved accuracy, Design-3 and Design-4 holds good with modest power, area consumption and delay.

7. ASIC IMPLEMENTATION

In the ASIC implementation power(nW),area(cell area) and delay(ps) parameters are analyzed for Exact, Design 1 and Design 2 compressors.

Table 1 Analysis using CADENCE

PARAMETERS	DESIGNS		
	Exact	Design-1	Design-2
Power (nW)	11847.548	2537.615	1949.708
Area (Cell area)	140	77	53
Delay (ps)	848	479	306

8. FPGA IMPLEMENTATION

In the FPGA implementation power(mW),area(Number of LUTs) and delay(ns) parameters are analyzed for 4 different multipliers.

Table 2 Analysis using Xilinx ISE

DESIGNS	PARAMETERS		
	Power (mW)	Area (No. of LUTs)	Delay(ns)
Exact Multiplier	59	136	20.468
Multiplier-1	52	127	18.251
Multiplier-2	47	125	19.757
Multiplier-3	59	133	19.329
Multiplier-4	56	133	20.218

9. APPLICATION : IMAGE PROCESSING

This proposed multipliers are applied on image processing to multiply two images on a pixel by pixel basis, therefore blending two images into a single image with high PSNR.The MATLAB tool is used here for image multiplication and for measuring the PSNR value.

The input images are shown in figure 10.

Fig.10 Input image 1 and image 2

The resulting output images for Multiplier 1, Multiplier 2, Multiplier 3 and Multiplier 4 is shown in figure 11.Multiplier 3 and 4 have good PSNR value compared to multiplier 1 and 2.

Fig.11 Output images of 4 multipliers

Table 3 infer the PSNR values of four different multipliers using approximate compression techniques.

Table 3 PSNR Values of 4 Different Multipliers

PSNR	Multi--plier 1	Multi--plier 2	Multi--plier 3	Multi--plier 4
	23.163	26.601	45.542	49.400

10. CONCLUSION

Thus the proposed approximate compressors with an implementation on Dadda multiplier has been discussed with its application on Image processing. The first and second multipliers have significant reduction on delay, area and power. The third and fourth multipliers have modest reduction with best accuracy. This proposed multipliers when applied on image processing to multiply two imageson a pixel by pixel basis, therefore blending two images into a single image results in high Peak-to-Signal Noise Ratio(PSNR) value i.e.,output image with good quality.

REFERENCES

[1] A. Ahmadi, S.M.Fakhraie, C.Lucas and H.R. Mahdiani, "Bioinspiredimprecise Computational Blocks for Efficient VLSI implementation of soft-computing applications", IEEE Trans. Circuits Syst. I: Reg. Papers, Vol. 57, No.4, 2010, pp. 850-862.

[2] B.E.S. Akgul, L.N. Chakrapani, S. Cheemalavagu, P. Korkmaz, P.K.V. Palem, "A Probabilistic CMOS Switch and its Realization by Exploiting Noise", Presented at the IFIP Int. Conf. Very Large Scale Integ., Perth, Australia, 2005.

[3] M. Aktan, D. Baran and V.G.Oklobdzija, "Energy Efficient Implementation of Parallel CMOS Multipliers with Improved Compressors", in Proc. ACM/IEEE 16th Int. Symp. Low Power Electron. Design, 2010, pp.147-152.

[4] S. Al-Sarawi, D.Kelly and B. Phillips, "Approximate Signed Binary Integer Multipliers for Arithmetic Data Value Speculation", in Proc.Conf. Design Architect. Signal Image Process, 2009, pp. 97-104.

[5] C. Chang, J.Gu and M. Zhang, "Ultra Low-voltage Low- power CMOS 4-2 and 5-2 Compressors for Fast Arithmetic Circuits", IEEE Trans. Circuits Syst., Vol. 51, No.10, 2004, pp.1985-1997.

[6] C. Chang, J.Hand Gu, "Ultra Low-voltage Low-power 4-2 Compressor for High Speed Multiplications", in Proc. 36th IEEE Int. Symp. Circuits Syst., Bangkok, Thailand, 2003, pp.v-321-v-324.

[7] M.D. Ercegovac, P.Gupta and P. Kulkarni, "Trading Accuracy for Power in a Multiplier Architecture", J. Low Power Electron., Vol.7, No.4, 2011, pp.490-501.

[8] S. Guan, T. Jeong, T. Krilavicius, J.Ma and K. Man "Implementation of High Performance Multipliers Based On Approximate Compressor Design", Presented at the Int. Conf. Electrical and Control Technologies, Kaunas, Lithuania, 2011.

[9] V. Gupta, D. Mohapatra, S.P.Park, A. Raghunathan and K. Roy, "IMPACT: IMPrecise Adders for Low-Power Approximate Computing", in Proc. Int. Symp. Low Power Electron. Design, 2011, pp.409-414.

[10] J. Han, J.Liang and F. Lombardi, "New Metrics for the Reliability of Approximate and Probabilistic Adders", IEEE Trans. Computers, Vol.63, No.9,2013, pp. 1760-1771.

[11] M.J. Schulte and E.E.SwartzlanderJr, "Truncated Multiplication with Correction Constant", in Proc. Workshop VLSI Signal Process.VI, 1993, pp. 388-396.

Measurement and Detection of Cisterna Magna in Fetal Brain based on LMS Method

V. Praveen Kumar and S. Deepak
Department of Electronics and Communication Engineering
K. S. R Institute for Engineering and Technology, Tiruchengode - 637 215, Tamil Nadu

Abstract

The Cisterna magna (CM) width reference ranges were constructed based on the measurements obtained from 80 healthy fetuses with normal postnatal outcome undergoing routine first-trimester ultrasound at 11–13 weeks, using the Lambda-Mu-Sigma method. CM was measured in the fetal midsagittal view, as routinely used for nuchal translucency assessment. A mixture model grouping algorithm is presented for robust ultra sound image segmentation in the presence of partial volume averaging. The method uses additional classes to represent Estimating tissue class parameters volume voxels of mixed tissue type in the data with their probability distributions modelled accordingly. The image model also allows for tissue-dependent variance values and voxel neighbourhood information is taken into account in the clustering formulation. The final result is the estimated fractional amount of each tissue type present within a voxel in addition to the label assigned to the voxel.

1. INTRODUCTION

Most posterior fossa anomalies are detected after visualization of an abnormally sized posterior fossa, which can be either enlarged or reduced [1]. Dandy–Walker malformation, Blake's pouch cyst, mega cisterna magna and posterior fossa arachnoid cysts frequently present with an enlarged posterior fossa, while Joubert's syndrome, cerebellar atrophy and Chiari malformation typically present with a reduced cisterna magna (CM) [2].

During the second-trimester anomaly scan, the CM is one of the structures routinely assessed together with the cerebellum [1–3]. In recent years, the diagnosis of many fetal structural anomalies has been made in the first trimester [4, 5], and since 2009 some groups have described intracranial markers of open spina bifida at 11–13 weeks 6–11. In 2010

Chaoui and Nicolaides [8] suggested the size of the fourth ventricle in a sagittal view of the fetal head, the 'intracranial translucency', as an early marker for spina bifida. More recently their group suggested the ratio of brain stem diameter to brain-stem-to-occipitalbone distance (BS/BSOB) as a better marker [10]. First-trimester reference ranges for the posterior fossa structures have been reported recently by two groups. Egle et al. [12] constructed reference ranges for transcerebellar diameter and the anteroposterior diameter of the CMand of the fourth ventricle in axial views using transabdominal sonography. In contrast, Papastefanou et al.[13] used a mid- sagittal view, the same one adopted by Lachmann et al.[10] to describe the BS/BSOB ratio, to establish their CM reference ranges. For practical reasons, the midsagittal view is preferable, given that this is the plane routinely used for nuchal translucency measurement and because the midbrain has become a landmark to define the correct mid-sagittal view. Surprisingly, there are substantial differences between these two reference ranges for CM diameter

The use of ultrasound imaging has resulted in the assessment of fetal structures along with various developed organs. In the past, gestational age has been established by a combination of the historical information and physical examination. Predictions were passed based on the menstrual history index, maternal sensation of fetal movement, assessment of uterine size by bi-manual examination in the first trimester, the initial detection of fetal heart tones by Doppler and uterine fundal height measurement. [1-6] Even in the best known cases it is reported that the menstrual history index and fundal height measurement techniques have been resulted in error [7]. With the known date of conception, the Timed Ovulation and in vitro fertilization the gestational age is expected to calculate accurately. But in most cases the date of ovulation or conception cannot be estimated accurately which ultimately results in calculating the gestational age using other methods [8-22].

2. FETAL CISTERNA MAGNA METHODS

A prospective cross-sectional study between March 2010 and February 2011, involving 69 normal pregnant women between 18 and 24 weeks was performed. This study was approved by the Research Ethics Committee of the Irmandade da Santa Casa de Miseric ordia de Sao Paulo, Brazil, and the patients who agreed to participate signed a term of consent.

This study was carried out at the Department of Obstetrics and Gynecology, Faculty of Medical Sciences of Santa Casa of S˜ao Paulo (FCMSCSP). The patients were randomly selected, and all evaluation made by a single examiner (FSBB), with five years experience in obstetric ultrasound. The examinations were performed on a SonoAce X8 (SamsungMedison, Seoul, Korea) device equipped with multifrequency volumetric convex transducer (3–7 MHz). The criteria for inclusion were (1) unique pregnancy with live fetus and (2) gestational age evaluated by last menstrual period and confirmed by ultrasound performed until the 14th week (crown-rump length-CRL: 4–84 mm). Exclusion criteria were (1) pregnant women carrying fetuses with structural anomalies detected at the time of the examination and (2) pregnant women carrying chronic diseases that would interfere with fetal growth.

Initially, a realtime 2D evaluation was performed in order to evaluate the biometry, morphology, and quantification of amniotic fluid volume. For the 2D measurement of transverse cerebellar and anterior-posterior cisterna magna diameter, it was performed a modified transversal slice of the fetal head slightly angled, through the thalamus, cerebellar hemispheres, cisterna magna, cave of septum pellucidum, the occipital bone, and nuchal fold. An insonation angle of the occipital bone was chosen, taking care that it was focused on an angle of 30æ%. It was performed a single measurement of transverse cerebellar and anteroposterior of the fetal cisterna magna diameter in each mother, and this image is saved in the memory of the device. The three-dimensional volume acquisition was performed on the same.

2D plane in which was performed the measurements of the transverse cerebellar diameter and anterior-posterior cisterna magna, to encompass the entire fetal skull (ROI-region of interest) (Figure 2(a)). In order to standardize all 3D measurements, the following preset was used on the device: scanning—3D static; display mode—three-dimensional extended imaging (multislice view); scanning speed—slow; angle scanning—70º%; overall gain of the device—50%. After the three-dimensional scanning, the image was displayed in the multiplanar mode (axial, sagittal, and coronal) (Figure 2(b)). The volumes were saved in the device memory and then stored on compact discs (CDs) and transferred to a personal computer. The analyses were performed offline in the same apparatus in a time period of 30 to 120 days after the volumetric capture.

3. RESEARCH CONTRIBUTION

Automatic detection and measurement of cisterna magna in fetal brain. In the LMS method, LMS parameters are estimated from the data, smoothed, and then used to create the desired percentiles. The lambda-mu-sigma (LMS) method calculates the lower limit of normal for Spiro metric values as the percentile of the distribution of scores. The cistern magna observations are features computed from LMS method neighborhoods surrounding the objects. In our algorithm, the order is selected such that the uncertainty of the detections is minimized.The analyses were performed offline in the same apparatus in a time period of 30 to 120 days after the volumetric capture.

4. METHODOLOGY

This was a retrospective study. CM width reference ranges were constructed based on the measurements obtained from 80 healthy fetuses with normal postnatal outcome undergoing routine first-trimester ultrasound at 11-13 weeks, using the Lambda-Mu-Sigma method. CM was measured in the fetal mid-sagittal view, as routinely used for nuchal translucency assessment. In addition, first-trimester ultrasound images in 11 fetuses with open spina bifida or posterior fossa anomalies, most of which were diagnosed later in pregnancy, were retrospectively reviewed, and CM measurements were compared against reference ranges. It have an good results in the automatic segmentation.

4.1. Block Diagram

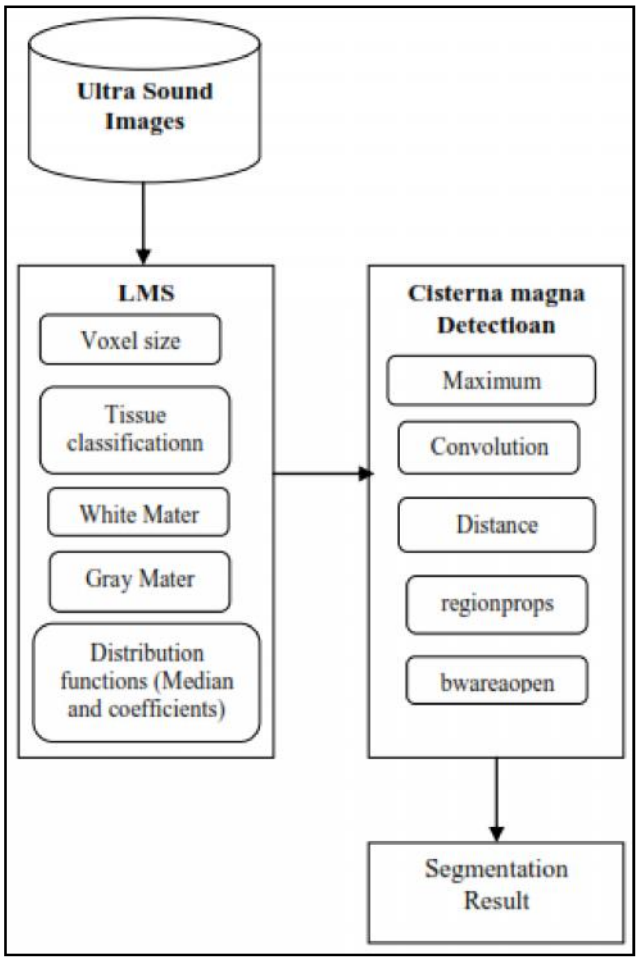

Fig.1 Block Diagram of Proposed Work

4.2 Lambda-Mu-Sigma Method

The LMS method summarizes the changing distribution by three curves representing the skewness expressed as a Box– Cox power (L), the median (M) and coefficient of variation (S).The resulting L-, M- and S-curves contain the information needed to draw any percentile curve. Degrees of freedom for each curve (L, M and S) were selected according to changes in the model deviance. In the LMS method, LMS parameters are estimated from the data, smoothed, and then used to create the desired percentiles. The lambda-mu-sigma (LMS) method calculates the lower limit of normal for Spiro metric values as the percentile of the distribution of scores. Only 10 principal components to represent the changes of shape since they captured 90 % of the total variation.

Grey Matter :Grey matter (or gray matter) is a major component of the central nervous system, consisting of neuronal cell bodies, neuropil (dendrites and unmyelinated axons), glial cells (astroglia and oligodendrocytes), and capillaries . Grey matter is distributed at the surface of the cerebral hemisphere's cerebellum, as well as in the depths of the cerebrum, cerebellar, brainstem, and spinal grey matter. In living tissue, grey matter actually has a grey-brown color, which comes from capillary blood vessels and neuronal cell bodies. Grey matter includes regions of the brain involved in muscle control, sensory perception, such as seeing and hearing; memory, emotions, and speech.

White Matter : A second major component of the central nervous system is white matter and it is composed of bundles of myelinated axons that connect various grey matter regions of the nervous system to each other and carry nerve impulses between neurons . White matter only contains the axons of the nerve cells, and not the cell bodies, which are found in grey matter. Myelin is a lipid that forms a thin layer, known as the myelin sheath, around the axons of white matter neurons acts as an electrical insulator, increasing the transmission speed of nerve signals by allowing the signal to jump down the axon. Myelin also gives white matter its characteristic color. At the age of 20, the total length of myelinated fibers in the body, if places end to end, is 176,000 km (109.4 miles) in males and is 149,000 km (92.6 miles) in females.

4.3 Cistrena Magna Detcetion

The cistern magna observations are features computed from LMS method neighbourhoods surrounding the objects. The likelihood (probability) of a hypothesized state that gives rise to observations is based on a deterministic model learned using a large annotated database of images. The transition model that describes the way the poses of objects are related is Gaussian filter. Employing the sequential sampling model allows us to use fewer samples of the object pose and formally extend this class of algorithms to multiple objects. In our algorithm, the order is selected such that the uncertainty of the detections is minimized. The fetal cisterna magna increases in size throughout pregnancy. The sample from fetuses with trisomy 18 was different and had a higher rate of small and large cisterna magna.

The cisterna may be so large that it extends laterally, posteriorly and superiorly far beyond the normal anatomic limits of the cisterna magna. The cisterna may also extend superiorly through a posterior dehiscence of the tentorium cerebelli .In this condition, borderline

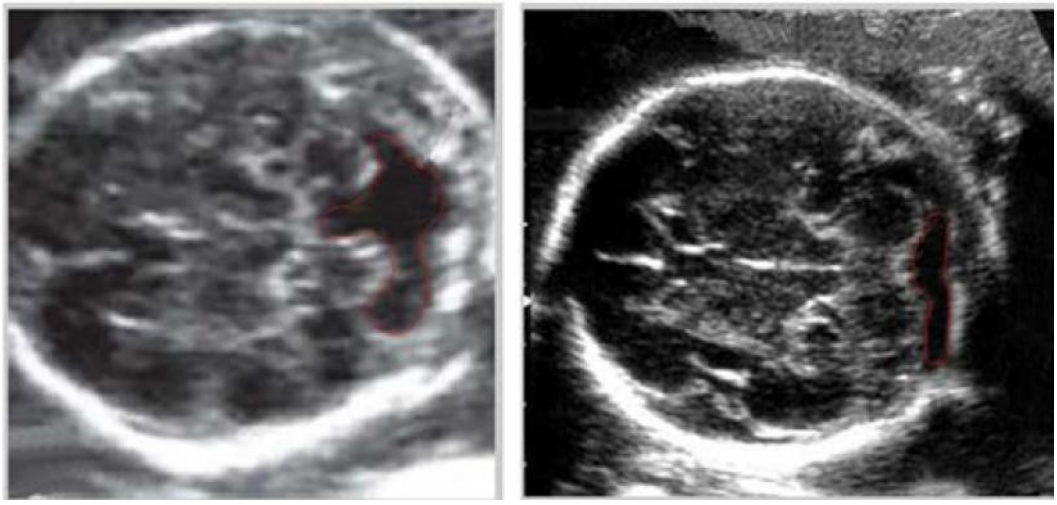

Fig.2 Automatic Detection Of Normal And Abnormal Images Of Citerna Magna

to overt ventriculomegaly and other neural/extra neural defects are generally present. Distinction between LMS variant and mega- cisterna magna in the fetus is difficult as definitive criteria have not been firmly established. The former condition should be suspected when a thin communication is found between the fourth ventricle and the cisterna magna, the latter when the cisterna magna has a depth greater than 10 mm.

5. DISCUSSIONS

The variation in size of the cisterna magna may be due to challenges in accurately measuring the cisterna magna in the third trimester. The cisterna magna is usually measured in an anteroposterior fashion from the posterior aspect of the cerebellar vermis to the inner edge of the occipital bone. Measurements of the cisterna magna should be performed at a level that includes visualization of the cavum septum pellucidum, cerebral peduncles, and cerebellar hemispheres.15 However, Laing et al16 established that if the transducer is angled in a semicoronal plane, the cisterna magna could appear falsely enlarged in approximately 40% of cases. Of the cases in which a pseudoenlarged cisterna magna was created in a semicoronal plane, approximately 70% occurred in the third trimester. Therefore, the smallest anteroposterior diameter in the axial plane from the cerebellar vermis to the inner edge of the occipital bone should be obtained, and in suspected abnormal cases, the cisterna magna should be measured in the midsagittal plane.

6. CONCLUSION

The proposed system constructed reference ranges for CM width at 11–13 weeks' gestation using midttal ultrasound images. It appears that first-trimester CM width can be used as a marker for the early detection of open spina bifida. However, our findings need to be confirmed in large prospective series.In our work presented an algorithm for Lambda-Mu-Sigma method partial volume segmentation of ultrasound images. Experimental results are comparable or superior to other published algorithms. Our method is an extension of a probabilistic grouping algorithm, to accommodate partial volume voxels and to allow class- dependent model values for the intensity variance. Although the convergence properties of the original technique are generally unknown, we have observed robust performance from our implementation as a function of the estimates used to initialize the class parameters. In the phase II work, the weighting function was augmented to favor spatially contiguous regions in the segmentation but other possibilities are being examined, including the use of prior anatomic information.

REFERENCES

[1] International Society of Ultrasound in Obstetrics&Gynecology Education Committee. Sonographic Examination of the Fetal Central Nervous System: Guidelines for Performing the 'Basic Examination' and the "Fetal Neurosonogram", Ultrasound Obstet Gynecol, Vol.29, 2007, pp.109–116.

[2] K. Shekdar, "Posterior Fossa Malformations. ", Semin Ultrasound CT MR, Vol.32, 2011, pp.228-241.

[3] S. Ni Scanaill, P. Crowley, M.Hogan and B.Stuart, "Abnormal Prenatal Sonographic Findings in the Posterior Cranial Fossa: A Case of Joubert's Syndrome", Ultrasound Obstet Gynecol, Vol.31, 1999, pp.71-74.

[4] M. Grande, M. Arigita, V.Borobio, JM.Jimenez, S, Fernandez and A. Borrell, "First-trimester Detection of Structural Abnormalities and the Role of Aneuploidy Markers", Ultrasound Obstet Gynecol, Vol.39, 2012, pp.157-163.

[5] V. Chalana, TC. Winter III, DR Cyr, DR. Haynor, K.Yongmin, "Automatic Fetal Head Measurements from Sonographicimages", Acad Radiol, Vol. 3, No.8, 1996, pp.628-635.

[5] A. Syngelaki, T.Chelemen, T.Dagklis, L.Allan, KH. Nicolaides, "Challenges in the Diagnosis of Fetal Non-chromosomal Abnormalities at 11–13 Weeks", Prenat Diagn, Vol.31, 2011, pp.90-102.

[6] R. Chaoui, B.Benoit, KS. Heling, KO. Kagan, V. Pietzsch, A. Sarut Lopez, I.Tekesin, K.Karl, " Prospective Prospective Detection Of Open Spina Bifida at 11–13 Weeks by Assessing Intracranial Translucency and Posterior Brain", Ultrasound Obstet Gynecol, Vol.38, 2011, pp.722-726.

[7] R. Chaoui, B.Benoit, H.Mitkowska-Wozniak, KS. Heling, KH. Nicolaides, "Assessment of Intracranial Translucency (IT) In the Detection of Spina Bifida at the 11–13- Week Scan", Ultrasound Obstet Gynecol, Vol.34, 2009, pp.249-252.

[8] R. Chaoui, KH.Nicolaides, "From Nuchal Translucency to Intracranial Translucency: Towards the Early Detection of Spina Bifida", Ultrasound Obstet Gynecol 2010; 35: 133–138.

[9] M. Finn, D. Sutton, S.Atkinson, K. Ransome, P. Sujenthiran, V.Ditcham, P.Wakefield, S.Meagher, " The Aqueduct of Sylvius: A Sonographic Landmark for Neural Tube Defects in the First Trimester", Ultrasound Obstet Gynecol 2011; 38:640–645.

[10] R. Lachmann, R.Chaoui, J. Moratalla, G. Picciarelli, KH. Nicolaides, "Posterior Brain in Fetuses with Open Spina Bifida at 11 to 13 weeks", Prenat Diagn, Vol.31, 2011, pp.103-106.

[11] M. Scheier, R.Lachmann, M. Petro's, KH. Nicolaides, "Threedimensional Sonography of the Posterior Fossa in Fetuses with Open Spina Bifida at 11–13 weeks' Gestation", Ultrasound Obstet Gynecol, Vol.38, 2011, pp.625-629.

[12] D. Egle, I.Strobl, V.Weiskopf-Schwendinger, E. Grubinger, F. Kraxner, IS. Mutz-Dehbalaie, A. Strasak, M. Scheier, "Appearance of the Fetal Posterior Fossa at 11+3 to 13+6 Gestational Weeks On Tran abdominal Ultrasound Examination"..

[13] I. Papastefanou, AP.Souka, A.Pilalis, P. Panagopoulos, D. Kassanos, "Fetal Intracranial Translucency And Cisterna Magna At 11 To 14 Weeks: Reference Ranges And Correlation With Chromosomal Abnormalities", Prenat Diagn, Vol.31, 2011, pp.1189-1192.

[14] PE. Shrout, JL.Fleiss, "Intraclass Correlations: Uses In Assessing Rater Reliability", Psychol Bull Vol.86, No.2, 1979, pp.420-428.

[15] "Fetal Medicine Foundation", www.fetalmedicine.com/fmf/online-education/01-11-136-week-scan.

[16] KW, Fong, A. Toi, N.Okun, E.Al-Shami and RJ . Menezes, "Retrospective Review of Diagnostic Performance of Intracranial Translucency in Detection of Open Spina Bifida at the 11–13-Week Scan", Ultrasound Obstet Gynecol, Vol.38, 2011, pp.630-634.

[17] R. Mangione, N.Lelong, M.Fontanges, S.Amat, J. Rosenblatt, B. Khoshnood, JM. Jouannic, " Visualization of Intracranial Translucency At The 11-13-Week Scan Is Improved After Specific Training", Ultrasound Obstet Gynecol, Vol.38, 2011, pp.635-639.

[18] NI. Weisenfeld and SK.Warfield, "Automatic Segmentation of Newborn Brain Ultrasound", Neuroimage, Vol.47, No.2, 2009, pp.564-572.

Fault Diagnosis of Three Phase Induction Motors by Using Kernal Based SVM Classifiers

R. Senthil Kumar and K. Sarasvathi
Department of Electrical and Electronics Engineering
M.Kumarasamy College of Engineering, Karur - 639 113, Tamil Nadu
E-mail: Senthilme90@gmail.com, sarasvathik.eee@mkce.ac.in

Abstract

Effective utilization of Induction Motor plays a vital role in industry environments. In order to reach this effective process, it has to stand with various types of faults which is rising from rugged environment. In this paper, unique performance of Squirrel cage induction is taken which is robustness, reduced size and low cost. When fault occurs, adjustable drive techniques should be tolerated to these faults. For this purpose, early detection of fault and its diagnosis progress should be applied to the drive techniques. Rotor fault, fault in short circuit winding, fault in air gap eccentricity, load fault are the various faults in this drive. To detect the fault in induction motor On-line condition monitoring is widely used. Here Initially normal operating condition of induction motor model is developed after that, various faults are analyzed. The simulation model of the setup is developed and the system performance is analysed afer the injection of fault in sequential order. The classifier used here is Support Vector Machine (SVM) which requires kernel function for non linear characteristics for obtaining the best results. For that here various kernel based functions are convolved with SVM which results in detection of faults at an accuracy of 91.4% with reduced training samples. Here Kernal based SVM classifiers for three phase induction motor is simulated using MATLAB/SIMULINK software.

Keywords: *Fault Diagnosis, Induction motor drive, Kernal based SVM Classifiers*

1. INTRODUCTION

In industry induction motors are widely used because of its inherent ruggedness and minimized cost. Adjustable speed drives are mostly used in many industrial applications. For applications requiring a constant speed induction motor is used because of its conventional method of speed control have either exclusive or highly ineffective. In order to prevent sudden failure and economic damage periodic maintenance is performed[1]. From the equation obtained from arbitrary reference frame of symmetrical induction machine, the simulation of various modes of operation is suitably obtained [2]. Figure 1.,.[3] shows entire block diagram of induction motor drive. The mathematical calculations and algorithms are used in the control scheme and it needs capable and precious controllers.. Here a novel theory is introduced to recover the performance of the motor running in various points at optimum voltage at optimum frequency for optimum motor efficiency.

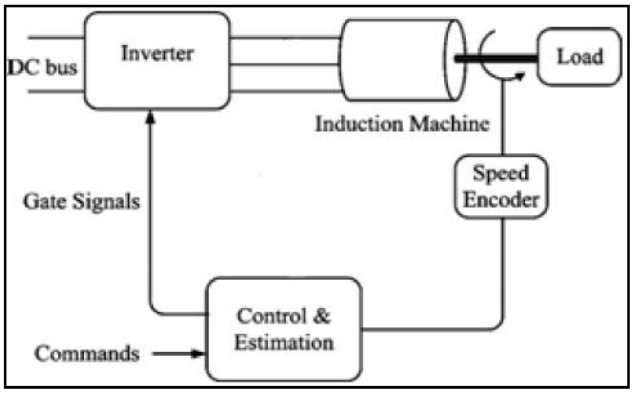

Fig.1 Typical Induction Motor Drive

To achieve the timely diagnostics of incipient IM faults the on-line IM diagnostic systems are being Developed. The detection of fault and the rotor fault analysis are critical so the a preventive fault diagnosis is important in industrial applications, while Faults in rotor share only about20% of the overall faults induction machine.

Most of the faults are occurred in induction motor like bearing fault effect(32-52%),stator winding fault (15-47%),rotor bar fault (5%),shaft fault (2%),external

disturbances are also produced 12-15%. Common rotor faults are break in rotor bars and the rotor to stator eccentricity. Due to short circuit of windings Stator faults are created. By monitoring the mechanical vibrations, current, reverse sequence pole and partial charges are measured for incipient fault detection[4].

To monitor the induction machine the spectral study of operational process parameters like temperature, pressure, stem flow etc.. are measured by the combination of advanced computerized data processing and acquisition intelligent techniques. The evaluation tools used are Time domain analysis, spectrum analysis, cestrum analysis. To resolve changes by trend setting, time domain analysis is used, to determine trends of frequencies spectrum analysis is used, to determine amplitude and phase relations, as well as to identify periodical Components of spectra cestrum analysisis used. In many situations, for incipient fault detection vibration monitoring methods are utilized. However, for stator current monitoring,[5] .

In this paper three phase induction motor dynamic model was developed and normal mode and faults modes are discussed. Then SVM classifiers are used to diagnosis the faults. Here Rotor fault, bearing fault, Eccentricity Faults are diagnosis by using kernel based SVM classifiers.

1.1 Dynamic Model of Induction Motor

The dynamic model in stationary reference frame with б-в reference frame variables of squirrel cage induction motor[SEIM] [6].

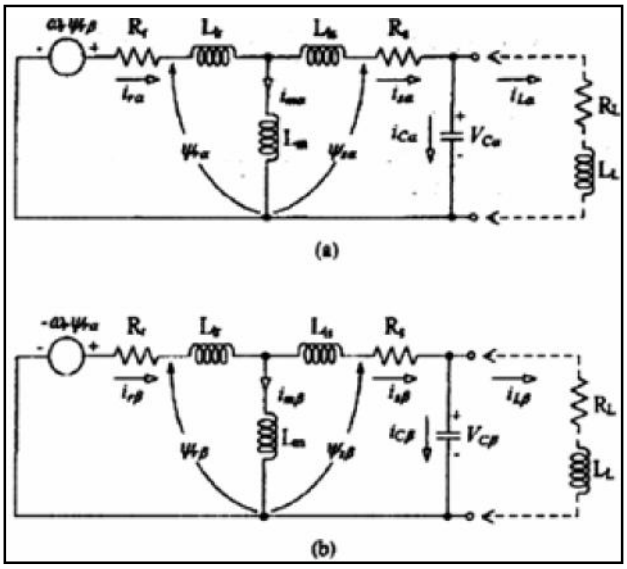

Fig.2 Equivalent Circuit of SCIM (a) á axis (b) â axis

From Figure 2, Components stator and rotor voltage of the induction motor can be expressed as follows:

$$V_{s\alpha} = R_s i_{s\alpha} + L_s \frac{d}{dt} i_{s\alpha} + L_m \frac{d}{dt} i_{r\alpha} \quad (1)$$

$$V_{s\beta} = R_s i_{s\beta} + L_s \frac{d}{dt} i_{s\beta} + L_m \frac{d}{dt} i_{r\beta} \quad (2)$$

$$0 = R_r i_{r\alpha} + L_r \frac{d}{dt} i_{r\alpha} + L_m \frac{d}{dt} i_{s\alpha} + \omega_r \Psi_{r\beta} \quad (3)$$

$$0 = R_r i_{r\beta} + L_r \frac{d}{dt} i_{r\beta} + L_m \frac{d}{dt} i_{s\beta} - \omega_r \Psi_{r\alpha} \quad (4)$$

The components of rotor flux linkage in the stationary reference can be written as

$$\Psi_{r\alpha} = L_m i_{s\alpha} + L_r i_{r\alpha} + \Psi_{r\alpha 0} \quad (5)$$

$$\Psi_{r\beta} = L_m i_{s\beta} + L_r i_{r\beta} + \Psi_{r\beta 0} \quad (6)$$

Where $\Psi_{r\alpha 0}$ and $\Psi_{r\beta 0}$ are the residual rotor flux linkages in α-β axis, respectively.

Then, ω_r electrical rotor speed ,the components of rotating voltage in the stationary reference frame are as the follows:

$$\omega_r \Psi_{r\alpha} = \omega_r L_m i_{s\alpha} + \omega_r L_r i_{s\alpha} + \omega_r \Psi_{r\alpha 0} \quad (7)$$

$$\omega_r \Psi_{r\beta} = \omega_r L_m i_{s\beta} + \omega_r L_r i_{s\beta} + \omega_r \Psi_{r\beta 0} \quad (8)$$

The expressions for capacitor voltages are,

$$V_{c\alpha} = \frac{1}{C} \int i_{C\alpha}\, dt + V_{c\alpha 0} \quad (9)$$

$$V_{c\beta} = \frac{1}{C} \int i_{C\beta}\, dt + V_{c\beta 0} \quad (10)$$

Using *"Fig. 2"*, equations (1)-(10), for the matrix equations of SCIM at no-load in the stationary reference frame are given by

$$\begin{bmatrix} 0 \\ 0 \\ 0 \\ 0 \end{bmatrix} = \begin{bmatrix} R_s + pL_s & 0 & pL_m & 0 \\ 0 & R_s + pL_s & 0 & pL_m \\ pL_m & \omega_r L_m & R_r + pL_r & \omega_r L_r \\ -\omega_r L_m & pL_m & -\omega_r L_r & R_r + pL_r \end{bmatrix} \begin{bmatrix} i_{s\alpha} \\ i_{s\beta} \\ i_{r\alpha} \\ i_{r\beta} \end{bmatrix} + \begin{bmatrix} V_{c\alpha} \\ V_{c\beta} \\ \omega_r \Psi_{r\beta 0} \\ -\omega_r \Psi_{r\alpha 0} \end{bmatrix} \quad (11)$$

From (11), can be written the state equations as follows:

$$A_p I_G + B I_G + V_G = 0 \quad (12)$$

Where,

$$A = \begin{bmatrix} L_s & 0 & L_m & 0 \\ 0 & L_s & 0 & L_m \\ L_m & 0 & L_r & 0 \\ 0 & L_m & 0 & L_r \end{bmatrix}, \quad B = \begin{bmatrix} R_s & 0 & 0 & 0 \\ 0 & R_s & 0 & 0 \\ 0 & \omega_r L_m & R_r & \omega_r L_r \\ -\omega_r L_m & 0 & -\omega_r L_r & R_s \end{bmatrix}$$

$$, I_G = \begin{bmatrix} i_{s\alpha} \\ i_{s\beta} \\ i_{r\alpha} \\ i_{r\beta} \end{bmatrix}, V_G = \begin{bmatrix} V_{c\alpha} \\ V_{c\beta} \\ \omega_r \Psi_{r\beta 0} \\ -\omega_r \Psi_{r\alpha 0} \end{bmatrix}$$

2. INDUCTION MOTOR FAULT ANALYSIS METHODS

2.1 Bearing Faults

Two concentric rings is arranged in rolling element bearing. In between the inner ring and outer ring set of

balls of rollers spin are placed in raceways. Defects of bearing may be classified as “distributed” and “local”. Defects in distributed system are having misaligned races, roughness in surface. These defects lead to vibrations immediately. This happens when a roller running over defected surface where the period and amplitude are deliberated by spot, speed, dimension of bearing of anomaly’s. The flawed bearings produces mechanical vibrations [7],[8].

2.2 Rotor Faults

Failures in electrical like bar defect or breakage of bar or mechanical failures includes rotor eccentricity will leads to faults that occur in rotor. During transient operations like start- up, initial faults arise from stresses produce from thermal or fatigue stresses in generous motors. Electrical failure like broken bar modifies torque often which leads to unsafe and inconsistent of an electrical machine. The other rotor fault is caused by air gap eccentricity [9]. Mechanical problems such as unbalance in load are related by these faults to some range in induction motors. The damage in bearings and house bearing causes load unbalance which influences air gap symmetry.

2.3 Eccentricity Faults

The eccentricity is the unequal airgap between stator and rotor of induction motor. It is of two types:

The eccentricity of static air-gap and the eccentricity of dynamic air-gap. The radial length of airgap is minimum and it is fixed in particular space for static air gap eccentricity. The mixed eccentricity and inclined eccentricity have also been reported. In adverse, midpoint of rotor and mid point of rotation does not concur for dynamic eccentricity. In this situation, air gap is not rigid in particular space but moves along with the rotor[10].

3. KERNAL BASED SVM CLASSIFIERS

Boser, Guyon, and Vapnik introduced a Support Vector Machine (SVM) in 1992 for a state-of-the-art classification method. Due to its high accuracy, ability to deal with high-dimensional data such as gene expression, and exibility in modeling diverse sources of data the SVM classifer is extensively used in bioinformatics.

SVMs belong to the common type of kernel methods:

A kernel method is an algorithm that depends on the data only through dot-products. The kernel function replaces the dot product which computes a dot product in some perhaps high dimensional feature space. This has two advantages: First, by methods designed for linear classifiers it has the ability to generate non-linear decision boundaries. Second, for no obvious fixed-dimensional vector space, the use of kernel functions allows the user to apply a classifier to data. sequence, either DNA or protein, and protein structure are the prime example of such data in bioinformatics. When supervising an SVM the practitioner needs to make a number of decision: how to preprocess the data, what kernel to use, and as a final point, setting the parameters of the SVM and the kernel. Uninformed choices could result in strictly reduced performance[10].

By mapping our data from input space X to a feature space F using a non-linear function Φ: X F is the resident way of making a non-linear classifier out of a linear classifier F. In the space F is the discriminant function is:

$$f(x) = W^{1} + \Phi(X)+b \qquad (13)$$

Non-separable data is modified from linearly separable data sheet applicable only for hard marigin SVM. Maximization of the geometric margin 1/||W|| is done by discriminant function which is equivalent to minimizing ||w||2. This leads to the following constrained optimization problem[11]:

Subject to: yi $(W^{T}+ \Phi(X)+b)e”1 \qquad i=1,2…n$

The kernel trick avoids the explicit mapping that is needed to get linear learning algorithms to learn a nonlinear function or decision boundary.

5. SIMULATION AND DISCUSSIONS

5.1 Simulations Procedure

By Simulations it is easy to evaluate even the most extreme faults, provided a simulation has been validated in hardware. Under fault condition,the observation of drive performance is not helpful in commercial drives having fault detection and isolation. Here, the various faults are analyzed by coding written on M-FILE. In this paper the following steps are used for analyzing various types of faults[14].

Step:1 The Manual Switch block’s open function sets
Step:2 Get Parameters for switching action on and off.
Step:3 Set parameter for deature for output variable dimention and size.

Step:4 Get the function of switch values either blocking mode or switch mode.
Step:5 Get parameter for orientation work for diagnosis the fault.
Step:6 Get parameter for plotting waveform like x axis, y axis, Radius.
Step:7 Get function for action allowed in all faults.
Step:8 Check for error thrown from the internal switch bloc

5.2 Simulation Results

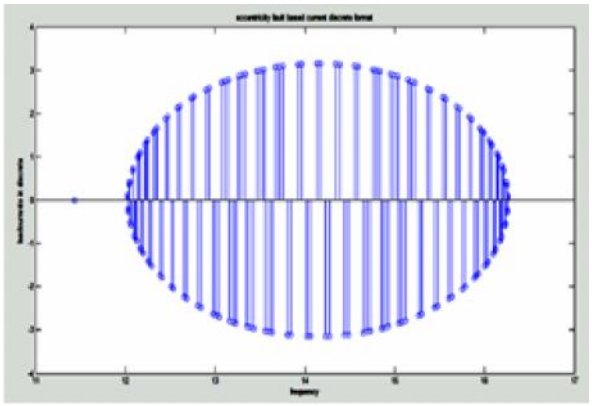

Fig.3 Eccentricity Fault based on Discrete Format

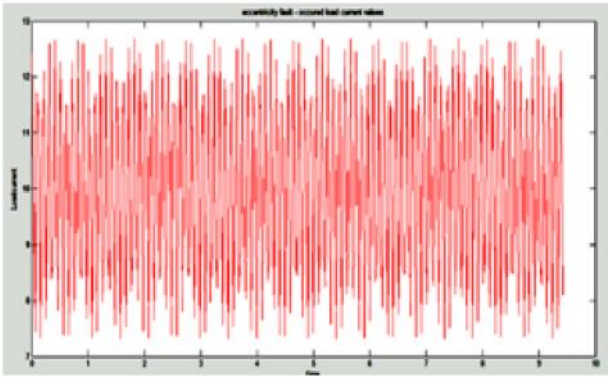

Fig.4 Eccentricity Fault Occurred on Load Current Values

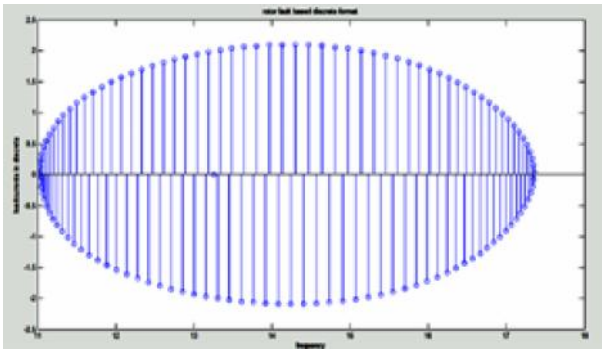

Fig. 5 Rotor Fault based on Discrete Format

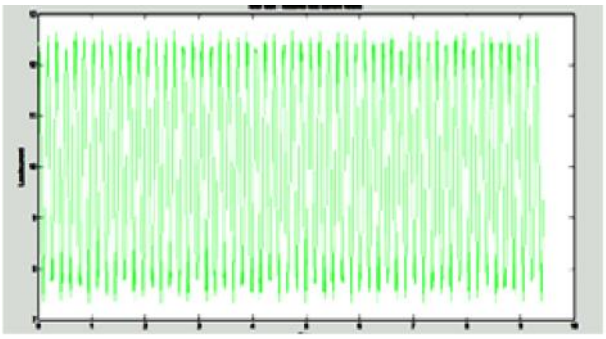

Fig. 6 Rotor Fault Occurred on Load Currentt Values

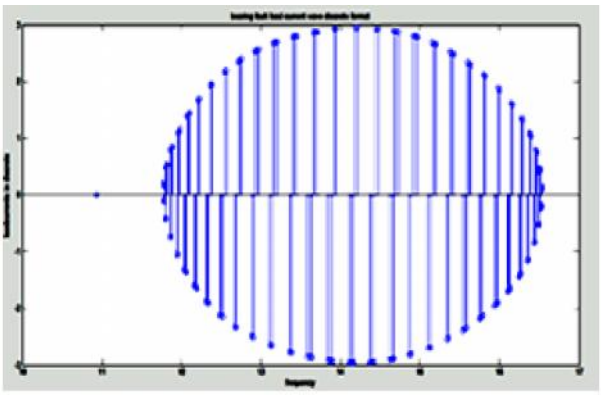

Fig. 7 Bearing Fault based on Discrete Format

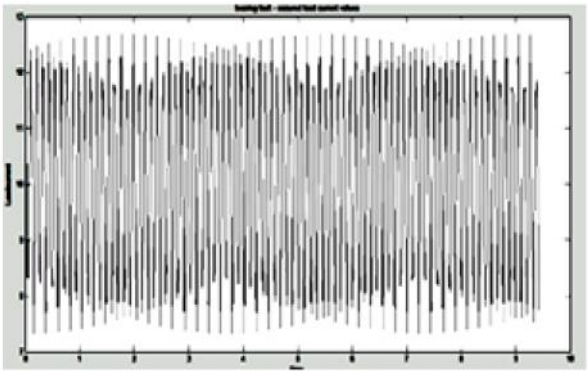

Fig.8 Bearing Fault on Load Current Values

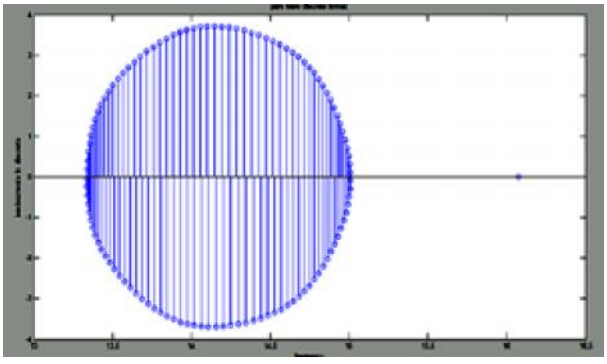

Fig.9 Pure Sine Wave Discrete Format

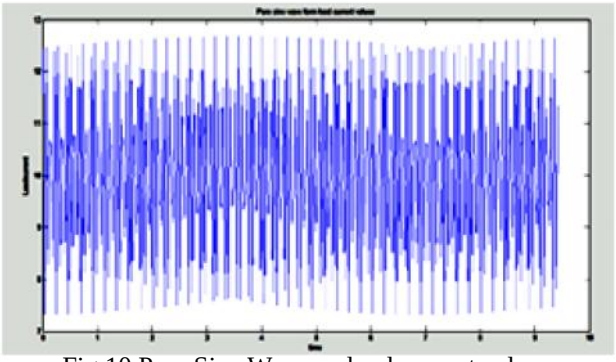

Fig.10 Pure Sine Wave on load current values

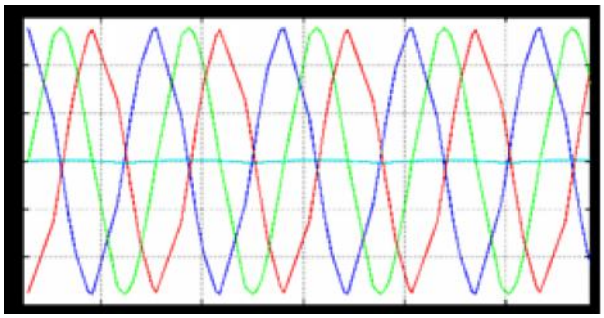

Fig.11Stator currents response after fault diagnosis

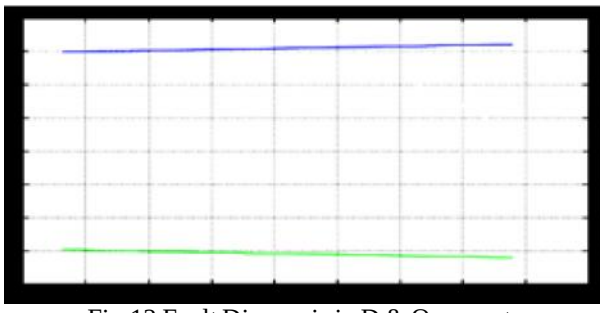

Fig.12 Fault Diagnosis in D & Q current

From Figure 3 to Figure 12 various faults like Eccentricity Fault, rotor fault, bearing faults discrete format as well as load current format also simulated using M-file.

7. CONCLUSION

This paper attempts to summarize recent developments in induction motor fault diagnostics and prognostics. Various techniques, models and algorithms have been analyzed and the suitability of a particular technique for a specific fault diagnosis has been focused upon in this paper.Here new algorithms are developed for detection and diagnosis the fault using MATLAB Mfile softwqare. Then Kernal based SVM classifiers model is also developed and bearing fault, rotor fault and Eccentricity faults are discussed. Here, various kernel based functions are convolved with SVM which results in detection of faults at an accuracy of 91.4% with reduced training samples.In future work the faults detection and diagnosis using more intelligent techniques and various control methods of induction motor also will be analysed.

REFERENCES

[1] A.M. Bazzi, A. D. Dominguez-Garcia and P.T. Krein, “A Method for Impact Assessment of Faults on the Performance of Field Oriented Control Drives: A First Step To Reliabilty Modeling”, in Proc. IEEE Appl. power Electron. Conf. Expo., 2010, pp. 256-263.

[2] Ali. M. Bazzi, Alejandro Dominguez-Garcia and Philip T. Krein, “Markov Reliability Modeling for Induction Motor Drives Under Field-Oriented Control”, IEEE Trans. Power Electron., Vol.2, Feb 2012.

[3] B. E. Boser, I. M. Guyon and V. N. Vapnik, “A Training Algorithm for Optimal Margin Classifiers”, In D. Haussler, editor, 5th Annual ACM Workshop on COLT, Pittsburgh, PA, 1992. ACM Press, pp.144-152.

[4] G.R. Slemon, “Modeling of Induction Machines for Electric Drives”, IEEE Trans. Ind. Appl., Vol.25, No.6, Nov/Dec 1989, pp.1126-1131.

[5] G.Loganathan, D.Rajkumar, M.Vigneshwaran, R.Senthilkumar, “An Enhanced Time Effective Particle Swarm Intelligence For The Practical Economic Load Dispatch”, IEEE 2nd International Conference on Electrical Energy Systems (ICEES), pp.44-50.

[6] G.K. Singh and Sa’ad Ahmed Saleh Al Kazzaz, “Induction Machine Drive Condition Monitoring and Diagnostic Research-A Survey”, Electric Power Systems Research, Vol.64, 2003, pp.145-158.

[7] I.Gerald Christopher Raj, P.Renuga, M.Arul Prasanna, “Improved Indirect Rotor Flux Oriented Control of PWM Inverter fed Induction Motor Drives”, International Journal of Recent Trends in Engineering and Technology,Vol.3, No.3,2010.

[8] J. Shawe-Taylor and N. Cristianini, “Kernel Methods for Pattern Analysis”, Cambridge UP, Cambridge, UK, 2004.

[9] J. Gouthaman and R.Bharathwajanprabhu, “Automated Urban Drinking Water Supply Control And Water Theft Identification System”, A Srikanth Students Technology Symposium (TechSym), 2011 IEEE, pp.87-91.

[11] R. Karthikeyan, S.Chenthur Pandian, " "Generalized Space vector PWM Algorithm for Minimizing THD in Hybrid Multilevel Inverters" , International Review of Electrical Engineering, Vol.6, No.5, 2011, pp2094-2099.

[12] R. Karthikeyan, SC. Pandian, "An Efficient Multilevel Inverter System for Reducing THD with Space Vector Modulation", International Journal of Computer Applications, Vol.23, No.2.

[13] K.Sundararaju and T.Rajesh, "Control Analysis of STATCOM under Power System Faults", International Journal of Communication and Computer Technologies(IJCCTS), Vol.4, No.1, Mar-2016, pp.4001-4006.

[14] M.Arul Prasanna, V. Rajasekaran, I.Gerald Christopher Raj and N.P.Selvam, "Modeling, Analysis and IFO Control Method for CSI fed 3 Phase Induction Motor Drive", Journal of Theoretical & Applied Information, 2014.

[15] P. C Krause and C. H Thomas, "Simulation of Symmetrical Induction Machinery", IEEE Trans., Power Apparatus and Systems, Vol. PAS-84, No. 11,1965.

[16] P. Santhoshini and P. Maniraj, "SEPIC Converter Based Dynamic Power Tracking From Wind Energy Conversion System", Journal of Chemical and Pharmaceutical Sciences., 2016, pp.41-45,

[17] R.Senthil kumar,S.Mahesh, "Fault Detection and Diagnosis of Induction Motor Using IFOC", International Journal Of Applied Engineering Research, Vol.11, No.3, April. 2016.

[18] S.Kirthika, P.Alageswari and R.Senthil kumar, "A Designed Method for 48 Pulsediode Rectifier with Coupled Three Phase Reactor", Journal of Advances in Chemistry, Vol.12, 2016, pp. 4959-4962.

[19] Shuo Chen, "Induction Machine Broken Rotor Bar Diagnostics Using Prony Analysis", A Ph.D Thesis Submitted to the School of Electrical and Electronic Engineering of the University of Adelaide, April 2008.

[20] T. Joachims, "Training Linear SVMs in Linear Time", In ACM SIGKDD International Conference On Knowledge Discovery and Data Mining (KDD), 2006, pp.217-226.

[21] W. R. Finley, M. M. Hodowanec, W.G. Holter, "An Analytical Approach to Solving Motor Vibration Problems", IEEE PCIC Conf., Sep 1999.

Deployment of IoT in Railway System

M. Gayathri Devi and E. Esakki Vigneswaran
Department of Electronics and Communication Engineering
Sri Ramakrishna Engineering College, Coimbatore - 641 022, Tamil Nadu

Abstract

A railway control system based on the Internet of Things (IoT) to control different railway components is proposed. The proposed system has the modules such as train system, railway station system and track system. The train system has GPS module to find the location of the train and transmit the message to the railway station system whenever the railway station system's GPS coordinates are met. The track system has GSM Module, servo motor, sensor and it is deployed on the railway track .The track system is to measure the sensor value for checking whether the train is in the track or not, and changes the track automatically by using proposed track mechanism. The track system is used to transmit the message to the railway station system for identifying the platform numbers of the train. The railway station system has GSM Module to transmit and receive messages from the track and train system. The railway station system updates the data to the cloud using Wi-Fi. The data in the cloud are updated automatically in the developed webpage. Users or passengers could be able to identify the train details by accessing the developed webpage.

Keywords: *GPS module, GSM module, Internet of Things (IoT).*

1. INTRODUCTION

The Internet of Things (IoT) is a rapidly evolving field that involves the interconnection and interaction of smart objects (objects or devices with embedded sensors, onboard data processing capability, and a means of communication) to provide automated services that would otherwise not be possible. IoT is not a single technology, but rather involves the convergence of sensor, information, communication, and actuation technologies. Now-a-days a hectic problem around the world is about traffic densities. This is also common to railway sectors too.

Recent years we often hearing the word train collision and it bags huge precious human life and time. Vehicle tracking is one of the very important issues in this world in recent years. And even train tracking and monitoring is also an important crisis now a days. A train collision takes huge amount of human life and creating a massive loss to the railway sector in terms of money and time. So the system what we are proposing here is a real time wireless based, which will track trains through wired and wireless communication. Railway control system is an essential part of railway infrastructure and is directly associated with the level of railway safety. Therefore in this project, the railway control system based on the Internet of Things (IoT) to controlling different railway components is proposed. In the railway station the Railway station system is kept and when the train arrives the message is transmitted to the track control system for changing the track through GSM.

In the track control system are used to have Arduino UNO board to change the track automatically. From Arduino UNO, servo motor changes the track and the signal is displayed after the track changes. The train control system is having GPS to find the location of the train and the location is send to the Arduino UNO. From Arduino UNO the location is send to the railway station system by using GSM.

2. RELATED WORK

The background of the work involves the selection of the hardware identification and the necessary software modules. Thus the implementation of the device in each module to get a clear idea about the process we have referred some of the papers and materials to develop the project. Some of reference papers are discussed here.

This revolutionary principle of connecting everything to the Internet, with the potential to bring many benefits and improve users life styles, is advancing quickly, where many applications are seeking to take advantage of the emerging infrastructure. Smart cities, smart energy, smart

mobility and transport, e.g., vehicular networks, smart healthcare are a few examples of the IoT smart-X applications.

The draw back of the paper is to develop a webpage is easily for user have discussed in [1]. The developed formal model is applied to demonstrate the design of passenger assistance software that interacts with the RIoT ecosystem and provides passengers with real-time information that is tailored to their requirements with run time. The changing system of the track automatically is not developed.[2].

In this paper, focus on the compression algorithm that reduce the amount of transmitted data and improve the system performance. Based on the analysis of the common algorithms, an efficient compression algorithm, named delta-encoding, is proposed[3]. Has discussed IoT is expected to provide the backbone of modern, smart societies and pave the way for the next generation of Internet technology[4].

The proposing system is a real time wireless based, which will track trains through wireless communication. Railway control system is an essential part of railway infrastructure. The transmitting data for message using 900MHZ operating frequency in GSM module. The railway station system is used to have raspberry pi 3 is having on chip Wi-Fi and is on the 2.4 GHZ operating frequency for network communication. The literature review is used to show the importance of the internet of things for the railway system.

The raspberry pi 3 are uses a Broadcom BCM2837 SoC with a 1.2 GHz 64-bit quad-core ARM Cortex-A53 processor, with 512 KB shared L2 cache. It comes with on-board wireless LAN and offers 50 percent more processing power compared to the previous versions. Networking can be done using 10/100Mbps Ethernet or 802.11b/g/n Wireless LAN. It consists of an onboard Bluetooth module which can be used for short distance communication between devices with data rate of 24Mbps. Interfacing with peripherals can be done using the 40 GPIO pins or the 4 onboard USB ports. This has significantly increased the number of peripherals that can be connected to the board. A wide range of operating systems is available for Raspberry Pi 3. For this system, Raspbian Jessie OS is used because the commonly used packages are automatically installed with the operating system. It consumes less power of 5V which can be sourced from GPIO headers or microUSB. Raspberry Pi 3 contains 1GB that can be used as cache for better performance of the system. In the Project Raspberry Pi is used as the core component which is interfaced with GSM module and the data is send to the cloud. Raspberry Pi is used due for its low cost, small form factor and power performance ratio.

Arduino is an open-source prototyping platform based on easy-to-use hardware and software. Arduino boards are able to read input, light on a sensor, a finger on a button and turn it into an output activating a motor, turning on an LED, publishing something online.Figure 3.4 shows arduino board. Arduino programming language (based on Wiring), and the Arduino Software (IDE) are used to send a set of instructions to the microcontroller on the board, based on Processing.The Arduino Uno R3 is a open source microcontroller board based on the ATmega328 chip. This Board has 14 digital input/output pins, 6 analog input pins, Onboard 16 MHz ceramic resonator, Port for USB connection, Onboard DC power jack, An ICSP header and a microcontroller reset button. It contains everything needed to support the microcontroller. Using the board is also very easy, simply connect it to a computer with a USB cable or power it with DC adapter or battery to get started.

In this project arduino uno are used as a train and track system. To communicate with railway station system. The device is used to find the location of the train by using GPS .The Arduino UNO microcontroller is connected with GPS and GSM to transmit message. It is fixed in the train.

The railway station system having raspberry pi receives the data and transmit the data to the track system by GSM .In the track system are used to have GSM to receive and transmit data ,IR sensor are used to find which track is free and according to the track it is used to turn the servo motor on and off. Then the message is transmitted to the railway station system .The railway station system are having in build Wi-Fi communication update the data in cloud.

The track system is to receive the message and check the infrared sensor value which is fixed in the track. According to the IR sensor value it is used to transmit the signal to the servo motor to turn (180 or 0) degree .Then the message is transmitted to the railway

station unit. The railway station system update the data in the cloud and send to the developed webpage. The passenger can view the train no and also the platform number with time.

3. BLOCK DIAGRAM

The block diagram of the project along with details of each hardware component that had been chose for its implementation is explained. The project uses Railway station system and Arduino UNO as the main hardware components for developing for train monitoring system. This embedded system consists of GSM module, GPS module, IR sensor, servo motor and android phone. The system involves the connection of module with the Arduino UNO and Railway station system .The project used 4 nodes for implementing the communication the android phone. The system uses the Train number to identify the train name with their location and time displayed in the mobile phone. The weaved cloud is used display the location and the platform number of the trains.

In the block diagram over all block diagram is shown in the Figure1 this diagram are used to represent the proposed system model. The train system are used to GPS which used to find the location of the train by using to check the GPRMC are used to find the location of the train and display the time. Then message is transmitted to the GSM which is connected with Arduino UNO.

The block diagram of railway station system in the railway station system is used to interface with GSM and Wi-Fi. The GSM are used to receive the message from the train control system. The stack overflow is checked and the message is transmitted to the track control system. After receiving the message from the track control system it is used to update the data in the cloud. The php code is added with the python code transmit data to the cloud and view the data from the mobile.

The block diagram of track control system in the "TRACK CONTROL SYSTEM" is having the Arduino UNO microcontroller are used to receive the message from railway station system and used to check the IR sensor . The IR sensor are used to check the train in the track or not according to sensor output the servo motor are to change the track automatically. Then the message is transmitted to the railway control system.

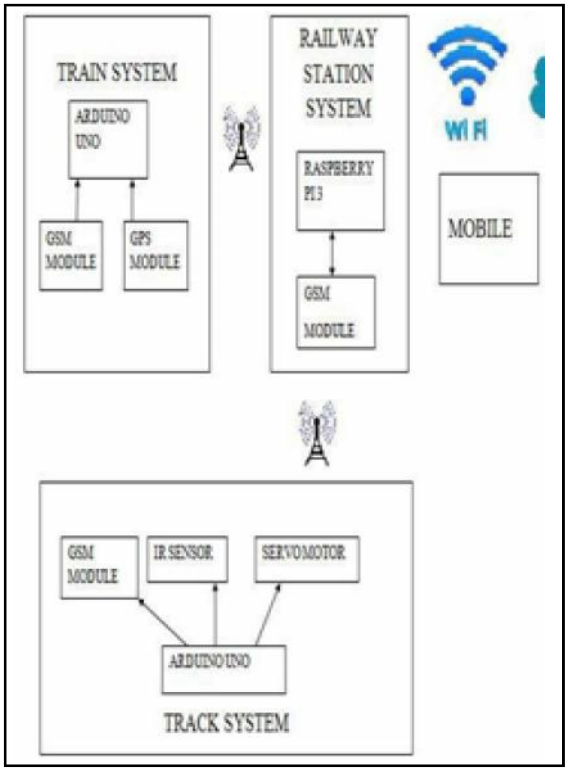

Fig.1 Overall Block Diagram

The overall block diagram is used to show the communication between the modules. The communications are done using the wireless communication. It is used for long distance communication.

4. EXPERIMENTAL RESULT

For experimentation result, the train system is having the GPS and GSM module. The railway station system is having raspberry pi 3 with inbuilt Wi-Fi and GSM module. The track system is having the GSM module, IR sensor and servo motor. The webpage is developed for the proposed system.

The Figure 2 shows the GPS and GSM connection with Arduino UNO microcontroller. The GPS are used to find the latitude and longitude of the train and time. The latitude and longitude location with the time and train number are transmitted to the railway station system using GSM Module, if the train arrived at particular range of the latitude and longitude. The GPS is connected with Tx to the pin0 of the Arduino UNO microcontroller and GSM Rx pin to the pin1 of the Arduino UNO microcontroller.

The Figure 3 shows the output of the train system. The message is transmitted to the railway station system with the location and the time.

The Figure 4 shows the connection between the Arduino UNO microcontroller, GSM module, IR sensor and servo motor. The Arduino UNO is connected with TX to the GSM module of RX, IR sensor is connected with pin 2 of the Arduino UNO, the servo motor are connected with pin 9 for Arduino UNO.

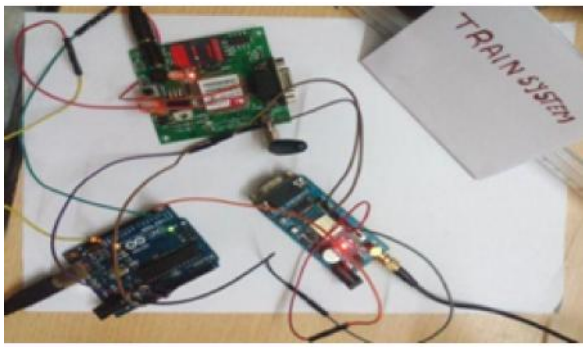

Fig. 2 Experimental Setup for Train System Module

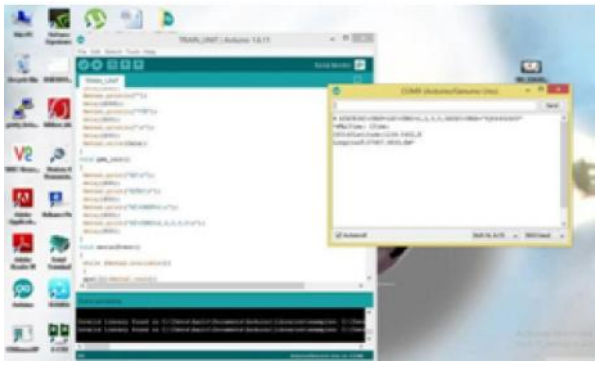

Fig.3 Train Control System Output

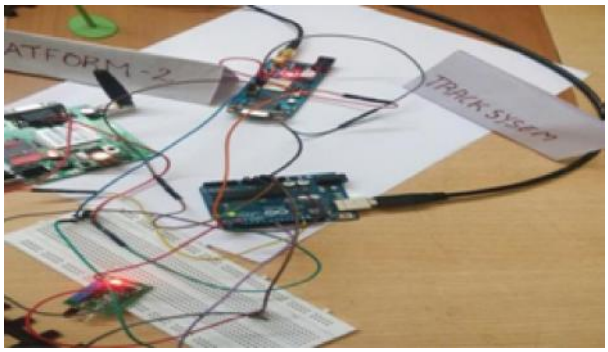

Fig.4 Experimental Setup for Track System

If the message is received from the railway station system then it check the IR sensor value and change the track automatically by using servo motor. The message is again transmitted to the railway station system. The Figure 5 shows the output of the track system. The message is transmitted to the railway station system.

The Figure 6 shows the connection between the railway station system and the GSM module. The GSM module are used to receive the message from train system and used to transmit the message to the track system .The GSM module of the RX pin to 10 pin of raspberry pi3 and TX pin to the 8 pin pd raspberry pi 3. The GND of the GSM is connected with pin 6 of raspberry pi 3.The railway station system is transmit the message automatically and wait for the message from the track unit to update the data in the cloud.

The Figure 7 shows the output of railway system. The message is received from the train system and transmitted to the track system. From the track system it received the message and transmit to the cloud.

5.RESULT ANALYSIS

The result is obtained when the IR sensor is high and the servo motor turn 180 degree .The message is transmitted to the railway station system with the train number and the platform1. It is shown in the Figure 8. The screen short shows the train number, platform number, location and time.

The result is obtained when the IR sensor is low and the servo motor turn on 0 degree. The message is transmitted to the railway station system with the train number and the platform1. It is shown in the Figure 9. The screen short shows the train number, platform number, location and time.

The online webpage is developed to get the data from the cloud. The experiment is done using the wireless devices to evaluate the effectiveness of the proposed system. The train system is transmitting the message to the railway system. The railway station system are used to update the data in cloud when it receives the message from the track system. The track system is received the message from the railway station system, change the track automatically and transmit the message to the railway station system.

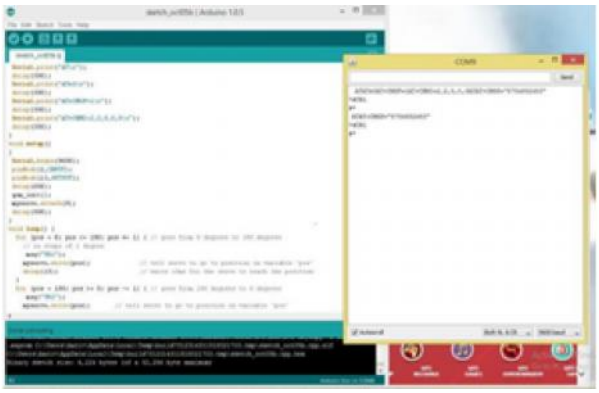

Fig.5 Track Control System Output

Fig. 6 Experimental Setup for Railway Station System Module

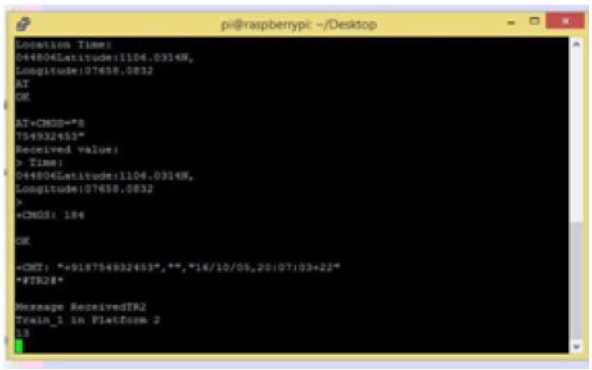

Fig.7 Railway Station System Module

Fig.8 Screen Shot Of Train 1 In Platform 1

Fig.9 Screen Shot In Train 1 In Platform 2

6.CONCLUSION

This prototype describes a deployment of IoT in railway system. The main goal of this project was to create a design for an efficient Deployment of railway station using Internet of things. The data is transmitted to the cloud. The automatic track changing mechanism is done by using servo motor. The cloud receives the data and plots the train number and the platform number of the train with the time and location. The changes in the cloud data is viewed in the webpage automatically. The passenger can access the webpage with the provided URL and passenger can view the location of the train by using mobile, smart phone and laptop. The proposed system can be a model for smart railway station in our country.

7.FUTURE WORK

The future work is to implement the gate control and the ABS system in the train. In the track control system, the Robot is developed to check the fault in the track. The MEMS system is designed to operate in harsh environments for the train.

REFERENCES

[1] M.H. Eiza, T. Owens and Q. Ni, "Secure and Robust MultiConstrained QoS aware Routing Algorithm for VANETs", IEEE Transactions on Dependable and Secure Computing, Vol.3, Jan 2015, pp.99-101.

[2] Mahmoud Hashem Eiza, Martin Randles, Princy Johnson, Nathan Shone, Jennifer Pang and Amhmed Bhih, "Rail Internet of Things: An Architectural Platform and Assured Requirements Model", in Proc. Int. Conf. Transportation Systems, 25 Jan 2015, pp.33-39.

[3] Yangxin Lin, Ping Wang, Jinlong Lin, Meng Ma, Ling Liu, Lin Ma, "Class-Based Delta-Encoding for High-Speed Train Data Stream" School of Software & Microelectronic, Peking University, Beijing, China, 2015.

[4] D. Mercer, "Connected World the Internet of Things and Connected Devices in 2020," Strategy Analytics, Oct 2014, pp.34-37.

[5] S. Yasunobu, S. Miyamoto, and H. Ihara, "Fuzzy control for automatic train operation system," in Proc. Int. Conf. Transportation Systems, Apr.5 2014, pp.33-39.

[6] Jordi Serra, David Pubill, Angelos Antonopoulos, and Christos Verikoukis, "Smart HVAC Control in IoT: Energy Consumption Minimization with User Comfort Constraints", The Scientific World Journal, Vol. 2014, Article ID 161874, Sep 2014, pp.11.

[7] L Li, XF Wang, X Lei, "The Design of Railway Information System Integration Based on IOT", Advanced Materials Research, 2013.

[8] Nazir Zafar and Others, "Towards the Safety Properties Of Moving Block Railway Interlocking System", International Journal of Innovative, Computing, Information and Control, Vol.8, No.8, Aug.2012.

[9] Xucong Zhang, Xiaoyun Wang and Yingmin Jia, "The Visual Internet ofThings System Based on Depth Camera", Proceedings of 2013 Chinese Intelligent Automation Conference, Part 2, pp. 447-455.

[10] IERC-European Research Cluster on Internet of Things, "Internet of Things Pan European Research and Innovation Vision", European Comm Systemies, Jan 2011.

[11] D. Mercer, "Connected World the Internet of Things and Connected Devices in 2020", Strategy Analytics, Oct 2014.

[12] M.H. Eiza and Q. Ni, "A Reliability-Based Routing Scheme for Vehicular Ad Hoc Networks (VANETs) on Highways", in Proc. Of the IEEE 11th International Conference on Trust, Security and Privacy in Computing and Communications (TrustCom), June 2012, pp.1578-1585.

[13] M.H. Eiza and Q. Ni "An Evolving Graph-Based Reliable Routing Scheme for VANETs," IEEE Transactions on Vehicular Technology, Vol. 62, No.4, May 2013, pp. 1493-1504.

[14] M.H. Eiza, T. Owens and Q. Ni, "Secure and Robust Multi Constrained QoS Aware Routing Algorithm for VANETs", IEEE Transactions on Dependable and Secure Computing, Jan 2015, Vol.62, No.99, pp.1-1.

[15] J. A. Stankovic, "Research Directions for the Internet of Things", IEEE Internet of Things Journal, Vol. 1, No. 1, 2014, pp.3-9.

[16] K. L. Lueth, "The 10 most Popular Internet of Things Applications Right Now", [Online]. Available: http://iot-analytics.com/10-internetof-things- applications/ [Accessed 24 08 2015].

[17] A. Scroxton, "How the Internet of Things Could Transform Britain's Railways", August 2014. [Online]could-transform-Britains-railways.[Accessed 18 05 2015].

Performance Analysis of MPPT Algorithms for PV Array Fed SEPIC Converter

S.Kirthika
Department of Electrical and Electronics Engineering,
M.Kumarasamy College of Engineering, Karur - 639 113, Tamil Nadu
E-mail: kirthikaselvam26@gmail.com

Abstract

This work deals with the application of Maximum Power Point Tracking (MPPT) Algorithm like Perturb and Observe and the Incremental Conductance algorithms for photovoltaic (PV) applications using MATLAB/ SIMULINK. These algorithms are applied to a Single Ended Primary Inductor Converter (SEPIC) using a mathematical model. The proposed methodology algorithm can be expanded to a various class of converters which is capable for photovoltaic applications. The SEPIC converter provides the close loop characteristics. The mentioned algorithms i.e. Perturb and Observe and Incremental Conductance algorithms are compared in terms of their fastness and error for the proposed Single Ended Primary Inductor Converter.

Keywords: *Incremental Conductance (INC), Maximum power point tracking (MPPT), Photovoltaic (PV), Perturb and Observe (P&O), SEPIC converter*

1. INTRODUCTION

Now a day, Renewable energy resource are becoming popular as they provide major part energy to energy of less consuming building [1]. Between the all renewable energy resource, solar power systems plays a vital role since they gives better opening to generate power and continues to grow in popularity [2],[3].

Photovoltaic (PV) array has variety of applications such as the power house appliances, solar car, and aircrafts. The solar panel output power changes in fraction of seconds due to rapid climatic changes like weather condition rises or reduce in ambient temperature [4]. In the lower efficiency of solar module, various techniques are introduced, the recent idea known as "maximum power point tracking" (MPPT). The MPPT algorithms are used to improve the output power of the PV panel. In the development of solar panels, maximum power point tracking algorithm is the electronic method of electrical load to attain the highest obtainable power, during second to second changes in sun light, shadow, heat from the sun, and solar PV system features. The single ended primary inductor converter (SEPIC converter) is used. The converter is used to avoid the fluctuation that is obtained by the solar panel output. This converter is connected between the load and the PV panel [5],[6]. The controller is used to trace the peak power of PV panel and control action is taken in the PV systems thereby improving efficiency of the overall systems.

This paper proposes a control scheme, how hill climbing and incremental conductance algorithms are used to track peak power obtained from solar panel that can be used to operate the load using SEPIC converter.

2. PROPOSED METHODOLOGY

The proposed system block diagram is shown in figure 1. This strategy of power production contains of PV panel, SEPIC converter, perturb and observe/ incremental conductance controller. The PV array converts the sun light into electrical power. The generated power is fed to the SEPIC converter and the activating pulse to the converter is given by perturb and observe algorithm or incremental conductance algorithm. The MPPT algorithm will continue until maximum power obtained from PV panel. Hence the load is sustained to operate at peak power.

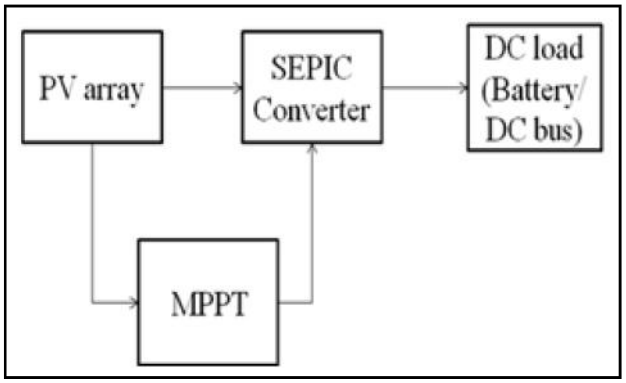

Fig. 1 Block Diagram of the Proposed Methodology

3. PHOTOVOLTAIC MODEL

Photovoltaic array is designed in series/shunt combination of solar cells [7], the circuit representation is shown in figure 2.

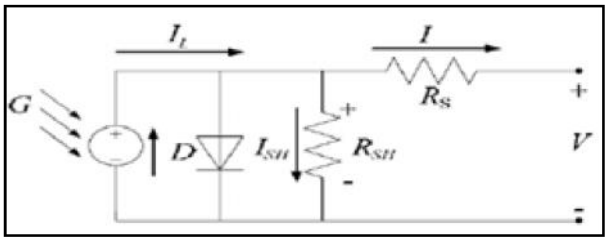

Fig. 2 Simplified circuit of PV panel

The current cell equation is given by,

$$I = I_L - I_D \qquad (1)$$

The current diverted through diode is given by,

$$I_D = I_o\left[\exp\left(\frac{V + IR_s}{nkT/q}\right) - 1\right] \qquad (2)$$

The current source that delivers short circuit current. The resistance is connected in series and parallel with the current source. The diode is connected parallel with the source that provides the p-n junction. That will provide either voltage or current. The current I_d is produced which is called diode current or dark current.

Where the symbol are given as follows,

I_O – Reverse saturation current, A
n – Diode ideality factor
T – Absolute temperature
e – Electron charge (1.602*10-19 C)
q – Elementary charge
k – Boltzmann constant (1.38*10-23 J/K)
I_D – Diode current, A
I_L – Photo generated current, A
R_S – Series resistance of cell

4. PROPOSED CONVERTER

While choosing an MPPT algorithm, the important thing is to select and design a very good converter, which is operated as the major part of MPPT. The switching mode supply DC-DC converter efficiency is mostly used. The high efficiency is obtained by using switching mode power supply [8]. Among the entire converters available, single ended primary inductor converter (SEPIC) is a DC-DC converter which is most efficient and popularly used. It can be work in all modes such as continuous, discontinuous, or boundary condition mode. The duty cycle of the SEPIC converter is controlled by the control transistor [12]. SEPIC converter has low ripple and no pulsating. It improves the tracking efficiency of the solar PV array. SEPIC's are useful in battery voltage that can vary the regulator's calculated output. A SEPIC converter consists of a coupling capacitor, C_1 and output capacitor, C_2, coupled inductors L_1 and L_2 and diode as shown in figure 3.

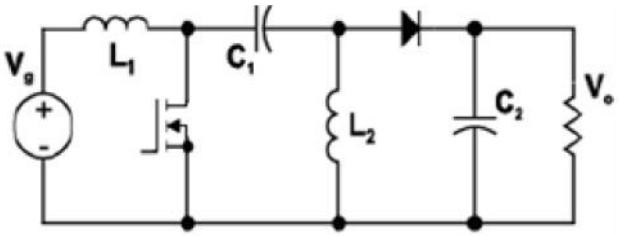

Fig.3 SEPIC converter circuit diagram

Figure 4 shows the converter when switch is on. The input voltage source is obtained by charging the inductor L_1 at this time. The energy is drawn from the inductor L_2 through the capacitor C_1, and the output capacitor is obtained by the load current. The load capacitor does not supply energy at that time. The polarity of the Inductor current and capacitor voltage are also decided.

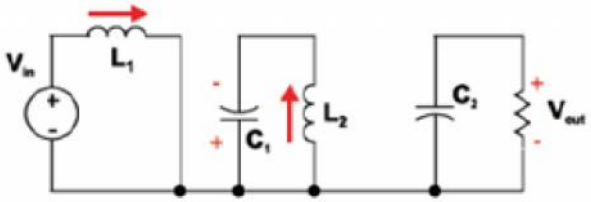

Fig. 4 SEPIC converter when switched ON

Figure 5 shows the converter when the switch is off, the current given to load system is obtained by charging the capacitor C_1 by inductor L_1. The load will be connected to the inductor L_2 at that time. This operation is done when the output capacitor will capture a current pulse, basically noisier than a buck converter. The SEPIC converter is most efficient and it will track maximum efficiency in solar array.

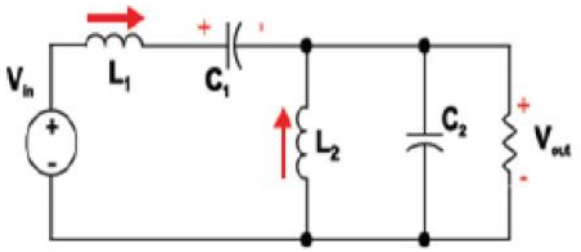

Fig.5 SEPIC converter when switched OFF

The duty cycle is formulae by,

$$Dmin = \frac{\text{Vout} + \text{Vd}}{\text{Vin(max)} + \text{Vout} + \text{Vd}} \quad (3)$$

$$Dmax = \frac{\text{Vout} + \text{Vd}}{\text{Vin(min)} + \text{Vout} + \text{Vd}} \quad (4)$$

5. PROPOSED ALGORITHM

There are wide number of algorithms used to trace maximum power. Some of the algorithms are simple and easy, such as current and voltage method, and some are more difficult, like hill climbing (P&O) and incremental conductance (INC) method. These algorithm changes in steady state, sensor essential, occurrence of speed , price, range of performance, acceptance, to perform more versatile, and its uses [10],[11].

P&O algorithm is the easier method. In this only one sensor is used, i.e. voltage sensor, to sense the solar panel voltage and the price of operation is lower. So it is easily implemented. INC conductance method is the one which is widely used in all type of weather conditions. In this topology, the output voltage of the solar cell is varied depend upon the peak power voltage. According to the incremental and instantaneous conductance the PV system is established.

5.1 Perturb and Observe MPPT

The P&O algorithm is also called as hill climbing method. This method is most widely used. The implementation of this method is easy and cost is less. This method will do track sudden changes and it will not reach maximum power. At the maximum power it rises or reduced repeatedly depends upon the reference voltage and current.

During dP/dV>0 the MPPT algorithm will trace maximum power available in solar cell. This method will continue to track in the same direction. During dP/dV<0 it will track above the maximum power obtained in solar cell. This topology will reverse the direction of search. This topology results in unstable output power. The algorithm is obtained in MATLAB/Simulink.

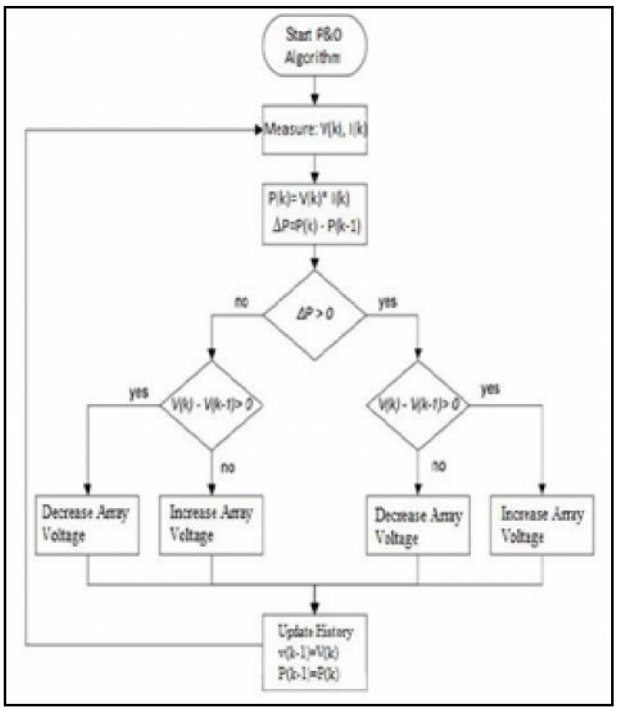

Fig. 6 Flowchart of P&O MPPT method.

5.2 Incremental Conductance MPPT

The output power from the solar PV is obtained by the incremental conductance method in reference to the voltage and the peak power will be equivalent to zero.

$$\frac{dP}{dV} = \frac{d(IV)}{dV} = I + V\frac{dI}{dV} = 0 \quad (5)$$

$$\frac{-I}{V} = \frac{dI}{dV} \quad (6)$$

The Eqn. (5) denotes the instantaneous and incremental conductance of PV array. In peak power, the parameters should be same in magnitude, but different polarities. The eqn. (6) that indicates the peak power voltage will be higher or lower the operating voltage. This relation is shown in eqns. (7, 8, 9).

$$\frac{\Delta I}{\Delta V} = -\frac{I}{V} \quad \text{at the MPP} \quad (7)$$

$$\frac{\Delta I}{\Delta V} > -\frac{I}{V} \quad \text{Left of the MPP} \quad (8)$$

$$\frac{\Delta I}{\Delta V} < -\frac{I}{V} \quad \text{Right of the MPP} \quad (9)$$

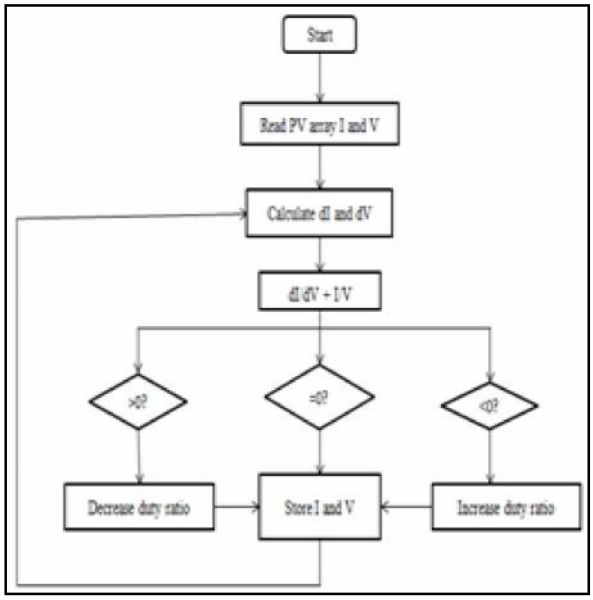

Fig. 7 Flowchart of INC MPPT method

The present and earlier value is calculated using dI and dV of the PV voltage and current. This incremental conductance method has an advantage that it can achieve the peak power and it also find out when it reaches the peak power. This method does not oscillate around the peak power point.

6. SIMULATION RESULT

The proposed system consists of the PV circuit model, SEPIC converter, MPPT algorithm and it is designed using MATLAB as shown in fig. 8. The PV panel output power is determined by the electrical circuit model of solar array. The PV array that provides voltage and current is given to the converter and controller simultaneously. The SEPIC converter will adjust the duty cycle directly.

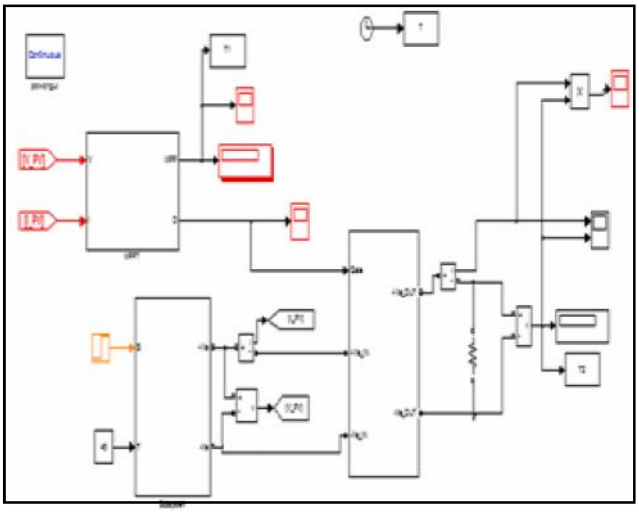

Fig. 8 Simulink diagram for proposed system

6.1 Simulation Result for P&O Method

The simulink for P&O algorithm is shown in fig. 9. The PV panel voltage and current is given to MPPT, that will track maximum peak power and the pulse is given to SEPIC converter.

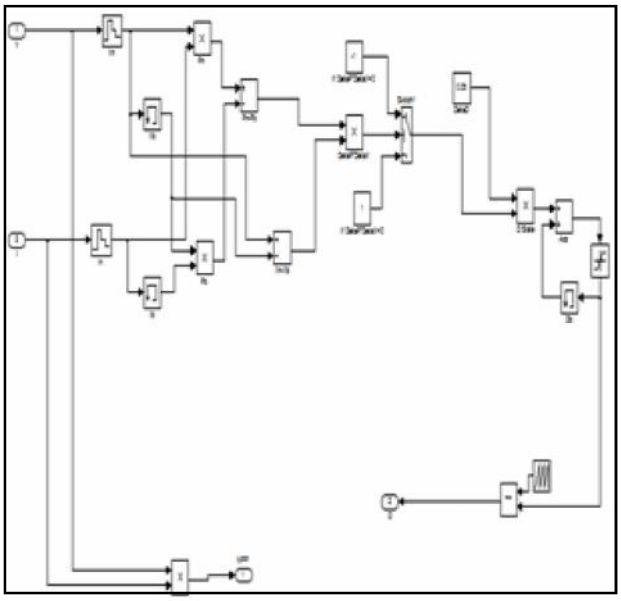

Fig. 9 Simulink of P&O algorithm

The algorithm is verified by using the temperature and irradiance. The MPPT output and output power waveforms will be obtained according to its temperature and irradiance. The waveforms are shown below.

(i) At constant temperature (T=25º) with the changes in irradiation (S=800 to 600w/m^2)

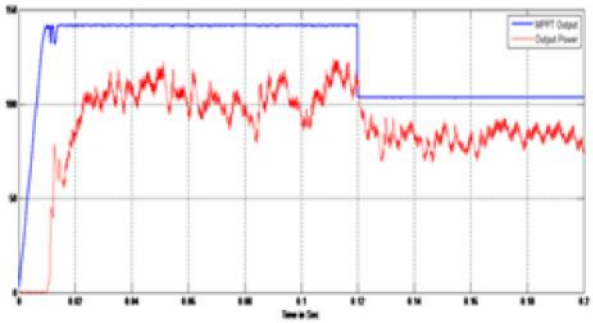

Fig.10 MPPT output and output power waveform (T=25º and S=800 to 600w/m^2)

Figure 10 shows two waveforms i.e. MPPT output and output power. If the temperature is reduced means, power will start to increase. Here T=25º so power starts to increase. If the irradiation increase means, the output power will increase. In P&O, the output power will not be steady.

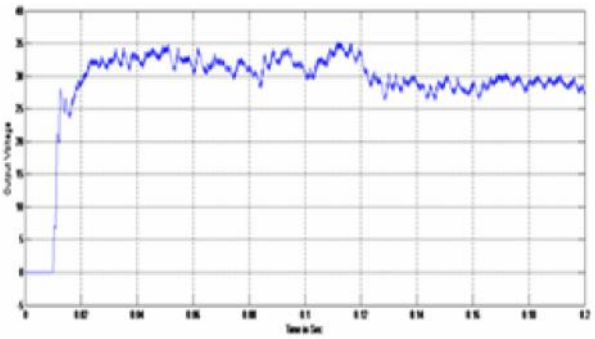

Fig.11 Output voltage waveform (T=25º and S=800 to 600w/m^2)

(ii)At constant temperature (T=70º) with the changes in irradiation (S=800 to 600w/m^2)

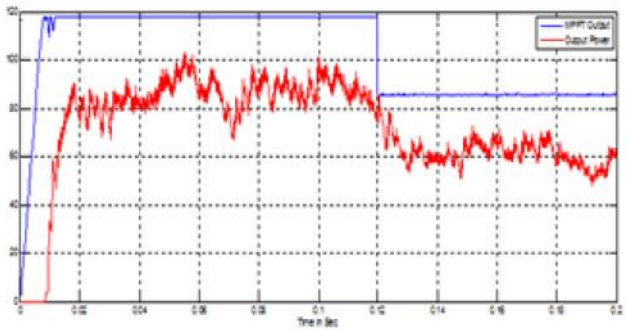

Fig.12 MPPT output and output power waveform (T=70º and S=800 to 600w/m^2)

Figure 12 shows two waveforms i.e. MPPT output and output power. If the temperature is increased means, power will starts to reduce. Here T=70º so power starts to reduced when compared to Fig. 10. If the irradiation increase means, the output power will increase.

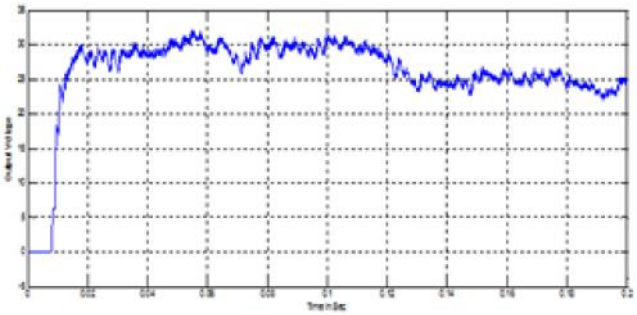

Fig.13 Output voltage waveform (T=70º and S=800 to 600w/m^2)

6.2 Simulation Result for INC Method

The simulink for INC conductance algorithm is shown in Figure 10. The first step is to read the PV array voltage and current. The next step is to calculate present and previous voltage and current in maximum peak power (MPP). By summing the present value and previous value, if it is greater than zero means duty ratio is reduced, if it is less than zero means duty ratio is increased, if it is equal to zero means voltage and current will be stored. This process is done until it gets maximum power output.

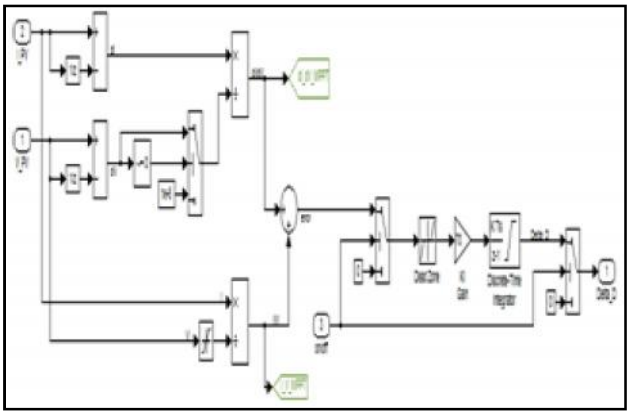

Fig.14 Simulink of the INC algorithm

(i) At constant temperature (T=25º) with the changes in the irradiation (S=800 to 600w/m^2)

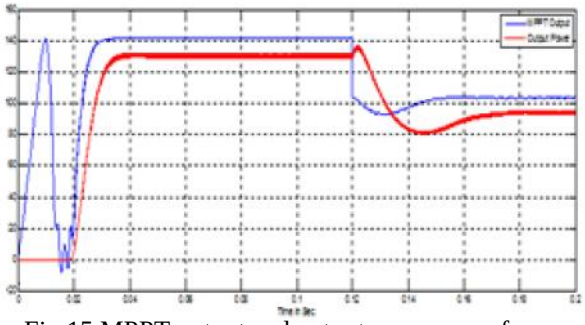

Fig.15 MPPT output and output power waveform (T=25º and S=800 to 600w/m^2)

Figure 15 shows two waveforms i.e. MPPT output and output power. If the temperature is reduced means, power will starts to increase. Here T=25º so power starts to increase. If the irradiation increase means, the output power will increase. In INC, the output power will be steady.

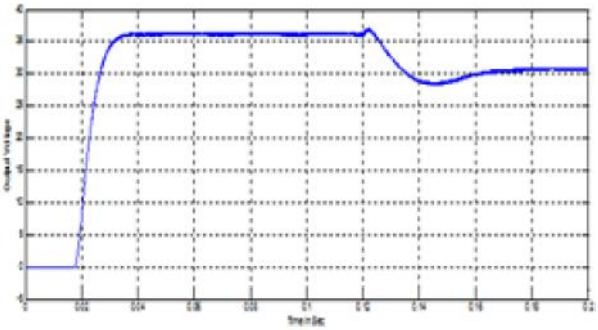

Fig.16 Output voltage waveform (T=25º and S=800 to 600w/m^2)

(ii)At constant temperature (T=70º) with changes in the irradiation (S=800 to 600w/m^2)

Figure 17 shows two waveforms i.e. MPPT output and output power. If the temperature is increased means, power will start to increase. Here T=70ş so power starts too reduced when compared with Fig. 15. If the irradiation increase means, the output power will increase.

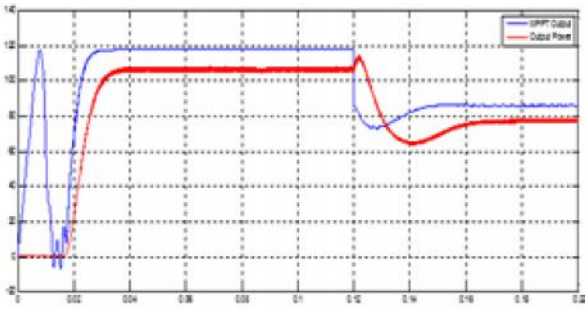

Fig.17 MPPT output and output power waveform (T=70º and S=800 to 600w/m^2)

7. CONCLUSION

This project presented the application of various Maximum Power Point Tracking (MPPT) like Perturb & Observe and Incremental Conductance Algorithms for photovoltaic (PV) applications using MATLAB/SIMLINK. These algorithms are applied to a Single Ended Primary Inductor Converter (SEPIC) using a mathematical model. The above algorithms i.e. Perturb & Observe and Incremental Conductance Algorithms are compared in terms of their fastness and error for the proposed Single Ended Primary Inductor Converter.

REFERENCES

[1] Dezso Sera, L.Mathe, T.Kerekes, "On the Perturb and Observe and Incremental Conductance MPPT Methods for PV Systems", IEEE Journal of Photovoltaics, Vol.3, No.3, July 2013.

[2] Nicola Femia, Giovanni Petrone, "Optimization of Perturb and Observe Maximum Power Point Tracking Method", IEEE Trans. Power Electron., Vol. 20, No.4, Jul. 2005, pp. 963-973.

[3] Omar Abdel-Rahim, Hamdy Radwan, Mahrous Ahmed, "Two Stages Maximum Power Point Tracking Algorithm for PV systems Operating Under Partially Shaded Conditions", IEEE Trans. Power Electron., Vol. 25, no.5, July 2010.

[4] Jay Patel, Vishal sheth, Gaursng Sharma, "Design & Simulation of Photovoltaic System Using Incremental MPPT Algorithm", International Journal of Advanced Research in Electrical, EIE, Vol.2, No.5, May 2013.

[5] Lokin Joshi, Kaumil Shah, "Incremental Conductance based Maximum Power Point Tracking for PV Multi-String Power Conditioning Systems", International Journal, Vol. 3, No.4, April 2013.

[6] S.Ravivarman, T.Samydurai, "Optimized Grid Power Injection with Maximum Power Point Tracking using Cascaded SEPIC Converter and Three Phase Inverter", International Journal, Vol.4, No.1, Jan 2015.

[7] M.G.Villalva, J.R.Gazoli, E.Ruppert, "Modelling and Circuit based Simulation of Photovoltaic Arrays", Brazilian Journal of Power Electronics, Vol. 14, No.1, Feb 2009, pp. 35-45.

[8] D.Velmurukan, Arun P Babu, Sandeep prasanth, "A Fuzzy algorithm based MPPT control for SEPIC Converter with Sliding Mode Controller", International Journal, Vol. 2, No.1, Feb 2015.

[9] R.Alonso, E.Roman, A.Sanz, V.Santos and P.Ibanez, "Analysis of Inverter Voltage Influence on Distributed MPPT Architecture Performance", IEEE Trans. Ind. Electron., Vol.59, No.10, Oct. 2012, pp. 3900-3907.

[10] K.Hussein, I.Muta, T.Hoshino, and M.Osakada, "Maximum Photovoltaic Power Tracking: An Algorithm for Rapidly Changing Atmospheric Conditions", IEEE Proceeding of Generation, Transmission and Distribution, Vol.142, No.1, 2005, pp.953-959.

[11] C.C.Hua and C.M.Shen, "Study of Maximum Power Point Tracking Techniques and Control of DC-DC Converter for Photovoltaic Power System", Proceeding of IEEE Power Electronics Specialists Conference, Vol. 1, 1998, pp.86-93.

[12] P.Mattavelli, L.Rossetto, G.Spiazzi and P.Tenti, "General Purpose Sliding Mode Controller for DC-DC Converter Applications", Processing IEEE PESC REc, Jun.1993, pp. 609-615.

Dynamic Power Tracking Using Intelligence Technique for WECS With Sepic Converter

P. Alageswari and S. Dinesh Kumar
M.Kumarasamy College of Engineering, Karur - 639 113, Tamilnadu.
E-mail: alageswariabi@gmail.co

Abstract

The global claim for electrical energy is constantly increasing while the production of fossil fuel based energy is declining and therefore the evident choice of clean energy source which is abundant and could provide security for the future development in renewable energy is essential. Among the renewable energy sources wind energy is one of the fastest growing power generation sectors. wind blows intermittent in nature so the necessary steps are carried out to give constant power to the load. The Proposed system employs wind turbine whose output is given to the permanent magnet synchronous generator to convert mechanical energy from wind turbine to electrical energy which uses a fuzzy logic controller for controlling the output power of the generator. This output power from PMSG is rectified to dc through rectifier and the rectified output is supplied to the SEPIC converter which increases or decreases the output power according to the load. The MPPT controller is used to control the duty cycle of the switch in the SEPIC converter. This system provides a constant DC power output to the load. In this perturb and observe algorithm and perturb and observe algorithm with ant colony algorithm is used to control the duty cycle and its output is compared to show improvement of power. Simulation results obtained using MATLAB validate the proposed method.

Keywords: *Wind Energy Convertion System (WECS), SEPIC converter, P&O algorithm, P&O with ant colony optimization, Fuzzy logic controller.*

1. INTRODUCTION

Energy is an important aspect of living organism. There are different forms of energy available in nature. Depending on its regeneration energy is classified into renewable and non renewable. Non-renewable energy is energy from fossil fuels like coal, crude oil, natural gas come from sources on our planet, once used they cannot be replaced or replenished. Burning of fossil fuel produce by-products like nitrous oxide, sulphur dioxide and produce green house gases causing the phenomenon of global warming. To overcome the above problems, renewable energy sources are preferred which can be replaced and used continuously without becoming depleted. Among the renewable energy sources wind energy is selected because of its availability and non polluting nature.[1],[2].The circulation of air in the atmosphere is caused by non uniform heating of earth by the sun, which cause air above a warm area expand, it is forced upward by cool, dense air which flows in surrounding areas causing a wind. Wind is a kinetic form of energy. Wind energy is converted to electrical energy by using wind turbine and electrical generator. The optimum power extraction [3]from wind is achieved by operating wind turbine in variable speed. To extract optimum power various intelligence techniques[4],[5] are used. If the turbine serves asa voltage source for an isolated area, huge amount of energy storage(battery) or other energy source(such as engine generator) is needed for stable operation due to the variable wind speed characteristics. So an inexpensive and efficient power converter for DC load connection is required for modern wind energy conversion systems. High flux density permanent magnet synchronous generators[6],[7],[8] are becoming popular in industrial applications especially for gearless drive systems with advantages such as small size, less weight and flexible in design structure. Considering these trends, one of the best topologies for wind power conversion system is the full size 3-phase diode rectifier with dc-dc chopper[9] is more cost effective solution for ac-dc converter than 3-phase IGBT PWM converter and the optimization techniques is used to control the switches[10][11][12].

2. SYSTEM OVERVIEW

The schematic diagram of proposed system comprises of two subsystems namely, the wind energy conversion system and power conversion system. The wind turbine system converts the wind energy into electrical energy. The wind energy conversion system includes wind turbine, pitch angle control, drive train, PMSG. By applying the MPPT scheme, the controlled torque is given as input for PMSG via controlling the electromagnetic torque and rotor speed of PMSG. The power conversion system includes rectifier and DC-DC converter. The rectifier converts the AC electrical energy from PMSG to DC. The SEPIC converter is used as a DC-DC converter. The controller 1 used here is Fuzzy logic controller and the controller 2 is P&O with ACO.

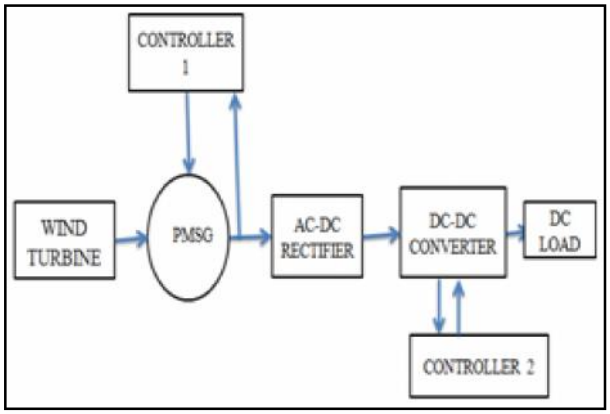

Fig.1 Block diagram of proposed system

2.1 Wind Turbine

Variable speed operation of wind turbines has more advantages over constant speed operation. Basically, variable speed wind turbines has the high inertia of the rotating mechanical parts of the system as a fly wheel, this helps to smoothen the power fluctuations and reduces the drive train mechanical stress. During partial load operations, variable speed systems could lead to maximize the capture of energy Alternatively, variable speed configurations provide the ability to control the rotor speed which allows the wind turbine system to operate constantly near to its optimum tip-speed ratio. The basic principle of wind turbine is to convert the linear motion of the wind into rotational energy, which is used to drive an electrical generator, where the kinetic energy of the wind to be converted to an electric power.

The kinetic energy(E) of the wind is given by

$$E = \frac{1}{2}mv^2 \quad (1)$$

The mass rate (m) is given by

$$m = \rho AV \quad (2)$$

By substituting (2) in (1),we get,

$$E = \frac{1}{2}\rho Av^3 \quad (3)$$

The available wind power is obtained by, applying

$$A = \frac{\pi}{4}D^2 \quad (4)$$

Available wind power,

$$P_a = \frac{1}{8}\rho\pi D^2 v^3 \quad (5)$$

The maximum power output from the turbine is given by

$$P_{max} = \frac{1}{2}\rho Av^3 c_p \quad (6)$$

Where,ρ = Air density in Kg\m^3,A= Area of the turbine blades in m^2,V= Wind velocity in m\s,Cp = Power coefficient .

The mechanical torque developed in the system is then,

$$T_W = \frac{P}{\omega} = \frac{\frac{1}{2}C_p\,\rho AV^3}{\omega} \quad (7)$$

The power coefficient is expressed in terms of the tip speed ratio λ and depends on the blade pitch angle β,

$$C_p(\lambda,\beta) = C_1\left(\frac{C_2}{\lambda_i} - C_3 * \beta - C_4\right)e^{\frac{-C_5}{\lambda_i}} + C_6\lambda \quad (8)$$

The tip-speed ratio is λ is

$$\lambda = \frac{\omega G}{R} \quad (9)$$

2.2 Drive Train

The rotational motion of the wind turbine rotor is transmitted to the electrical generator by means of mechanical transmission called drive train. Its structure frimly depends on each particular WECS technology. Figure 3 shows the drive train model of WECS. Therefore, the electrical machine will experience an increased rotational speed and a reduced electromagnetic torque. A two mass shaft model is used in wind turbine system drive train. One mass represents the turbine inertia and the other mass represents the PMSG inertia.

$$T_W - T_{SH} = 2H_T \frac{d\omega_T}{dt} \quad (10)$$

$$T_{SH} - T_E = 2H_G \frac{d\omega_T}{dt} \quad (11)$$

$$\frac{d\theta}{dt} = \omega_T - \omega_G \quad (12)$$

$$T_{SH} = K\theta - D\frac{d\theta}{dt} \quad (13)$$

where H_T is the inertia constant of the turbine, H_G is the inertia constant of the PMSG, θ is the shaft twist angle, ω_T is the angular speed of the wind turbine in p.u, ω_G is the rotor speed of the PMSG in p.u., K is the shaft stiffness and D is the damping coefficient.

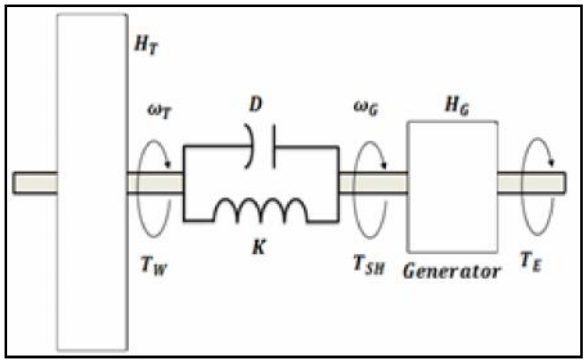

Fig.2 Equivalent diagram of wind turbine drive train

2.3 PMSG Modelling

Doubly fed induction generators are generally used as the generator in a variable speed wind turbine system. In case of DFIG, gearbox is required to match the turbine and rotor speed. The gearbox frequently suffers from faults and it have need regular maintenance, which makes the system unreliable. The reliability of the variable speed wind turbine can be improved by using a direct drive-based permanent magnet synchronous generator (PMSG). PMSG has received much attention in wind energy applications as a result of its self-excitation capability, leading to a high power factor and high efficiency operation.

The voltages of d- and q- axes in PMSG can be given by:

$$v_d = -i_d R_S - \omega\lambda_q + p\lambda_d \quad (14)$$

$$v_q = -i_q R_S - \omega\lambda_d + p\lambda_d \quad (15)$$

Where, λ_d and λ_q are the *d*- and *q*- axes stator flux linkages and are given by the following equations

$$\lambda_d = -L_d i_d + \lambda_M \quad (16)$$

$$\lambda_q = -L_q i_q \quad (17)$$

The torque equation of an interior permanent magnet synchronous generator is given by

$$T_e = -\frac{3}{2}P\left(\lambda_q i_q - \lambda_q i_d\right) \quad (18)$$

$$T_e = -\frac{3}{2}P\left[\lambda_M i_q + \left(L_d - L_q\right) i_d i_q\right] \quad (19)$$

For a surface PMSG, which is used in this paper *Ld=Lq*, therefore, the torque equation becomes

$$T_e = -\frac{3}{2}P\left[\lambda_M i_q\right] \quad (20$$

The generator torque and rotor speed are related by

$$T_g = T_m - J\frac{d\omega_m}{dt} - B\omega_m \quad (21)$$

In equations (14-21), *vd*, *vq*, *id*, *iq*, *Ld* and *Lq* are the *d* and *q* axes stator voltages, currents and inductances respectively, *Rs* is the stator resistance, λM is the amplitude of the flux linkage (Wb) in the stator due to permanent magnet in the rotor, ω is the electrical angular velocity in rad/sec, ω_m is the rotor speed, *B* is the damping coefficient (Nm.s), *J* is the moment of inertia (kg.m2), and *P* is the number of pole pairs. *p* is the operator *d/dt*. The torque equation consists of two terms represented in (18). The first term represents the excitation torque and the second term represents the reluctance torque due to rotor saliency.

2.4 POWER ELECTRONIC CONVERTER

A DC-DC converter is a converter which converts a source of direct current (DC) from one voltage level to another voltage level. It is a class of power converter.DC-DC converters may be operated in two modes, according to the current in the main magnetic component.The DC-DC converter topologies are classified as Buck converter, Boost converter, Buck-boost converter. The Buck converter is also known as step down converter which produces lower output voltage than the dc input voltage. The Boost converter is also known as step up converter which produces higher output voltage than the dc input voltage. The buck-boost converter produces the output voltage either higher or lower than the dc input voltage. In the proposed work SEPIC converter is used as DC-DC converter.

3.SEPIC CONVERTER

The single ended primary inductor converter is a DC/ DC converter whose output voltage is greater than, less than, or equal to the input voltage. By controlling the duty cycle of control switch, the output of the SEPIC is controlled. A SEPIC is typically a boost converter pursued by a buck-boost converter, therefore it is similar to a traditional buck-boost converter, but it has advantages of having non-inverted output, and being capable of reducing the voltage drop across the switch.

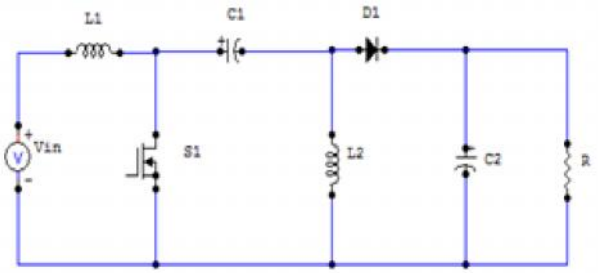

Fig.3 Circuit diagram of SEPIC Converter

The design equations of SEPIC converter is given by

$$L_2 = \frac{1}{2} * \frac{V_{in} * D}{\Delta i_L * f_s} \quad (22)$$

$$C_{OUT} \geq \frac{I_{OUT} * D}{\Delta V * 0.5 * f_s} \quad (23)$$

$$C_1 = C_2 = \frac{I_{OUT} * D}{\Delta V * f_s} \quad (24)$$

Where,

D=Duty cycle,V_{in} is the input voltage in Volts, ΔV and Δi_L is the ripple voltage and current, f_s is the supply frequency. In mode 1 operation of SEPIC converter, switch S1 is turned on, the current in the inductor L1 increases and the current in inductor L2 goes more negative. The input source V_{in} is used to increase the magnitude of current I_{L1}. While S1 is closed, the instantaneous voltage V_{C1} is approximately equal to V_{IN}, the voltage V_{L2} is approximately "V_{IN}. Therefore, the capacitor C1 is used to supply energy to increase the magnitude of the current in L2 and thus increase the energy stored in L2. The resistive load R is supplied by a capacitor C2.

In mode 2 operation of SEPIC converter, switch S1 is turned off, the current IC1 = IL1, since inductors do not allow sudden changes in current. The current inductor L2 will continue in the negative direction, in fact it never reverses its direction. In this mode, the negative I_{L2} will add to the current I_{L1} to increase the current delivered to the load. Using Kirchoff's Current Law, the current flowing through diode, $I_{D1} = I_{C1} - I_{L2}$. It can then be concluded, when S1 is off, the inductor L1 and L2 deliver power to the load from both L2 and L1. During this off cycle, C1 is being charged by L1, and will in turn recharge L2 during the on cycle.Calculated value of design variables are

Table 1 Parameter Values of SEPIC converter

PARAMETERS	VALUE
Input voltage, V_{in}	100V
Output Voltage for D=40%,D=75%	64V,295V
Switching frequency	500kHz
L_1	5Mh
L_2	5mH
C_1	470µF
C_2	22000
R	100Ω

3. CONTROLLER USED IN PROPOSED WORK

3.1 Fuzzy Logic Controller

Fuzzy controllers are the rule based system. FLC consists of 3 stages namely, input stage, a processing stage, and an output stage. The input stage maps the input given to FLC to the appropriate membership functions and truth values. The processing stage invokes appropriate rule and generates a result for each, then combines the results of the rules. Finally, the output stage converts the result from processing stage into a specific control output value.In the proposed work Fuzzy logic controller is used to control the input torque given to the PMSG. It consists of Mamdani fuzzy inference system and the input given to the fuzzifier is electromagnetic torque and rotor speed. The triangular membership function is used to represent the inputs and the output. The output got from defuzzifier is controlled torque which is given as input to PMSG. In this system 9 rules are set to get the required output.

3.2 P &O ALGORITHM WITH ACO

The P&O algorithm is used to control the switching pulse of the SEPIC converter. It is mathematical optimization technique used to find a local maximum point. In this system, voltage and current are taken from the SEPIC converter is given as a input to the MPPT block and the output got from the block is given as a pulse to the switch. In the controller 2 block the pulse from P&O and ACO is combined to produce the pulse. According to the load, the pulse is given to the switch to supply a constant power to the load.

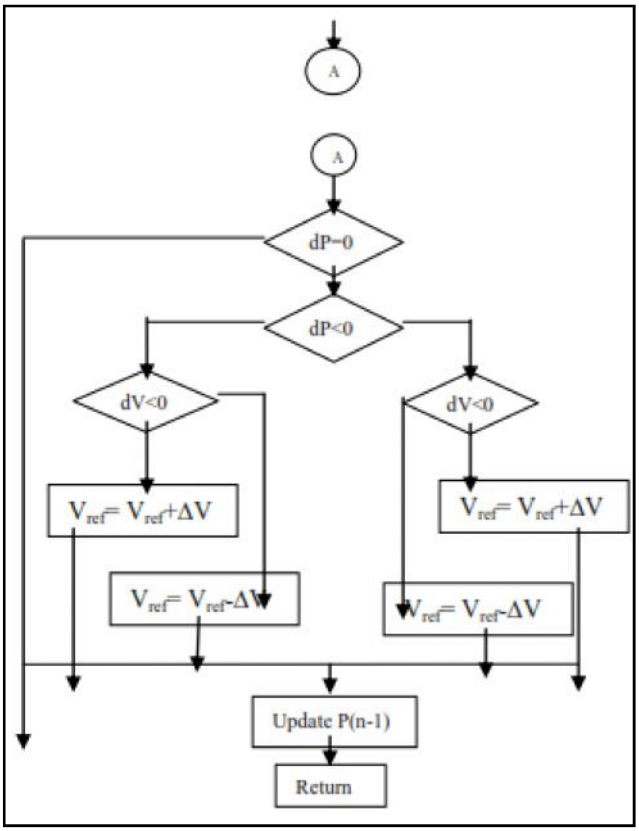

Fig.4 Flow chart of P&O algorithm

4. SIMULATION MODEL, RESULT AND ITS DISCUSSIONS

The simulink model of the SEPIC converter based WECS is developed using MATLAB(2011a) which consists of wind turbine, two mass drive train, PMSG, SEPIC converter, fuzzy logic converter, P&O algorithm, P&O with ACO algorithm. The main objective of this model is to improve the voltage obtained from variable speed wind turbine and to give the constant power to the load. Figure 5 shows the loop MATLAB/Simulink block of the wind turbine.The output of the wind turbine is given to the drive train model and its output is given to PMSG to convert mechanical energy to electrical energy. The rating of PMSG is selected according to the requirement.

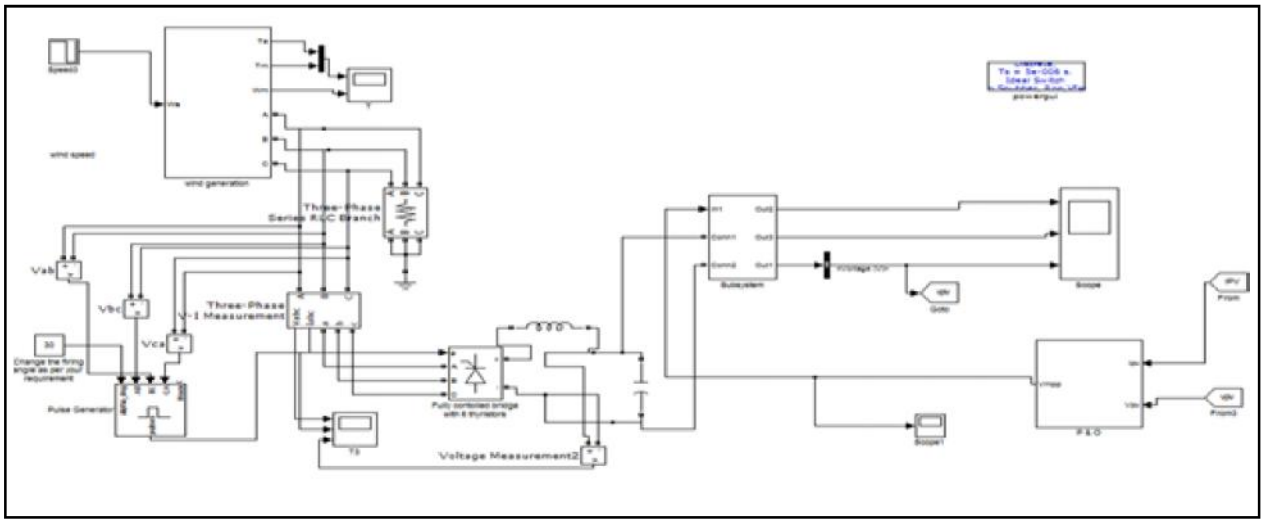

Fig. 5 Simulation of SEPIC based wind energy conversion system

Figure 6, gives the output voltage and current from the PMSG which was obtained from mechanical input given to PMSG and it gives the rectified output voltage of PMSG output voltage.

Figure 7, shows the output current and voltage waveform across the SEPIC converter which is obtained by giving pulse using P&O algorithm.

Figure 8, shows the output current and voltage waveform across the SEPIC converter which is obtained by giving pulse using P&O algorithm with ACO.

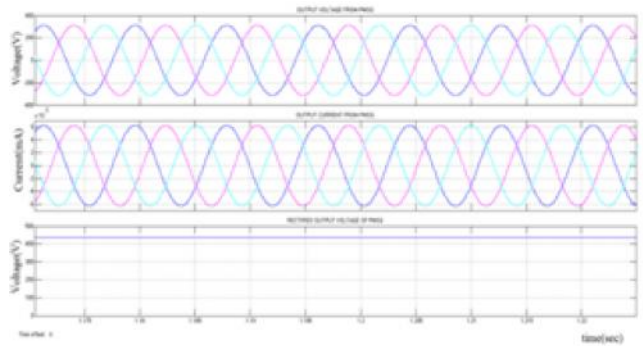

Fig. 6 Voltage and Current waveform from PMSG and rectified voltage waveform

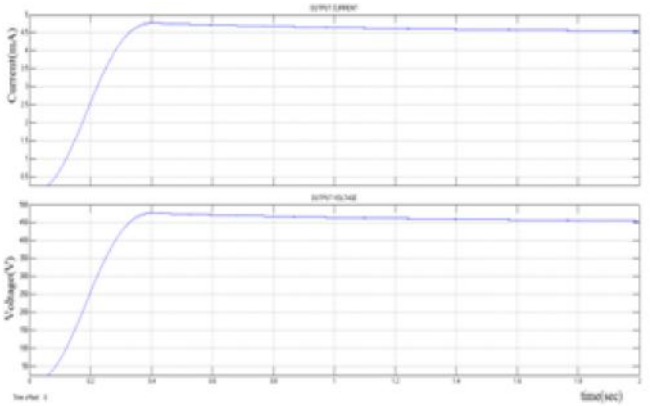

Fig.7 Current and Voltage waveform across the SEPIC converter using P&O

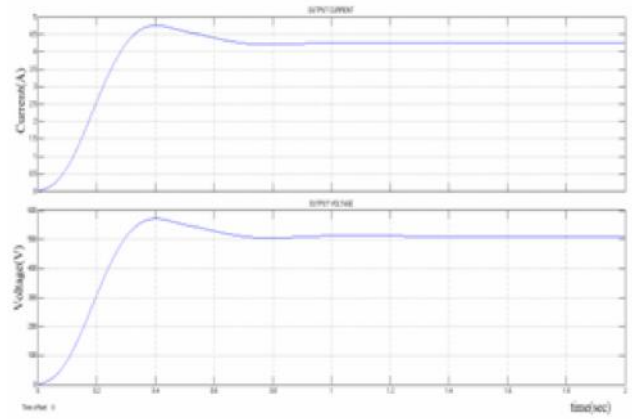

Fig 8: Current and Voltage waveform across the SEPIC converter using P&O with ACO

5. HARDWARE IMPLEMENTATION OF SEPIC CONVERTER

The hardware implementation of SEPIC converter with variable input voltage is given using RPS is shown in figure 5.3 and 5.4. From this it is observed that the output voltage of SEPIC converter with 12 V input is 29.76V. the output voltage of SEPIC converter with 20V input is 30.16V.

Table 2 Components for Hardware Implementation

Sl. No.	Name of the Components	Range	Quantity
1	Battery	6V	2
2	Regulator	7805	1
3	Dc series motor	50W, 1500rpm 50W,150 rpm	1 1
4	Dc series generator	50W,150 rpm	1

Fig. 9 Hardware implementation of SEPIC converter with 12V input

Fig.10 Hardware implementation of SEPIC converter with 20V input

Fig.11 SEPIC converter with WECS

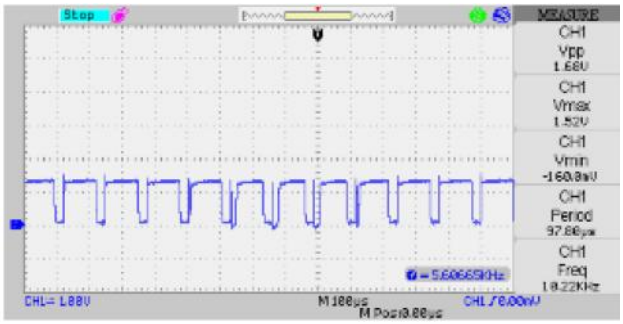

Fig.12Switching pulse for SW in resistive load condition

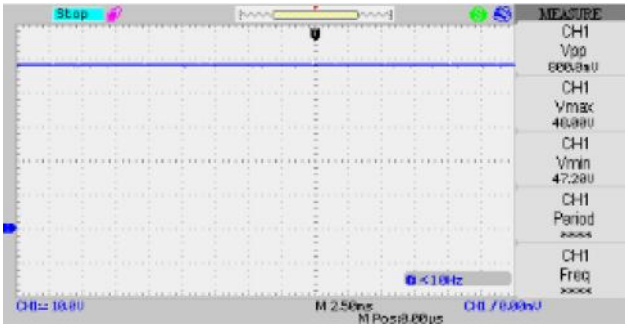

Fig.13Output voltage waveform of proposed work with resistive load

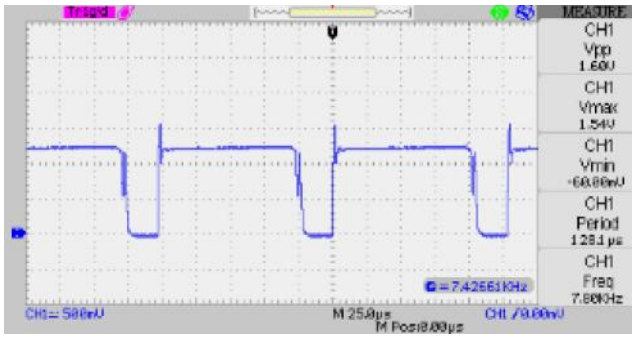

Fig.14 Switching pulse for SEPIC converter with motor load

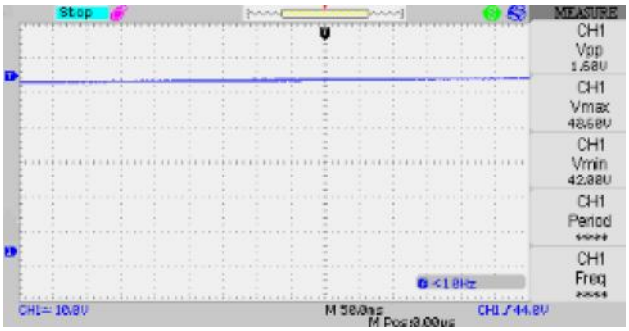

Fig.15 Output waveform of proposed work with motor load

6. CONCLUSION

From the simulation, it is observed that the proposed system works efficiently by improving output voltage by using P&O with ant colony optimization. As compared to P&O algorithm the P&O algorithm with ant colony optimization works more efficiently and by using fuzzy logic controller the PMSG is controlled for variable wind speed and the hardware for SEPIC converter with result had been implemented.

REFERENCES

[1] Vivek Agarwal., Rakesh K. Aggarwal., Pravin Patidar and Chetan Patki, “A Novel Scheme for Rapid Tracking of Maximum Power Point in Wind Energy Generation Systems”, IEEE transactions on Energy Conversion., Vol. 25, No.1, 2010, pp.228-236.

[2] Yun Yang., Kwan-Tat Mok., Siew-Chong Tan, “Nonlinear Dynamic Power Tracking of Low-Power Wind Energy Conversion System”, IEEE Transactions on Power Electronics., Vol.30, 2015, pp.5223-5236.

[3] Yuanye Xia., Khaled H. Ahmed and Barry W. Williams, “A New Maximum Power Point Tracking Technique for Permanent Magnet Synchronous Generator Based Wind Energy Conversion System”, IEEE Transactions on Power Electronics., Vol. 26, No.12, 2011, pp.3609-3620.

[4] Hany M. Hasanien and S. M. Muyeen, “Design Optimization of Controller Parameters Used in Variable Speed Wind Energy Conversion System by Genetic Algorithms”, IEEE transactions on Sustainable Energy., Vol.3, No.2, 2012, pp. 200-208.

[5] Eftichios Koutroulis and Kostas Kalaitzakis, “Design of a Maximum Power Tracking System for Wind-Energy-Conversion Applications”, IEEE transaction on Industrial Electronics., Vol.53, 2006, pp.486-494.

[6] V. Krishnakumari, Suji Muhammed “Performance Analysis of a PMSG Based Wind Energy Conversion System”, International Journal of Engineering Research & Technology., Vol.3, 2014, pp.2278-0181.

[7] C. N. Bhende, S. Mishra and Siva Ganesh Malla , “Permanent Magnet Synchronous Generator-Based Standalone Wind Energy Supply System”, IEEE transactions on Sustainable Energy., Vol. 2, No.4, 2011, pp. 361-372.

[8] M. E. Haque, K.M.Muttaqi and M. Negnevitsky, "A Control Strategy for Output Maximisation of a PMSG-based Variable-speed Wind Turbine", Australian Journal of Electrical and Electronics Engineering., Vol.5, 2009, pp.263-270.

[9] Ebrahim Babaei., Mir Esmaeel Seyed Mahmoodieh "Calculation of Output Voltage Ripple and Design Considerations of SEPIC Converter", IEEE transaction on Industrial Electronics.,Vol.61, No.3, 2014, pp.1213-1222.

[10] Ahmad El Khateb, Nasrudin Abd Rahim, Jeyraj Selvaraj and Mohammad Nasir Uddin, "Fuzzy-Logic-Controller-Based SEPIC Converter for Maximum Power Point Tracking", IEEE transaction on Industrial Electronics., Vol.50, 2014, pp.2349-2358.

Design of High Throughput Redundant Binary Technique for Image Processing Application

P. Nathiya, S. Padmapriya and K. Dhatchayani
Sri Ramakrishna Engineering college, Coimbatore - 641 022, Tamil Nadu

Abstract

Redundant Binary (RB) method can be used for high modularity and carry-free addition for high performance multipliers. An additional Error Correcting Word (ECW) is generated in a conventional RB multiplier and requires both radix-4 Modified Booth Encoding (MBE) and RB encoding. In MBE multiplier the additional RBPP accumulation stage occurs. In this method a new RB Modified Partial Product Generator (RBMPPG) is proposed. An extra Error Correcting Word (ECW) is removed and saves a one accumulation stages. Than conventional RB MBE multiplier the proposed RBMPPG generates fewer partial product rows. The proposed RB MBE method simulation results show significantly improves the area and delay for the word length of each operand in the multiplier is at least 8bits. The area delay product can be reduced up to 50 percent compared with existing RB multipliers.

Keywords: *Modified booth encoding, Redundant binary, RB partial product generator, RB multiplier*

1. INTRODUCTION

The arithmetic units of Microprocessor, multimedia, and digital signal processors are applied in digital multipliers. To design a high speed and low power multipliers many algorithm and architectures are proposed. There are three steps to include the Normal Binary (NB) multiplication by digital circuits. First step generation of partial product, second step to remain two partial product rows all partial products are added by partial product reduction tree. In third step, the fast carry propagation adder can be added by using two partial product rows. To perform a partial product reduction two methods can used.

To perform signed-digit arithmetic the redundant binary number representation has been introduced by avizienis [1]. The capability of RB number can be represented in different ways. By using redundant binary addition trees the fast multipliers can be designed [6].Floating point processor and redundant binary representation are implemented in VLSI[5].Due to advantageous features, high performance of RB multipliers become popular such as high modularity and carry-free addition [8].

$$NRBPPAS = [\log_2(N/4+1)] \quad (1)$$

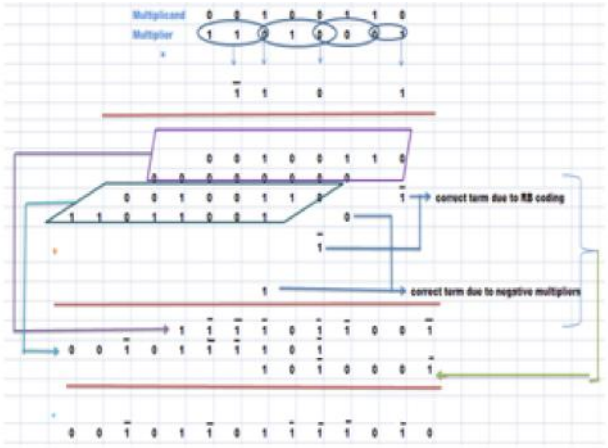

Fig.1 Conventional 8 bit NBBE multiplier

2. ANALYSIS OF BOOTH ENCODING AND RB PARTIAL PRODUCT GENERATOR

2.1 Radix-4 Booth Encoding

Booth encoding is used to facilitate the two's complement multiplication of binary numbers. The sets of three adjacent bits are formed in the multiplier bits. In neighboring groups the two side bits are overlapped in which it is {b1,b0,0}. The decoded partial product are selected by a each group. And 2A from the table1 shows the twice the value of multiplicand, it can be performed by left shifting. Each bit of A and adding '1' the negation operation can be obtained. For RB MBE multipliers the problem cannot be solved.Radix-4 booth encoding is used to solve the problem in correcting bits for multiplier of (NBBE-2) multipliers. By inverting

each bit of A and adding '1'the negation operation is achieved. The encoder and decoder operations are used in a partial product reduction tree.

Table 1 Scheme of MBE

b2i+1,b2i, b2i-1	Operation
000	0
001	+A
010	+A
011	2A
100	-2A
101	-A
110	-A
111	0

2.2 RB PARTIAL PRODUCT GENERATOR

RBPP is generated from two NB partial products, one RB digit is used to represent by two bits. Using two's complement representation the addition of two N-bit partial products X and Y are used. Adding -1 from the NB partial product to the LSB and RBPP is generated. The errors are introduced in both the MBE and RB coding. 1) -1 must be added to the LSB of RB number when RB format is converted by a NB number. 2) During the booth encoding the multiplicand is multiplied by -1 or -2. From both the radix-4 and RB encoding a single ECW can compensate the errors. The N/4 RBPP rows and one ECW included by a N-bit- CRBBE-2.

$$ECW = E(N/4)0\,F(N/4)0 \ldots .0E_{i2}0F_{i0} \ldots 0E_{i2}0F_{10} \qquad (2)$$

Where i represents the i^{th} row in the RBPP's. Booth encoding is determined by using the errorcorrectingdigit.

$$Ei_2 = \begin{cases} 0, no\ negative\ encoding \\ 1, negative\ encoding \end{cases}$$

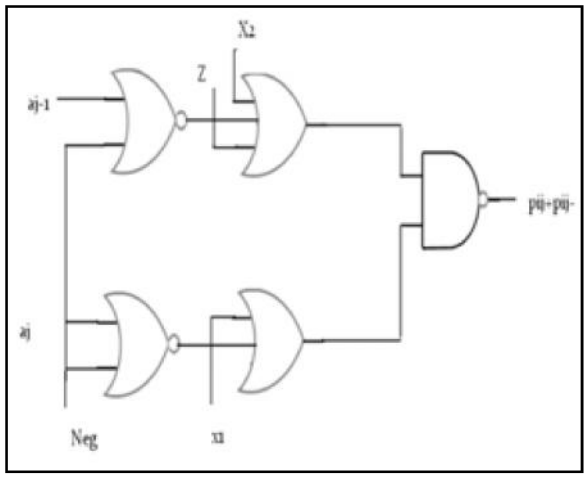

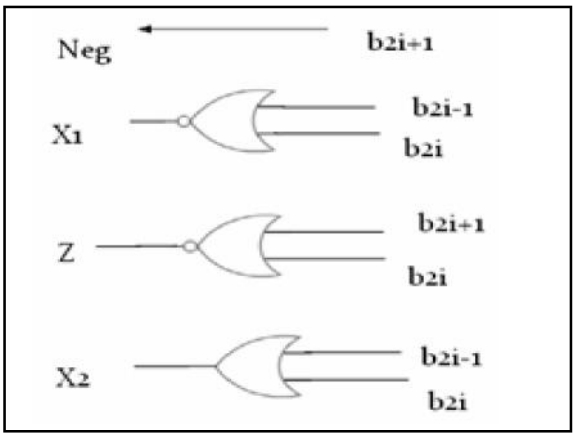

Fig.2 MBE scheme of encoder and decoder

An encoder accepts an active level on one of its input level representing digit such as decimal or octal digits and converted in to coded output such as BCD or Binary. Decoder is a logic circuit that accepts a set of inputs that represents the binary number and activates only the output that corresponds to input number.

Table 2 RB Encoding

X_i^+	X_i^+	RB digit (X_i)
0	0	0
0	1	-1
1	0	1
1	1	0

3. METHOD OF PROPOSED RB PARTIAL PRODUCT GENERATOR

In this method error correction is eliminated using new RB modified partial product generator and partial product rows are reduced from 3 to 2 stages. The error correcting words are combined in free space of partial product terms and shown in Figure3. (b) and by combining the number of accumulation stages.

$$ECW_1 = 0E_{12}\,0F_{10} \qquad (3)$$

By using PP_1 the ECW_1 is generated.

$$ECW_2 = 0\,E_{22}\,0\,F_{20} \qquad (4)$$

PP_1 and PP_2 are to be combined with ECW_2 to eliminate the RBPP accumulation stages. The first (PP_1^+)MSB of first partial product row and ($PP^-_{N/4}$) last partial product of two LSBs of last partial product row are eliminated using Error Correction Word (ECW). The area and delay product can be reduced.

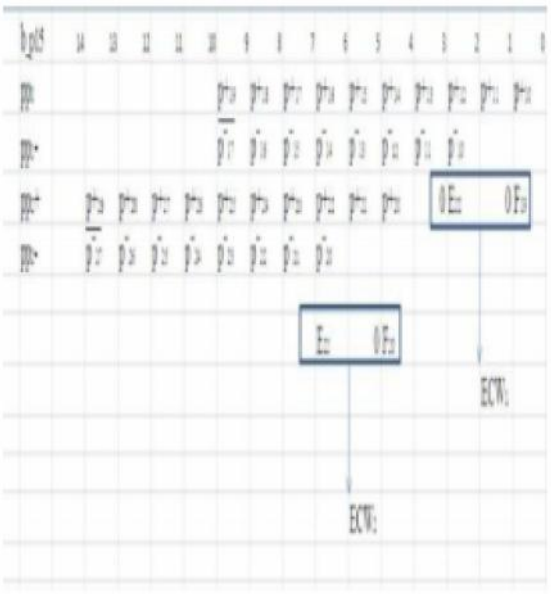

Fig.3 (a) 8-bit MBE multiplier of a new RBMPPG architecture

Fig.3 (b) Proposed RBMPPG-2 architecture eliminating ECW2.

The partial product terms are generated in a Stage-1 RBPPA and shown in Figure 4. the 8 bit values are combined in a stage-2 RBPPA to convert a Redundant Binary to Normal Binary convertor. Finally the product term is generated.

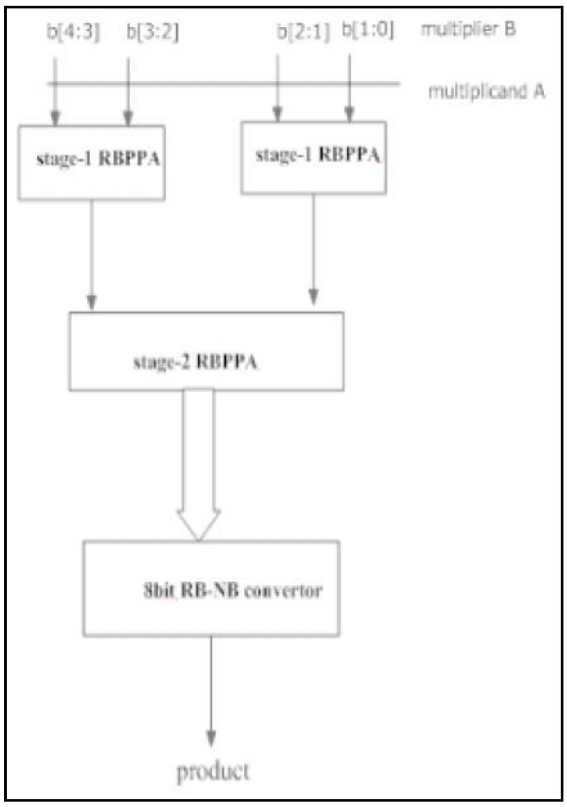

Fig.4 Block diagram of 8-bit RB multiplier

3.1 Proposed RBMPPG-2

The pp1 and pp2 are incorporated to eliminate the RBPP accumulation stages. The area delay process can be reduced. Than other gates the two input NAND gate and Transmission gate (TG) are faster.

By generating Q_{18}^{+}, Q_{19}^{+}, Q_{20}^{+}, Q_{21}^{+} the delay of RBMPPG-2 is reduced. Whereas Q_{18}^{+} shows a longest path delay.

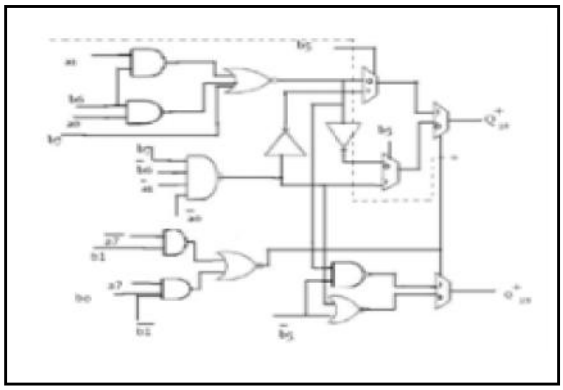

Fig.5.Modified partial product variables Q_{18}^{+} and Q_{19}^{+}

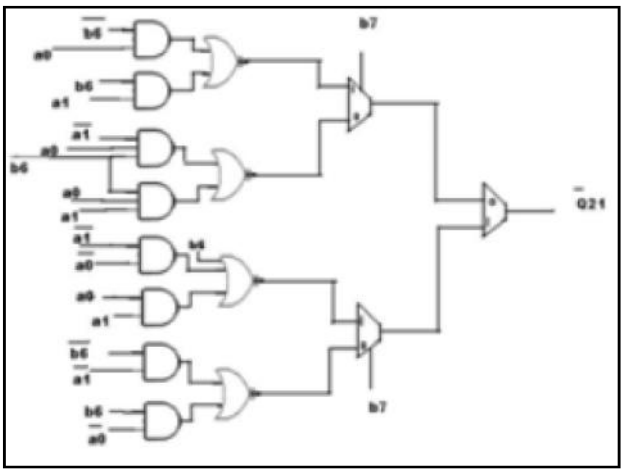

Fig.6 Modified partial product variables Q^{-}_{21}.

By eliminating the invertors from mux the number of stages can be reduces easily.

$$Q^{+}_{18} = (b_7 \oplus b_5 + b_7 b_6 b_5).p^{+}_{18} + \bar{b}_7 \bar{b}_5.(\overline{p^{-}_{21} + p^{-}_{20}}) \oplus p^{+}_{18})$$

$$+ b_7 \overline{b_6} b_5 . (p^{-}_{21} p^{-}_{20} \oplus p^{+}_{18})$$

$$Q^{+}_{19} = (b_7 \oplus b_5 + b_7 b_6 b_5).p^{+}_{19} + \bar{b}_7 \bar{b}_5.(\overline{p^{+}_{18} + p^{-}_{21}}) + p^{-}_{20} p^{+}_{19})$$

$$+ b_7 \overline{b_6} b_5 . (p^{+}_{18} p^{-}_{21} p^{-}_{20} \oplus p^{+}_{19})$$

$$Q^{-}_{21} = (b_7 \oplus b_5 + b_7 b_6 b_5).p^{+}_{21} + \bar{b}_7 \bar{b}_5.(\overline{p^{-}_{21} + p^{-}_{20}})$$

$$+ b_7 \overline{b_6} b_5 . p^{-}_{21 \oplus} p^{-}_{20})$$

4. PERFORMANCE ANALYSIS

The performance of RBMPPG is proposed using Xilinx tool. The NBBE-2, CRBBE-2 and RBBE results are compared. In final stage RB multiplier is converted into NB multiplier to form a two's complement number. Compared with existing covalent redundant binary booth encoding the proposed redundant binary booth multiplier is more efficient. In Table 3. The area and delay are to be shown using the covalent redundant binary booth encoding (CRBBE) and redundant binary booth multiplier.

Table 3 Design Results of CRBBE and RBBE Multipliers Using Xilinx ISE Tool

Techniques	Area in Slices	Area in LUTs	Delay (ns)
Normala Binary Booth Encoding Multiplier (NBBE)	320	840	21.2
Covalent Redundant Binary Booth Encoding (CRBBE)	281	725	14
Covalent Redundant Binary Booth Multiplier	233	600	3.2

5. APPLICATION : IMAGE PROCESSING

The proposed multipliers are applied on image processing to multiply two images on pixel by pixel basis, by using MATLAB tool, therefore blending two images into a single image there will not be any noise in the output images the PSNR value will be a infinity for both the proposed and existing method.

The input images are shown in figure 7

Fig.7 Input image 1 and image 2

By multiplying input image 1 and 2 the images are blended using MATLAB and resulted output images are shown below in figure 8.

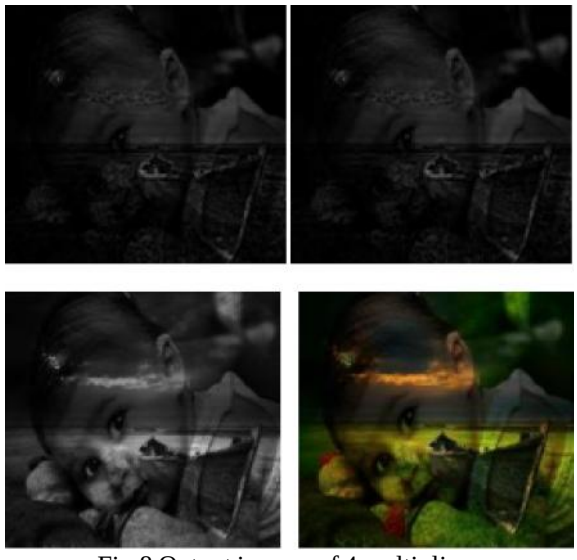

Fig.8 Output images of 4 multipliers

6. CONCLUSION

In this paper, a new modified RBPP generator method is proposed. In previous stage the additional ECW (Error Correction Word) is introduced. Due to elimination of ECW the RBPP accumulation stage is saved. To reduce the number of RBPP rows from N/4+1 to N/4 the RB partial product generation technique can be applied to any 2^n-bit RB multipliers. The performance of RB MBE multipliers using the proposed RBMPPG-2 is improved and shown in simulation results. The area delay product can be reduced more than 50percent using proposed RB multipliers. Hence, designing area delay efficient power of two RBMBE multipliers is very useful technique using proposed RBPP generation method. The proposed RBPP are to be applied in image processing.

REFERENCES

[1] AvizienisA, "Signed-digit Number Representations for Fast Parallel Arithmetic", IRE Trans. Electron. Computers, Vol.EC-10, 1961, pp.389-400.

[2] N.Besli and R.Deshmukh, "A Novel Redundant Binary Signeddigit (RBSD) Booth's Encoding", in Proc. IEEE Southeast Conf., 2002, pp.426-431.

[3] C. Chang, J.Gu and M. Zhang, "Ultra Low-voltage Low-power CMOS 4-2 and 5-2 Compressors for Fast Arithmetic Circuits", IEEE Trans. Circuits Syst. I, Reg. Papers, Vol.51, 2004, pp. 1985-1997.

[4] C. Chang, and Y. He, "A Power-delay Efficient Hybrid Carry Lookahead Carry-select Based Redundant Binary to Two's Complement Converter", IEEE Trans. Circuits Syst. I, Reg. Papers, Vol. 55, 2008, pp.334-336.

[5] H. Edamatsu, T. Taniguchi, T.Nishiyama and S. Kuninobu, "A 33 MFLOPS Floating Point Processor using Redundant Binary Representation", in Proc. IEEE Int. Solid-State Circuits Conf. (ISSCC), 1988, pp.152-153.

[6] Y. Harata, Y.Nakamura, H. Nagase, M.Takigawa and M. Takagi, "A High Speed Multiplier using A Redundant Binary Adder Tree", IEEE J. Solid-State Circuits, vol. SC-22, 1987, pp. 28-34.

[7] J. Kang and J. Gaudiot, "A Simple High-speed Multiplier Design", IEEE Trans. Computers, Vol. 55, 2006, pp.1253-1258.

[8] F. Lamberti, H.Antelo, N.Andrikos and P. Montuschi, "Reducing the Computation Time in (short bit-width) Two's Complement Multipliers", IEEE Trans. Computers, Vol.60, 2011, pp. 148-156.

[9] H. Makino, H.Shinohara and Y.Nakase, "A 8.8-ns 54x54-bit Multiplier using New Redundant Binary Architecture", in Proc. Int. Conf. Comput. Design (ICCD), 1993, pp.202-205.

[10] D. Nikolos, G. Dimitrakopoulos, "High-speed Parallel Prefix VLSI Ling Adders", IEEE Trans. Computers, Vol.54, 2005, pp.225-231.

Estimation of Micro Calcification in Mammogram Images

C. Santhi, S.M. Shayeela Banu, S. Suvetha, V. Thenmozhi and M. Manikandan
Department of Electronics and Communication Engineering,
M.Kumarasamy College of Engineering, Karur - 639 113, Tamil Nadu

Abstract

In upcoming years, an increased interest is seen in area of medical image handling, outcome, and Computer Aided Diagnostic (CAD) frameworks. The fundamental reason for CAD framework helps specialist during the time spent determination. Computer aided design frameworks, be that as it may are very costly, particularly in the vast majority of the creating nations. Our emphasis is on building up an ease CAD framework. Today, the greater part of the CAD frameworks with respect to mammogram grouping target programmed recognition of calcification and anomalous mass. Calcification regularly demonstrates an early manifestation of bosom disease in the event that it shows up as a little size brilliant spot in a mammogram picture. Based on the perception that calcification shows up as little brilliant spots on a mammogram picture, we propose another scale-particular blob identification strategy in which the scale is chosen through directed learning. By figuring vitality for every pixel at two unique scales, another component "Proportion Energy" is presented for proficient blob discovery. Because of the forced straightforwardness of the element and post preparing, the running time of our calculation is direct concerning picture measure.

1.INTRODUCTION

Breast tumor is one of the significant reasons for death among ladies everywhere throughout the world. The genuine reason for bosom growth is still obscure. Along these lines, early location of breast tumor and its treatment is the best way to perhaps longer life and enhanced personal satisfaction of patients. Computer aided design frameworks help significantly in diagnosing bosom growth.

What's more, these frameworks may likewise be utilized as a moment feeling by radiologists for the check of demonstrative outcomes. In such CAD frameworks, exactness of results is of essential significance. A minor wrong location or false miss can prompt to wrong or poor treatment. Because of the affectability of the issue, numerous specialists are doing work in the field of mammogram division and rivaling each other to accomplish better outcomes.

Our examination predominantly concentrates on ease handling mammogram pictures those outcomes in the division of both irregular mass and calcification. Insights demonstrate that 30–50 % of tumor has micro calcification and abnormal mass is likewise a reasonable manifestation of bosom disease. Along these lines, early location of such strange mass and small scale calcification can help radiologists in better diagnostics, bringing about appropriate and auspicious treatment of patients. Division of mammograms for distinguishing calcification and different masses is a dynamic territory of research.

2. PROPOSED METHOD

It has been watched that a variation from the norm, particularly microcalcification zone, happens as a modest blob in mammograms having more shine, subsequently force, contrasted with its near by pixels [Figure 5]. We register vitality at every pixel in a mammogram for two diverse window capacities. By captivating the proportion of vitality figured for a little window (3 X 3) to the vitality processed for an expansive window (11 X 11), we distinguish the apprehensive territory contain a variation from the norm by thresholding the vitality proportion to 80 % of most extreme vitality proportion and by applying power edge steps a while later. At that point, we concern post processing on conclusive outcomes utilizing morphological operations. We concern pre-preparing ventures toward the begin of the calculation to sort out ordinary pictures, i.e., pictures have no variation from the norm. The motivation behind applying this sifting is to dispose of the additional handling required in preparing ordinary pictures. A piece chart depicting the strategy utilized is appeared as a part of Figure 6.

Table 1 Small Window(3x3)

P(x-1, y-1)	P(x-1,y)	P(x-1,y+1)
P(x,y-1)	P(x,y)	P(x,y+1)
P(x+1,y-1)	P(x+1,y)	P(x+1,y+1)

Fig.1 Input image

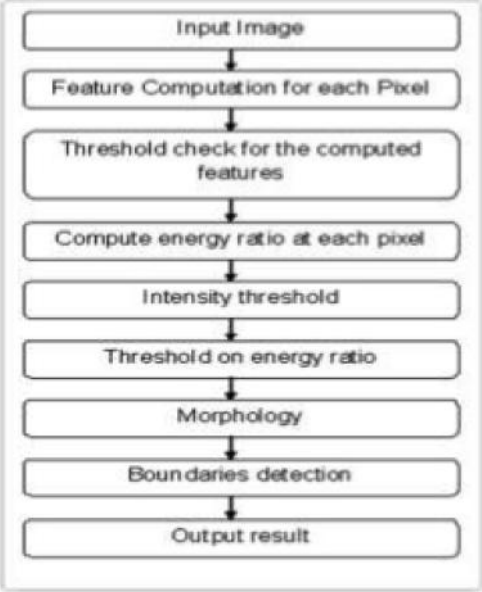

Fig.2 Steps of the proposed algorithm

2.1 Preprocessing

The reason for the preprocessing tread is to sift through standard pictures from the dataset. This spares instance from extra preparing the typical pictures and to diminish the fake helpful outcomes. Along these lines, if a picture is ordinary, it is accounted for quickly. To sift through ordinary pictures, we register kurtosis and skewness for a 20 × 20 sliding window. The particular pixel is accounted for as typical if kurtosis estimation of a pixel focused at the 20 × 20 window surpasses 14 and skewness esteem surpasses 2.3. In the event that we don't discover any pixel in the entire picture that has a place with these edge breaking points of skewness and kurtosis, we think the picture to be a typical picture, have no variations from the norm.

2.2 Energy Computation

After the preprocessing tread our calculation find the doubtful districts inside the mammogram. For algorithm, pick the little window range 3 × 3 and the bigger window size 11 × 11 window sizes later traverse approving outcomes on various window sizes. Energy pixel is registered aggregate intensities of the pixels secured by window focused at thee pixel. Assume P(x, y) speaks power of pixel situated at arrange x, y in a picture. At that point the 3 × 3 and 11 × 11 windows focused at P(x,y) are spoken to by Tables 1 and 2, individually.

The vitality at P(x, y) for a window w (wr, wc), w, is registered as takes after:

$$w(x,y) = \sum_{i=-wr}^{wr} \sum_{j=-wc}^{wc} P(x+i, y+j).$$

For the tiny window w=s and wr=wc=3. For the big window w=l and wr=wc=11. The Ratio Energy (RE) is computed by Eq. (1).

$$RE_{(x,y)} = \frac{{}^{s}(x,y)}{{}^{l}(x,y)} \times 100 \qquad (1)$$

RE is registered for each pixel in the picture. We then dispose of anomalies from the picture for even judgment of additional limits Fig 7(a) demonstrates the come about subsequent to taking supplement of Ratio Energy processed at every pixel.

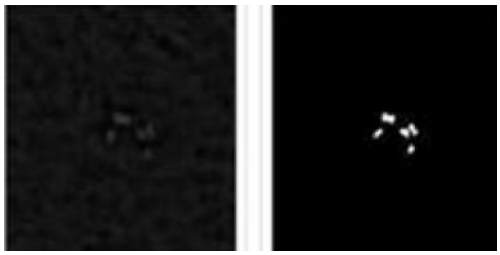

(a) (b)

Fig.7 (a) Image showing complement of Ratio Energy computed at each pixel (b) Image after thresholding RE image to maximum energy and intensity

2.3 Threshold computation

To maintain a strategic distance from consideration of exception pixels, we relate limit on the pixel forces. Pixels that are of no enthusiasm for discovery of anomalous lots cannot add vitality edge. Thus, in the underlying stride of thresholding it can be disregard RE's of every pixel that recline beneath our characterized power edge χ, as spoke to by Eq. (2).

$$\chi = 90/100 \times \max(\text{Intensity}(x, y)) \quad (2)$$

Most extreme force utilized as a part of Eq. (2) is in use from a capacity that take beat two most extreme powers from the picture. It then thinks about the contrast between these forces. On the off chance that the distinction is more noteworthy than a specific edge, it implies there exists an anomaly in the picture and the force determination work essentially chooses the second power to be the power edge. Else, it gives back the main vitality to be the power edge.

Subsequent to applying force edge, we register the most extreme of all vitality proportions, as indicated by Eq. (3).

$$= \max(REp(x, y)) \quad (3)$$

We contrast RE of every pixel and the vitality edge δ, characterized in Eq. 4.

$$\delta = 80/100 \times \varepsilon \quad (4)$$

In the event that RE of a pixel P(x, y), is more prominent than eequivalent to δ, pixel is marked as frontal area pixel i.e., it has a place with microcalcification or irregular mass. Figure 7(b) demonstrates the irregular range after vitality and power edges. We conform our edges in an approach to reduce the possibility of tall fake harmful charge notwithstanding, this biasness in thresholding presents several fake encouraging points in our outcomes, for which we relate the position handling tread.

2.4 Post Processing

In this progression, we diminish the quantity of artificial positives. We utilize the morphological operation with the precious stone molded organizing component for this reason. Since microcalcifications show up as brilliant and modest acne and regularly have a mass not any more than 20 pixels on the mammograms. Contingent upon this property we pick the extent of organizing component bigger than 20 pixels.

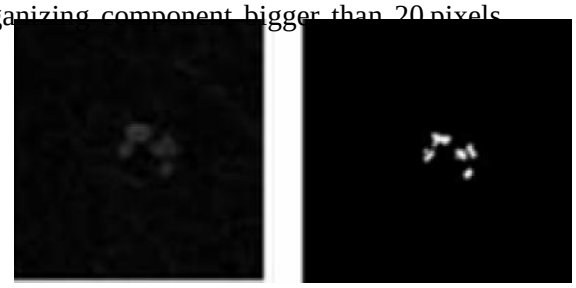

(a) (b)

Fig.8 (a) Outcome of tophat morphological operation on original image (b) Image shows thresholding after the tophat operation

Assume P(x, y) speaks to a dim size mammogram picture and S is the organizing component, fundamental morphological operation Erosion o and Dilation •" are characterized as takes after:

$$\text{Erosion:}[\ PoS](x,y) = \min(u,v)\ \varepsilon S\ P(x + u, y + v)$$
$$\text{Dilation:}[\ P+S](x,y) = \max(u,v)\ \varepsilon S\ P(x - u, y - v)$$

Base ahead essential morphological process cavity morphological process o is characterizes as Erosion took after by Dilation

$$PoS = (P\ S) + S.$$

On relating the TopHat morphological operation of dark level mammogram picture by registering morphological opening of the picture and subtract it from our unique picture, f, as appeared in Eq. (5) [Figure 8 (a)].

$$\text{TopHat}(P) = P - (PoS) \quad (5)$$

We utilize the imTopHat capacity of Mat lab to affect the morphological TopHat operation. At that point we binarize the picture that is acquired by Eq. (5) by captivating pixels having force > 4.0 σ, where σ is standard deviation [Figure 8(b)].

After this procedure, we have two pictures:

Ie = Image in the wake of figuring and thresholding the vitality work, and

It = Image in the wake of applying TopHat and thresholding.

The crossing point of these pictures, Ir, appeared in Eq. (6) is the normal result of calcification [Figure 9], where calcification incorporates both microcalcification and full scale calcification.

$$Ir = Ie \Lambda It \quad (6)$$

Where '" is the sensible AND operation.

At long last, the limit circle is wan in the region of an irregularity by evaluating the middle and span of the circle concerning the thickness of the forefront pixels. Fig 10 demonstrates confident means required in recognizing and picture circle in the region of the irregular locale.

2.5 Results

The choice of a CAD framework can be categorized as one of the four classifications. A picture locale can be call anomalous (positive) or ordinary (negative), and a choice can also be right (genuine) or off base (false). Computer aided design can produce two sorts of incorrect yields, i.e., False Positive (FP) and False Negative (FN). Genuine Positive (TP) and True Negative (TN) are the two right choices. Two execution detects of a discovery framework is identified with choices recognized over are "Affectability" and 'Specificity'. Affectability is the likelihood of a positive check, the patient is unwell while specificity is probability of a negative check the patient is healthy hhigh estimations of affectabilityy, specificity are alluring. "Exactness" and "Accuracy" are likewise utilized for execution assessment in CAD frameworks. To survey the execution of our calculation, we tried it on 84 pictures from the DDSM database. 54 (64 %) of these pictures were typical and 30 (36 %) were malignant.

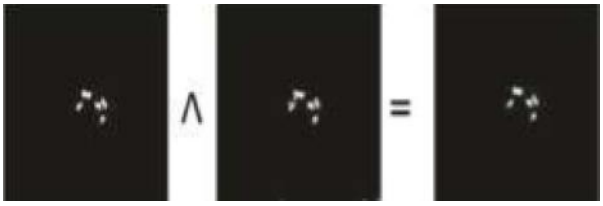

Fig. 9 The image after applying the logical AND operation on the RE image and the tophat image

2.6 Detection criteria

Execution of CAD conspires created for mammogram arrangement require sure criterion for deciding TP and FP group discovery. The evaluation outcomes, honest to goodness groups of calcificationn can be recognized by a specialist radiologist. Criterion are utilized for tallying quantity of TP identifications can be a group as effectively distinguished if at least three pixels are determined inside the area set apart as contain calcification by a radiologist. Every extra district, if distinguished, is thought to be FP.

As appeared in Table 2, our calculation has 91 % sensitivity, 97 % specificity, 93 % exactness, and 85 % accuracy. Two master radiologists1 observed our outcomes to be extremely attractive and dependable.

Table 2 Analysis of Results

Performance Measure	Abnormal cases		Normal cases	
	30 (36%)		54 (64%)	
	TP	FN	TN	FP
	29 (97%)	01 (3%)	49 (91%)	05 (9%)
Sensitivity	91%			
Specificity	97%			
Precision	85%			
Accuracy	93%			

2.7 Algorithm Complexity

Every pixel in picture, RE count take O(window estimate) instance since it distinguish spot at a particular level paying little mind to the span of the picture, i.e., the window level is settled (consistent). Along these lines, time multifaceted nature of RE calculation at every pixel is O(1) that collects O(n) of this picture have n pixels. The charge of thresholding for together vitality and force in additionally straight as far as the quantity of pixels in the picture. In this manner, the time many- sided quality of thresholding is O (n).

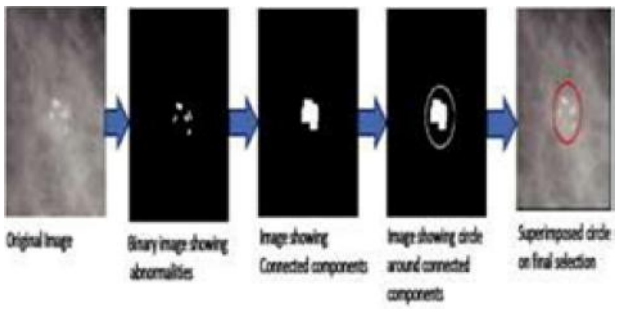

The alteration of definite outcomes incorporates the morphological operation, as morphology require difficulty of the organizing component over the entire picture. In view of settling the scale, the extent of organizing component is additionally settled bringing about the time many-sided quality of the aggregate difficulty to be O(n). The development charge of the entire calculation, T(n), will be T(n) = time cost for figuring R.E at every

pixel + time cost for thresholding + Time cost for morphology = O(n) + O(n) + O(n) = O(n). Along these lines, the calculation is straight as far.

3.CONCLUSIONS

Computer aided design frameworks can help significantly in the early identification of disease. Mammogram order is significant utilize of CAD frameworks are utilized. A mammogram picture is typically very loud so it is difficult to identify district of intrigue (ROI). Indeed, a specialist radiologist can't relate to 100 % certainty that the territory of concern is constantly recognized accurately. As per an overview, just about 25 % of microcalcification is miss by radiologists at early on stage Countless picture examinations is one reason of this miss proportion.

Computer aided design frameworks are unrivaled in that once created, they can work with a similar exactness on any number of pictures. Equipment disappointments might be a purpose behind the framework to crash; however expanded examination stack does not influence the execution of the framework.

Computer aided design frameworks created for mammogram order assist radiologists to obtain a moment supposition and reduction a radiologist's failure proportion. Radiologists contrast the opinion and aafter effects of CAD framework and construct their last findings with respect to a "twofold perusing" of results. A definitive objective of CAD framework for mammography is distinguishing cancer to be felt by a doctor radiologist. This advance recognition enormously enhances ladies odds of fruitful treatment of her bosom malignancy.

Our exploration for the most part spotlights on the extremely fundamental property of microcalcification are luminous blob on a mammogram picture when contrasted with the rest of the bosom outskirts. We utilize proportion vitality (RE) as a component that separates the territory containing variation from the norm from whatever remains of the region in a mammogram picture. In the wake of getting most extreme RE we then contrast the vitality of every pixel with threshold greatest RE so as to judge whether the pixel has a place with calcification or not. At long last, we tidy up our outcomes utilizing morphology. We likewise watch some area based properties of ordinary pictures (without cancer) that are unique in relation to anomalous pictures (with tumor) and utilize these properties to sift through typical pictures at early phases of our calculation and keep away from their more dispensation This progression diminishes the quantity of FP outcome.

Utilizing an exceptionally basic component of a picture, our framework is profoundly effective and makes a consistent number of outputs of the picture to create last outcomes. Assist, the outcomes are locale based rather than pixel based on the grounds that microcalcification happens as thick groups.

REFERENCES

[1] J. Dengler, S. Behrens and J.F. Desaga, "Segmentation of Microcalcifications in Mammograms", IEEE Transactions on Medical Imaging, Vol.12, 1993, pp.634-642.

[2] A. Przelaskowski and P. Surowski, "Methods of Medical Image Data Optimization Applied to Archiving and Telemedical Transmission", Research Project of the State Commit-tee for Scientific Research No. 7T11E03920, (in Polish), 2002.

[3] S. Quadrades and A. Sacristan, "Automated Extraction of Microcalcifications BI-RADS Numbers in Mammograms", Proc. IEEE ICIP, 2001, pp.289-292.

[4] J.Dengler, S. Behrens and J. Desaga, "Segmentation of Microcalcifications in Mammograms", IEEE Trans. Medical Image. Vol.12, 1993, pp.231-238.

[5] D. Betal, N. Roberts, and G. Whitehouse, "Segmentation and Numerical Analysis of Micro calcifications on Mammograms using Mathematical Morphology", British J. Radiology Vol.70, 1997, pp.903-917.

[6] J. Kim and H. Park, "Statistical Textural Features for Detection of Micro Calcifications in Digitized Mammograms", IEEE Trans. Medical Image. Vol.18, 1999, pp.231-238.

[7] H. Chany, B. Sahiner, N. Petrick, M. Helvie, K.Lam, D. Adler, and M. Goodsitt, "Computerized Classification Of Malignant And Benign Micro Calcifications On Mammograms: Texture Analysis Using An Artificial Neural Network", Phys. Med. Biol., Vol.42, 1997, pp.549-567.

[8] Y. Jiang, "Classification of Breast Lesions From Mammograms", in Handbook of Medical Imaging, Academic Press, New York, 2000, pp. 341-357.

[9] L. Shen, R. Rangayyan, and J. Desautels, "Shape Analysis Of Mammographic Calcifications", Proc., 5th Annual IEEE Symposium on Computer-Based Medical Systems, 1992, pp.123-128.

[10] T. Kohonen, "Self-organizing Maps in Information Sciences", in Sprinter Series in Information Sciences, 1995, pp.30.

[11] Y. Jiang and R. Nishikawa, "Malignant and Benign Clustered Microcalcifications: Automated Feature Analysis and Classification", Radiology, Vol.198, 1996, pp.671-678.

[12] Conselleria de Sanitat Monografies Sanitaries, Programa de Prevenciyn de cбncer de mama en la Comunidad Valenciana, serie E25, 1998.

Indian Journal of Engineering, Science, and Technology (IJEST)

(ISSN: 0973-6255)
(A half-yearly refereed research journal)

Information for Authors

1. All papers should be addressed to The Editor-in-Chief, Indian Journal of Engineering, Science, and Technology (IJEST), Bannari Amman Institute of Technology, Sathyamangalam - 638 401, Erode District, Tamil Nadu, India.
2. Two copies of manuscript along with soft copy are to be sent.
3. A CD-ROM containing the text, figures and tables should separately be sent along with the hard copies.
4. Submission of a manuscript implies that : (i) The work described has not been published before; (ii) It is not under consideration for publication elsewhere.
5. Manuscript will be reviewed by experts in the corresponding research area, and their recommendations will be communicated to the authors.

Guidelines for submission

Manuscript Formats

The manuscript should be about 8 pages in length, typed in double space with Times New Roman font, size 12, Double column on A4 size paper with one inch margin on all sides and should include 75-200 words abstract, 5-10 relevant key words, and a short (50-100 words) biography statement. The pages should be consecutively numbered, starting with the title page and through the text, references, tables, figure and legends. The title should be brief, specific and amenable to indexing. The article should include an abstract, introduction, body of paper containing headings, sub-headings, illustrations and conclusions.

References

A numbered list of references must be provided at the end of the paper. The list should be arranged in the order of citation in text, not in alphabetical order. List only one reference per reference number. Each reference number should be enclosed by square brackets.

In text, citations of references may be given simply as "[1]". Similarly, it is not necessary to mention the authors of a reference unless the mention is relevant to the text.

Example

[1] M.Demic, "Optimization of Characteristics of the Elasto-Damping Elements of Cars from the Aspect of Comfort and Handling", International Journal of Vehicle Design, Vol.13, No.1, 1992, pp. 29-46.

[2] S.A.Austin, "The Vibration Damping Effect of an Electro-Rheological Fluid", ASME Journal of Vibration and Acoustics, Vol.115, No.1, 1993, pp. 136-140.

SUBSCRIPTION

The annual subscription for IJEST is Rs.600/- which includes postal charges. To subscribe for IJEST a Demand Draft may be sent in favour of IJEST, payable at Sathyamangalam and addressed to IJEST. Subscription order form can be downloaded from the following link http:// www.bitsathy.ac.in./ ijest.html.

For subscription / further details please contact:

IJEST
Bannari Amman Institute of Technology
Sathyamangalam - 638 401, Erode District, Tamil Nadu Ph: 04295 - 226340 - 44
Fax: 04295 - 226666 E-mail: ijest@bitsathy.ac.in Web:www.bitsathy.ac.in

Indian Journal of Engineering, Science, and Technology

Volume 11, Number 2, July - December 2017

CONTENTS

Design of Compact Microstrip Dipole Antenna 01
S.Anusha and L.Gomathi

An efficient Compression Technique for Image Multiplication 08
N. Savithaa, C.S. Manikandababu and G.G. Renuga Devi

Measurement and Detection of Cisterna Magna in Fetal Brain based on LMS Method 14
V. Praveen Kumar and S. Deepak

Fault Diagnosis of Three Phase Induction Motors by Using Kernal Based SVM Classifiers 19
R. Senthil Kumar and K. Sarasvathi

Deployment of IoT in Railway System 25
M. Gayathri Devi and E. Esakki Vigneswaran

Performance Analysis of MPPT Algorithms for PV Array Fed SEPIC Converter 31
S.Kirthika

Dynamic Power Tracking Using Intelligence Technique for WECS With Sepic Converter 37
P. Alageswari and S. Dinesh Kumar

Design of High Throughput Redundant Binary Technique for Image Processing Application 45
P.Nathiya, S.Padmapriya and K.Dhatchayani

Estimation of Micro Calcification in Mammogram Images 50
C.Santhi, S.M.Shayeela Banu, S.Suvetha, V.Thenmozhi and M.Manikandan